Theory and observations of tropical waves

Juliana Dias

- **Equatorial Waves**
- **Convectively Coupled Equatorial waves**
- **Madden-Julian Oscillation**
- Easterly Waves

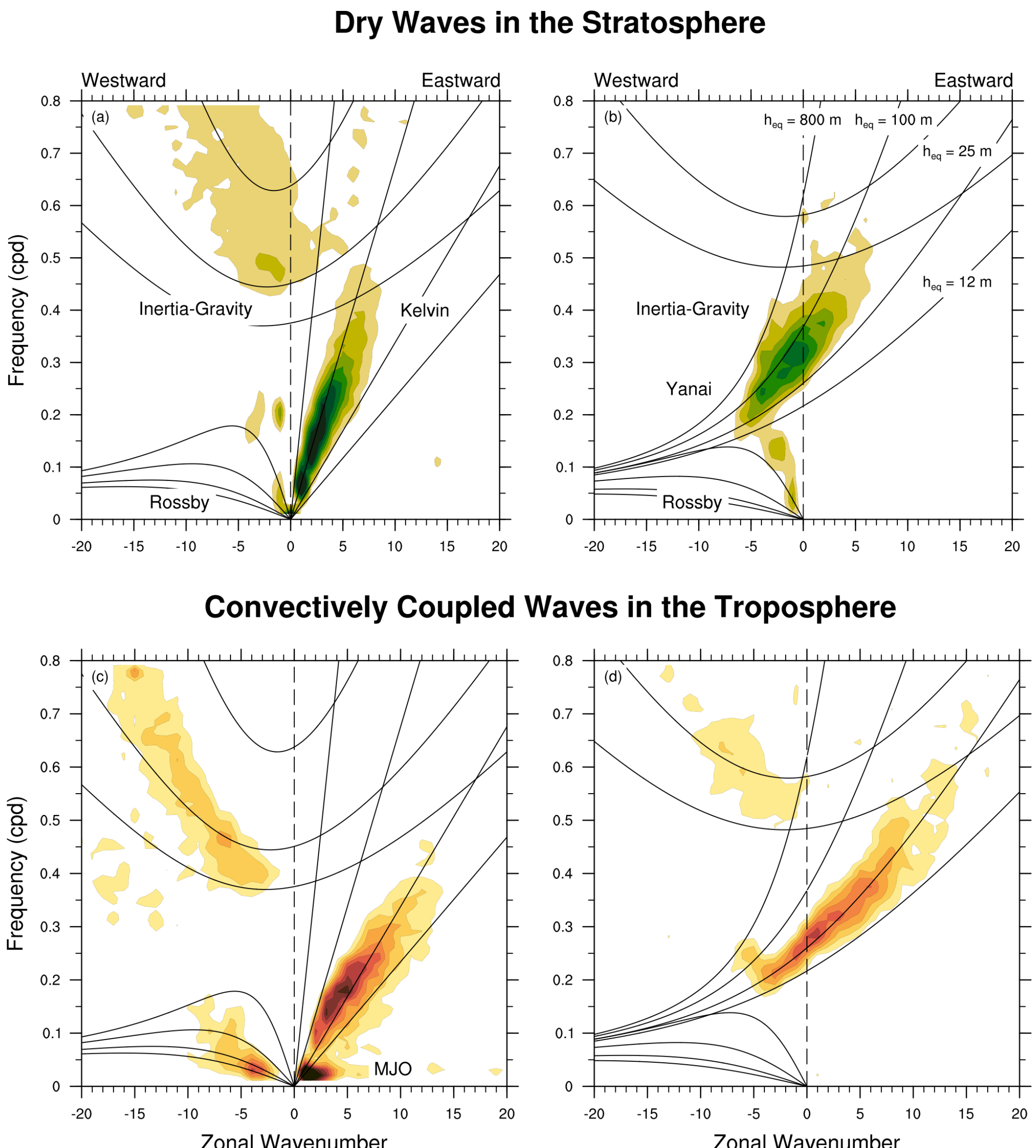

Theory and observations of tropical waves

and predictions

Juliana Dias

- **Equatorial Waves**
- **Convectively Coupled Equatorial waves**
- **Madden-Julian Oscillation**
- Easterly Waves

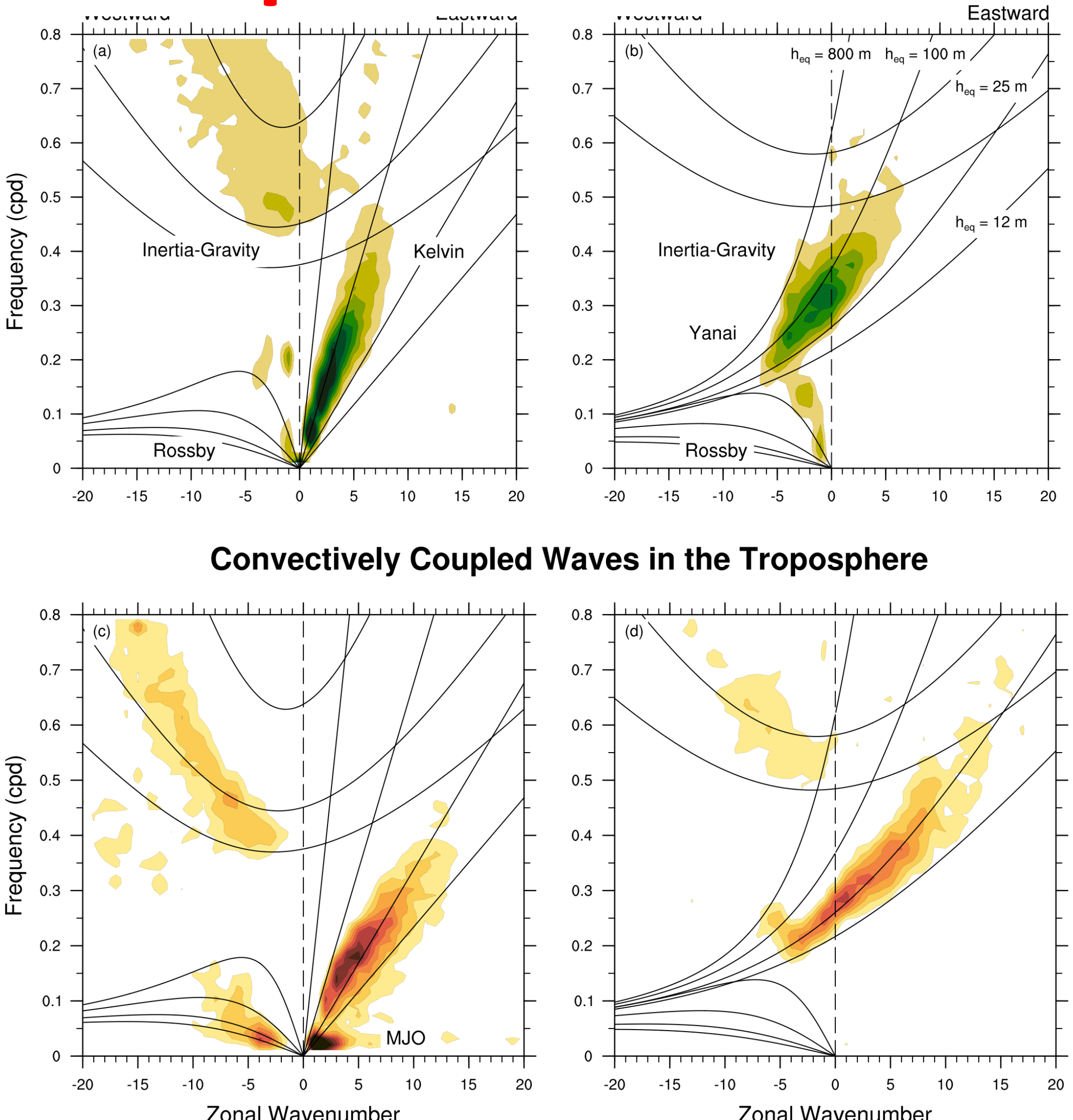


CANADA
Boulder
New York
UNITED STATES
MEXICO
CUBA
VENEZUELA
COLOMBIA
BRAZIL
PERU
BOLIVIA
CHILE
PARAGUAY
ARGENTINA
Sao Paulo


EXPERIMENTO METEOROLÓGIC
Realização: USP/UNESP
Apoio: FABESP/


C A N A D A
Boulder
New York
UNITED STATES
MEXICO
CUBA
VENEZUELA
COLOMBIA
B R A Z I L
PERU
BOLIVIA
CHILE
ARGENTINA
Sao Paulo

Key takeaways:

- Planetary waves are trapped along the equator due to the change in the Coriolis parameter's sign.
- The equatorial wave spectrum includes fast-oscillating inertia-gravity waves and low frequency Rossby waves, with mixed Rossby-gravity wave branch and an eastward-propagating equatorial Kelvin wave filling the frequency gap.
- Linear theory works well to interpret observations, providing mechanistic insights into the global scale atmospheric response to tropical convective heating.
- Important questions remain about the role of moisture in convectively coupled

equatorial waves and the Madden-Julian Oscillation (MJO).

Part 1: Theory of Tropical Waves

- Matsuno's theory for free equatorial waves
- Dispersion diagrams
- Convectively coupled equatorial waves
- MJO theor(~~y~~)ies

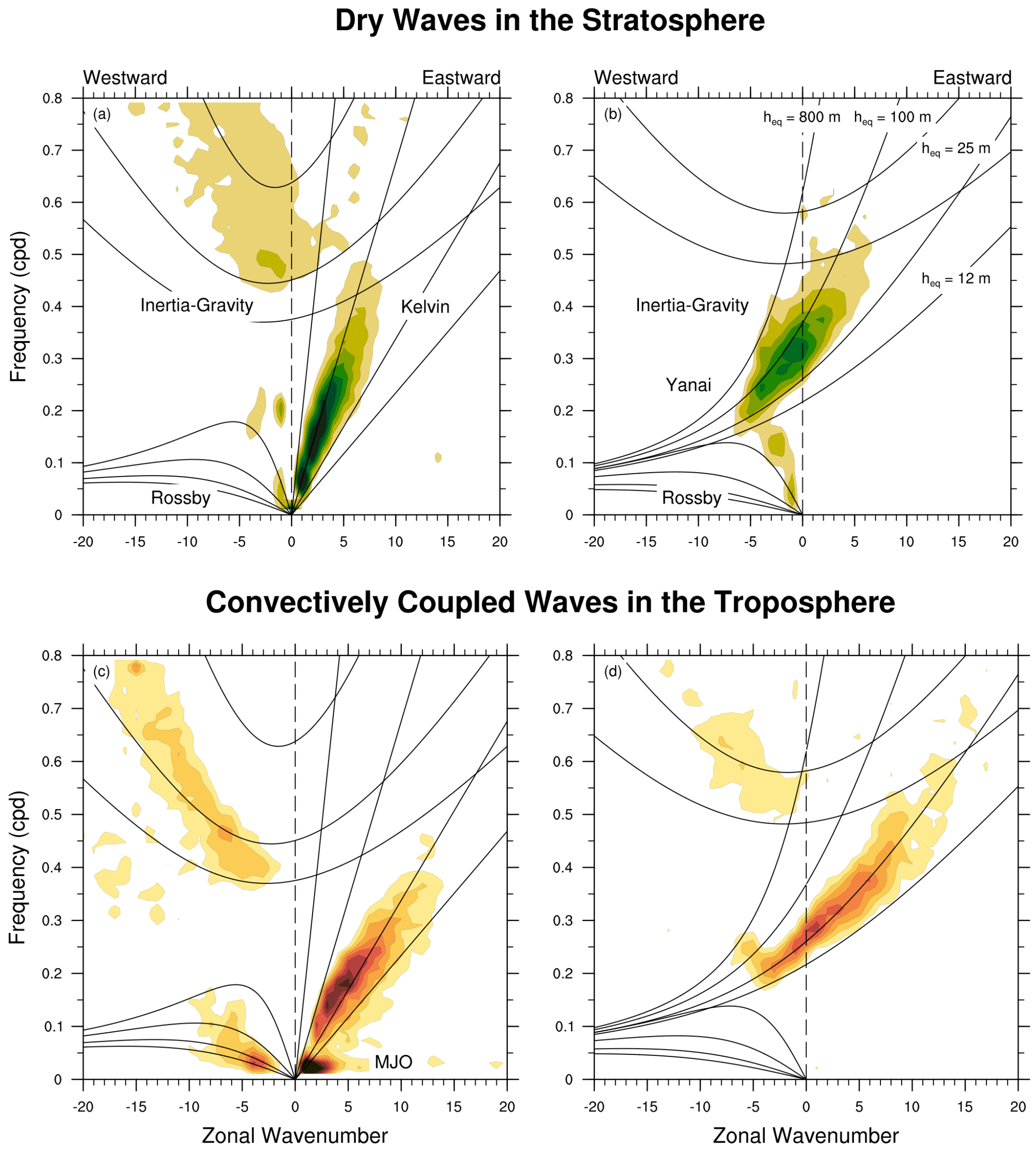

Part 1: Theory of Tropical Waves

- Matsuno's theory for free equatorial waves
- Dispersion diagrams
- Convectively coupled equatorial waves
- MJO theor(~~y~~)ies

Atmospheric Dynamics
Volume A. Large-scale Atmospheric Dynamics

Editors: Riwal Plougonven, Gwendal Rivière & Caroline Muller

20 juin 2024

Chapitre 13. Equatorial waves

Matsuno's theory for free equatorial waves

Tropical dynamics is markedly different from the midlatitudes because as one crosses the equator, the vertical component of the Earth's rotation vector (Ω) changes sign.

$$f = f_o + \beta y$$

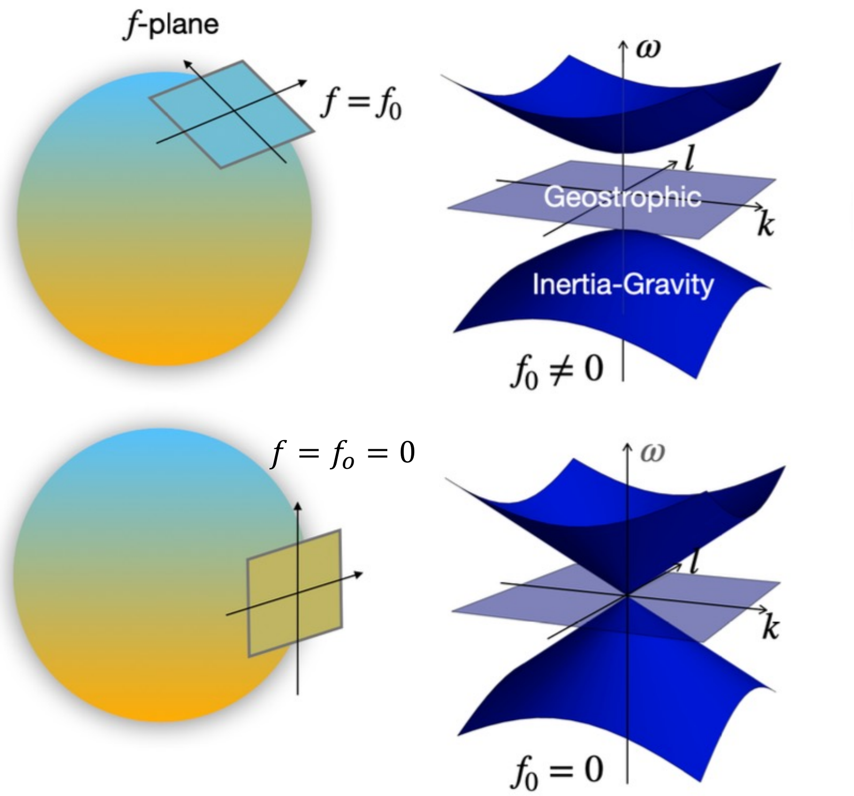

$$f = 2\Omega \sin(\text{lat})$$

Matsuno's theory for free equatorial waves

Tropical dynamics is markedly different from the midlatitudes because as one crosses the equator, the vertical component of the Earth's rotation vector (Ω) changes sign.

$$f = f_o + \beta y$$

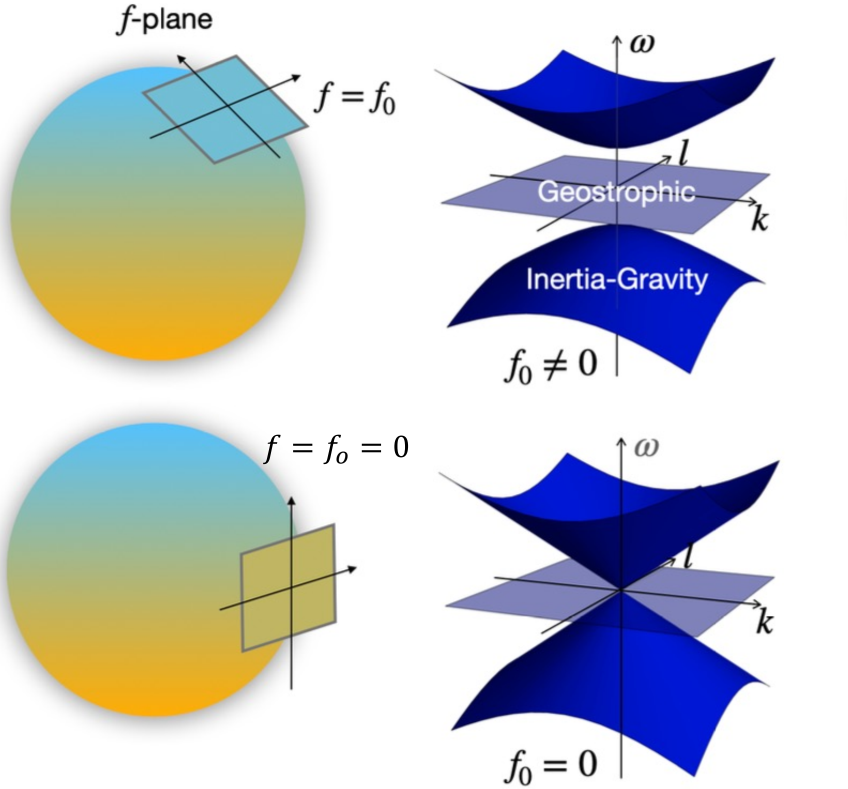

Matsuno's looked for wave solutions when:

$$f = \beta y$$

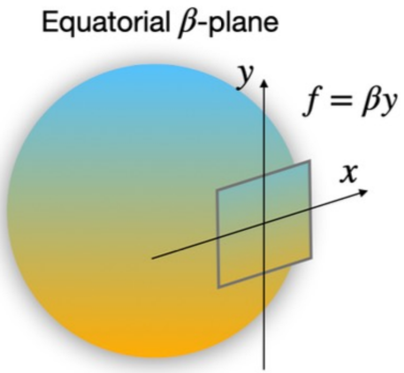

$$f = 2\Omega \sin(\text{lat})$$

Matsuno's theory for free equatorial waves

On a local cartesian coordinate system (Fig. 1), the equations of motion and of the mass conservation are written as;

$$\frac{\partial u}{\partial t}-fv+g\frac{\partial h}{\partial x}=0$$

$$\frac{\partial v}{\partial t}+fu+g\frac{\partial h}{\partial y}=0 \qquad (1)$$

$$\frac{\partial h}{\partial t}+H\left(\frac{\partial u}{\partial x}\right)=0$$

where u, v, are the velocities in the x and y directions respectively and h is the small deviation of the elevation of the top surface, the mean value of which is denoted by H. f is the Coriolis parameter and g the acceleration of gravity. As shown in Fig. 1 the x-axis is taken so as to coincide with the equator directing eastward, and the y-axis is taken northward. Here we shall assume

Here we shall assume that the Coriolis parameter f is linearly proportional to the latitude,

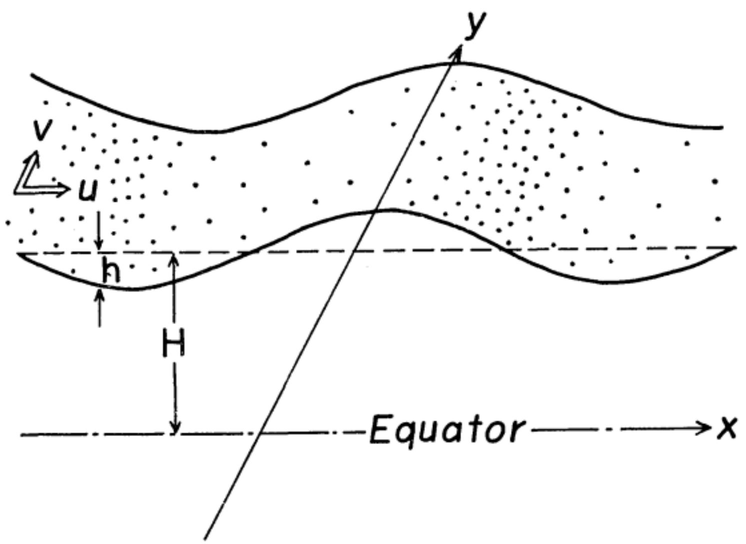

Fig. 1. Model and Coordinates.

$$f=\beta y.$$

Matsuno's theory for free equatorial waves

Introducing rescaled velocity and interface height perturbations

$$u' = \frac{u}{c}, \quad v' = \frac{v}{c}, \quad \eta' = \frac{h - H}{H}, \quad c \equiv \sqrt{gH},$$

The equatorial beta plane linear shallow equations configuration leads to a solvable wave problem

$\hat{v}$

Matsuno's theory for free equatorial waves

The equatorial beta plane linear shallow equations configuration leads to a solvable wave problem

Introducing rescaled velocity and interface height perturbations

$$u' = \frac{u}{c}, \quad v' = \frac{v}{c}, \quad \eta' = \frac{h-H}{H}, \quad c \equiv \sqrt{gH},$$

the linear dynamics around a state of rest can be written as

$$\frac{\partial}{\partial_t}\begin{pmatrix} u' \\ v' \\ \eta' \end{pmatrix} = \begin{pmatrix} 0 & f(y) & -c\partial_x \\ -f(y) & 0 & -c\partial_y \\ -c\partial_x & -c\partial_y & 0 \end{pmatrix}\begin{pmatrix} u' \\ v' \\ \eta' \end{pmatrix}$$

$\hat{v}$

Matsuno's theory for free equatorial waves

The equatorial beta plane linear shallow equations configuration leads to a solvable wave problem

Introducing rescaled velocity and interface height perturbations

$$u' = \frac{u}{c}, \quad v' = \frac{v}{c}, \quad \eta' = \frac{h-H}{H}, \quad c \equiv \sqrt{gH},$$

the linear dynamics around a state of rest can be written as

$$\frac{\partial}{\partial_t}\begin{pmatrix} u' \\ v' \\ \eta' \end{pmatrix} = \begin{pmatrix} 0 & f(y) & -c\partial_x \\ -f(y) & 0 & -c\partial_y \\ -c\partial_x & -c\partial_y & 0 \end{pmatrix}\begin{pmatrix} u' \\ v' \\ \eta' \end{pmatrix}$$

Assuming wave solutions in the x-direction

$\hat{v}$

$$(u, v, \eta) = (\hat{u}(y), \hat{v}(y), \hat{\eta}(y))\, e^{i\omega t - ikx}\,.$$

Matsuno's theory for free equatorial waves

The equatorial beta plane linear shallow equations configuration leads to a solvable wave problem

Introducing rescaled velocity and interface height perturbations

$$u' = \frac{u}{c}, \quad v' = \frac{v}{c}, \quad \eta' = \frac{h-H}{H}, \quad c \equiv \sqrt{gH},$$

the linear dynamics around a state of rest can be written as

$$\frac{\partial}{\partial_t}\begin{pmatrix} u' \\ v' \\ \eta' \end{pmatrix} = \begin{pmatrix} 0 & f(y) & -c\partial_x \\ -f(y) & 0 & -c\partial_y \\ -c\partial_x & -c\partial_y & 0 \end{pmatrix}\begin{pmatrix} u' \\ v' \\ \eta' \end{pmatrix}$$

Assuming wave solutions in the x-direction

$$(u, v, \eta) = (\hat{u}(y), \hat{v}(y), \hat{\eta}(y))\, e^{i\omega t - ikx}\,.$$

leads to a linear system of equations

$$\omega \begin{pmatrix} \hat{u} \\ \hat{v} \\ \hat{\eta} \end{pmatrix} = \begin{pmatrix} 0 & -i\beta y & ck \\ +i\beta y & 0 & ic\partial_y \\ ck & ic\partial_y & 0 \end{pmatrix}\begin{pmatrix} \hat{u} \\ \hat{v} \\ \hat{\eta} \end{pmatrix},$$

$\hat{v}$

Matsuno's theory for free equatorial waves

The equatorial beta plane linear shallow equations configuration leads to a solvable wave problem

Introducing rescaled velocity and interface height perturbations

$$u' = \frac{u}{c}, \quad v' = \frac{v}{c}, \quad \eta' = \frac{h-H}{H}, \quad c \equiv \sqrt{gH},$$

the linear dynamics around a state of rest can be written as

$$\frac{\partial}{\partial_t}\begin{pmatrix} u' \\ v' \\ \eta' \end{pmatrix} = \begin{pmatrix} 0 & f(y) & -c\partial_x \\ -f(y) & 0 & -c\partial_y \\ -c\partial_x & -c\partial_y & 0 \end{pmatrix}\begin{pmatrix} u' \\ v' \\ \eta' \end{pmatrix}$$

Assuming wave solutions in the x-direction

$$(u, v, \eta) = (\hat{u}(y), \hat{v}(y), \hat{\eta}(y))\, e^{i\omega t - ikx}\,.$$

leads to a linear system of equations

$$\omega\begin{pmatrix} \hat{u} \\ \hat{v} \\ \hat{\eta} \end{pmatrix} = \begin{pmatrix} 0 & -i\beta y & ck \\ +i\beta y & 0 & ic\partial_y \\ ck & ic\partial_y & 0 \end{pmatrix}\begin{pmatrix} \hat{u} \\ \hat{v} \\ \hat{\eta} \end{pmatrix},$$

Which can be combined into a single equation for $\hat{v}$

$$\frac{\mathrm{d}^2\hat{v}}{\mathrm{d}y^2} + \left(\frac{\omega^2 - \beta^2 y^2}{c^2} - \frac{\beta k}{\omega} - k^2\right)\hat{v} = 0$$

Matsuno's theory for free equatorial waves

Meridional wind wave solutions are proportional to the solutions for the 1D quantum harmonic oscillator

$$\frac{\mathrm{d}^2\hat{v}}{\mathrm{d}y^2} + \left(\frac{\omega^2 - \beta^2 y^2}{c^2} - \frac{\beta k}{\omega} - k^2\right)\hat{v} = 0 \qquad (*)$$

This equation is formally analogous to the 1D quantum harmonic oscillator, with a known set of orthonormal solutions given by

$$\varphi_n(y) = H_n\left(\frac{y}{\sqrt{c/\beta}}\right) e^{-\frac{1}{2}\frac{y^2}{c/\beta}}, \quad n \in \mathbb{N}.$$

Where each basis element. φ_n is a solution of the Eq. (*) provided that:

$$\omega^2 - k^2 c^2 - \frac{\beta c^2 k}{\omega} = (2n+1)\,\beta c,$$

Matsuno's theory for free equatorial waves

Meridional wind wave solutions are proportional to the solutions for the 1D quantum harmonic oscillator

$$\frac{d^2\hat{v}}{dy^2} + \left(\frac{\omega^2 - \beta^2 y^2}{c^2} - \frac{\beta k}{\omega} - k^2\right)\hat{v} = 0 \qquad (*)$$

This equation is formally analogous to the 1D quantum harmonic oscillator, with a known set of orthonormal solutions given by

$$\varphi_n(y) = H_n\left(\frac{y}{\sqrt{c/\beta}}\right) e^{-\frac{1}{2}\frac{y^2}{c/\beta}}, \quad n \in \mathbb{N}.$$

Where each basis element. φ_n is a solution of the Eq. (*) provided that:

$$\omega^2 - k^2c^2 - \frac{\beta c^2 k}{\omega} = (2n+1)\,\beta c,$$

The functions $H_n(\xi)$ are Hermite polynomials of order *n* :

$$H_0(\xi) = 1,\ H_1(\xi) = 2\xi,$$

$$H_{n+1}(\xi) = 2\xi H_n(\xi) - 2nH_{n-1}(\xi), \qquad \frac{dH_n}{d\xi} = 2nH_{n-1}(\xi).$$

Matsuno's theory for free equatorial waves

Meridional wind wave solutions are proportional to the solutions for the 1D quantum harmonic oscillator

$$\frac{d^2\hat{v}}{dy^2} + \left(\frac{\omega^2 - \beta^2 y^2}{c^2} - \frac{\beta k}{\omega} - k^2\right)\hat{v} = 0 \qquad (*)$$

This equation is formally analogous to the 1D quantum harmonic oscillator, with a known set of orthonormal solutions given by

$$\varphi_n(y) = H_n\left(\frac{y}{\sqrt{c/\beta}}\right) e^{-\frac{1}{2}\frac{y^2}{c/\beta}}, \quad n \in \mathbb{N}.$$

Where each basis element. φ_n is a solution of the Eq. (*) provided that:

$$\omega^2 - k^2c^2 - \frac{\beta c^2 k}{\omega} = (2n+1)\,\beta c,$$

The functions $H_n(\xi)$ are Hermite polynomials of order *n* :

$$H_0(\xi) = 1,\ H_1(\xi) = 2\xi,$$

$$H_{n+1}(\xi) = 2\xi H_n(\xi) - 2nH_{n-1}(\xi), \qquad \frac{dH_n}{d\xi} = 2nH_{n-1}(\xi).$$

The equatorial Rossby radius of deformation

$$L = \sqrt{c/\beta}$$

Matsuno's theory for free equatorial waves

Zonal wind and perturbation height fields can be obtained from the meridional wind solution

If $\hat{v} = \varphi_n/\sqrt{c\beta}$, then $\hat{u}$ and $\hat{\eta}$ are

$$i\left(\omega - ck\right)\left(\hat{u} + \hat{\eta}\right) = -\varphi_{n+1},$$
$$i\left(\omega + ck\right)\left(\hat{u} - \hat{\eta}\right) = -2n\varphi_{n-1}\ .$$

A solution $v \propto \varphi_n$ with $n \neq 1$ is thus admissible only if

$$\omega \neq \pm ck$$

which can be combined as

$$\begin{pmatrix} \hat{u} \\ \hat{v} \\ \hat{\eta} \end{pmatrix}_{n,\omega} = A_{k,\omega} \begin{pmatrix} \frac{1}{2}\left(\omega + k\right)\varphi_{n+1} + n\left(\omega - k\right)\varphi_{n-1} \\ -i(\beta c)^{-1/2}\left(\omega^2 - c^2k^2\right)\varphi_n \\ \frac{1}{2}\left(\omega + k\right)\varphi_{n+1} - n\left(\omega - k\right)\varphi_{n-1} \end{pmatrix}, \quad \omega^2 - k^2c^2 - \frac{\beta c^2 k}{\omega} = \left(2n+1\right)\beta c$$

Matsuno's theory for free equatorial waves

There is a discrete spectrum of shallow water waves on the equatorial beta plane

With some algebra, three types of solutions ($(\omega\,(k))$ for the dispersion relation can be derived:

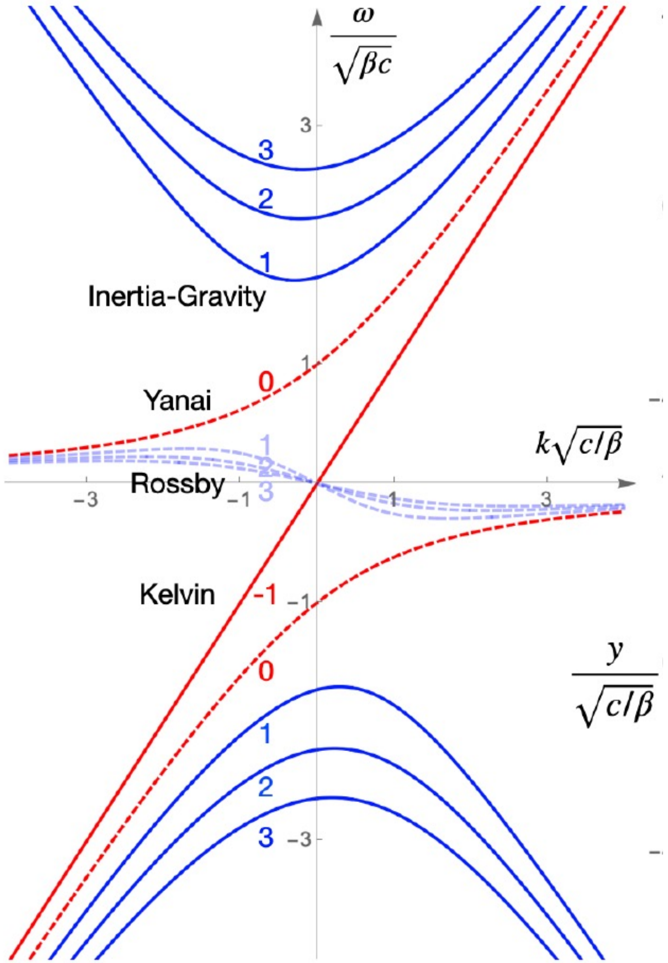

Dispersion relation:

$$\omega^2 - k^2c^2 - \frac{\beta c^2 k}{\omega} = (2n+1)\,\beta c,$$

Discrete wave solutions:

n=-1 (Kelvin)

n=0 (Yanai)

n≥1 (Inertia-Gravity and Rossby)

Matsuno's theory for free equatorial waves

There are eastward and westward moving Inertia-Gravity waves. Rossby waves move westwards

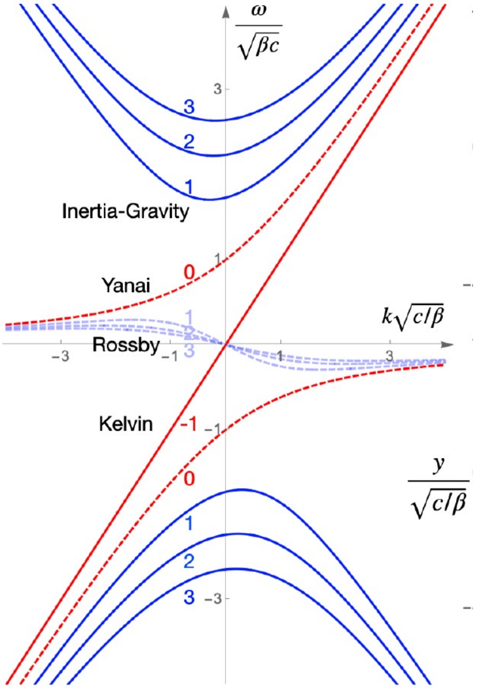

Inertia-Gravity waves:

- When n>0, there are three solutions to the dispersion relation equation. The two high frequency solutions are denoted Inertia-Gravity waves.
- If the term $\beta c^2 k/\omega$ is small in the dispersion relation then

$$\omega = \pm\sqrt{c^2k^2 + \beta c(2n+1)}.$$

is the approximate frequency of inertia-gravity waves

Rossby waves:

- The remaining low frequency solution is close to geostrophic balance. Neglecting the term ω^2 in the dispersion relation,

$$\omega = \frac{-\beta k}{k^2 + (2n+1)\beta/c}$$

is the approximate frequency of Rossby waves

Dispersion relation:

$$\omega^2 - k^2c^2 - \frac{\beta c^2 k}{\omega} = (2n+1)\,\beta c,$$

Phase velocity:

$$c_p = \frac{\omega}{k}$$

Group velocity:

$$c_g = \frac{\partial \omega}{\partial k}$$

Matsuno's theory for free equatorial waves

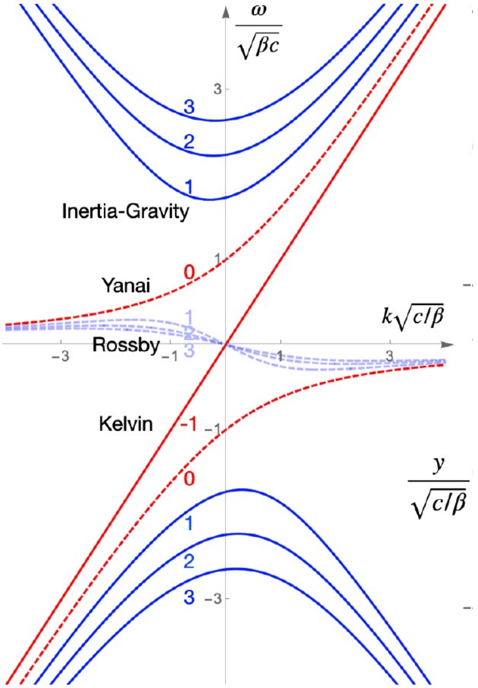

Inertia-Gravity waves:

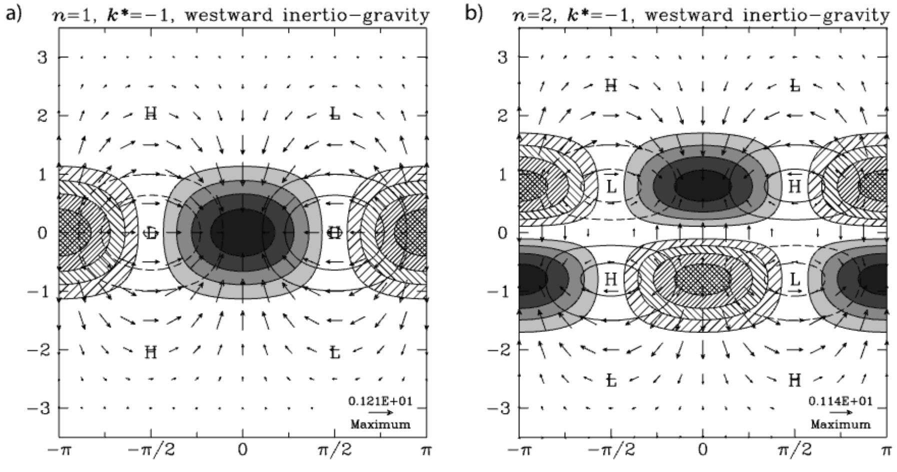

Rossby waves:

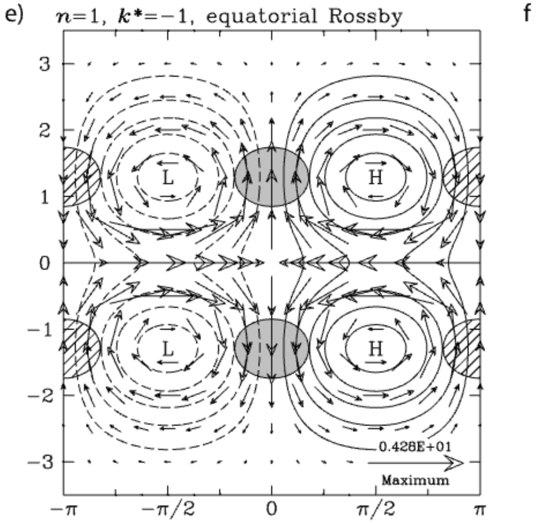

Even n yields a v structure that is symmetric across the equator, and odd yields antisymmetric v structure

$$i\left(\omega - ck\right)\left(\hat{u} + \hat{\eta}\right) = -\varphi_{n+1},$$

$$i\left(\omega + ck\right)\left(\hat{u} - \hat{\eta}\right) = -2n\varphi_{n-1}$$

Matsuno's theory for free equatorial waves

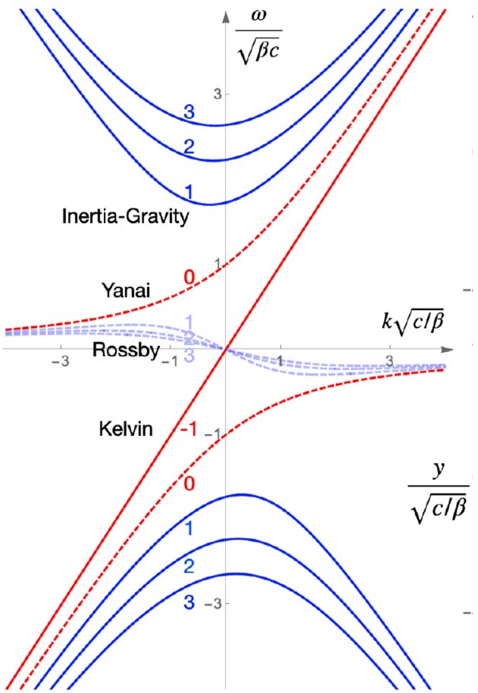

Yanai Waves:

- Yanai waves correspond to solutions to the dispersion equation when n=0:

$$\omega = \frac{kc}{2} \pm \frac{1}{2}\sqrt{k^2c^2 + 4\beta c}.$$

- The positive frequency solution corresponds to a single branch that transits from the low frequency Rossby wave band to the high frequency inertia-gravity wave band as k is increased from negative to positive values. For this reason, this solution is often called a mixed Rossby-gravity wave mode.
- The phase velocity is positive if $k > 0$ and negative if $k < 0$, but the group velocity is always positive.
- Those modes are commonly called Yanai waves, in honor of M. Yanai who discovered them in observations.

Yanai waves behave as Rossby waves as $\mathrm{k} \to -\infty$ and as a Inertia-Gravity wave as $\mathrm{k} \to \infty$

Matsuno's theory for free equatorial waves

For Yanai waves v is symmetric across the equator

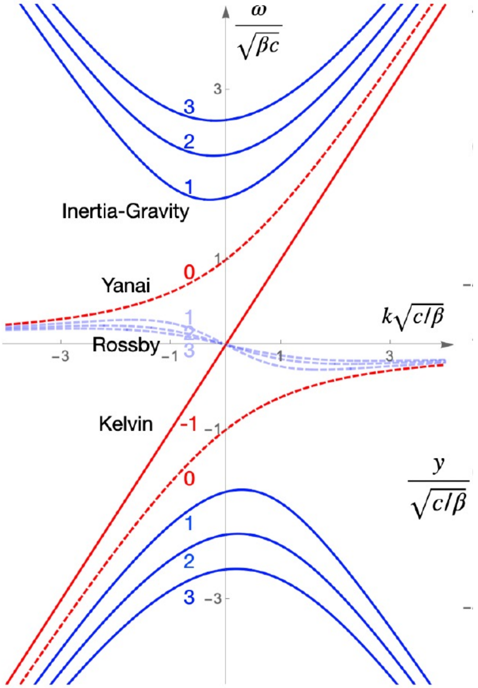

Yanai Waves horizonal structure:

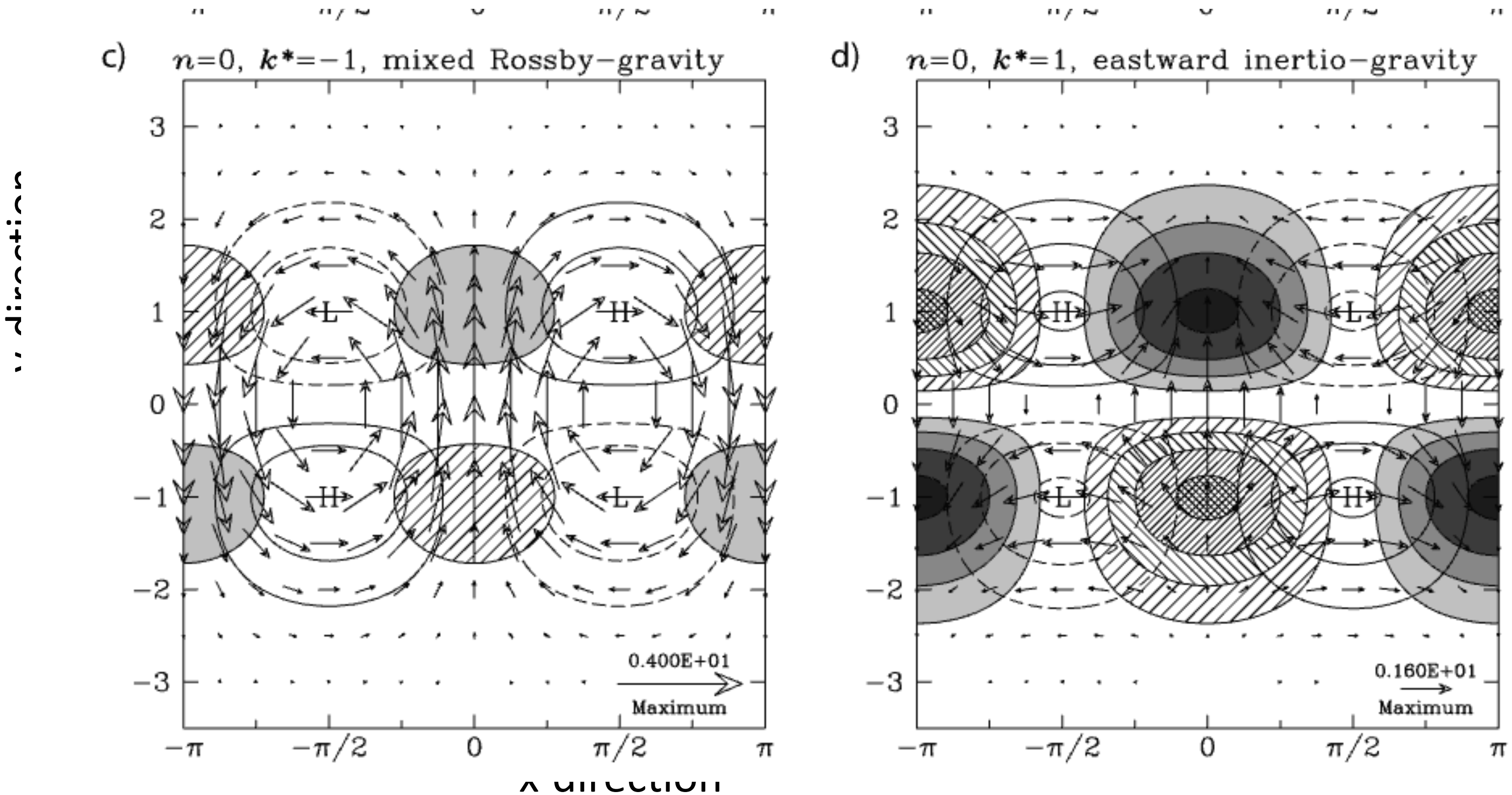

Matsuno's theory for free equatorial waves

Kelvin waves have zero meridional wind component and are non-dispersive

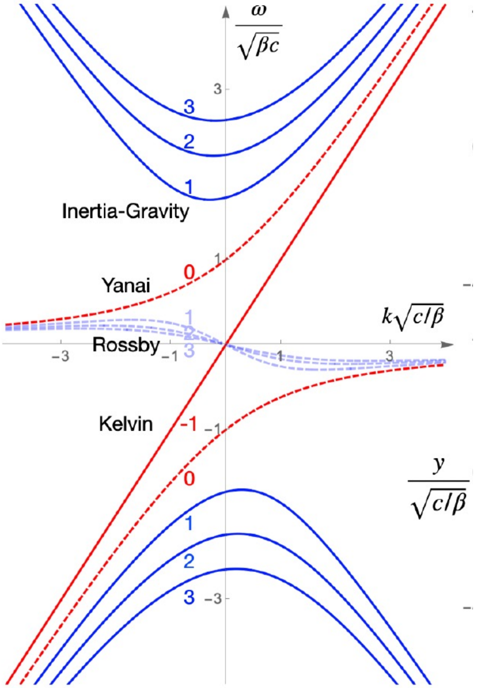

Kelvin Waves:

- Are solutions of the shallow water system when $v = 0$
- A vanishing meridional velocity implies geostrophic balance in the meridional direction :

$$\beta y \hat{u} = -c\partial_y \hat{\eta}$$

- The eastward non-dispersive propagating mode $\omega = ck$ is the only admissible solution. The westward mode does not vanish as $\mathrm{y} \rightarrow \infty$ (i.e. rotation plays an important role by selecting the eastward propagating mode)
- Because this solution is a root for the dispersion relationship when n=-1, this mode is often labeled by the index n=-1

Matsuno's theory for free equatorial waves

Kelvin Waves horizonal structure:

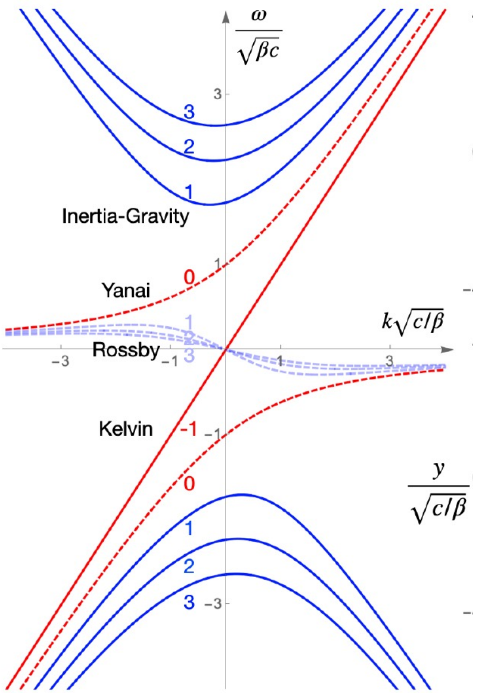

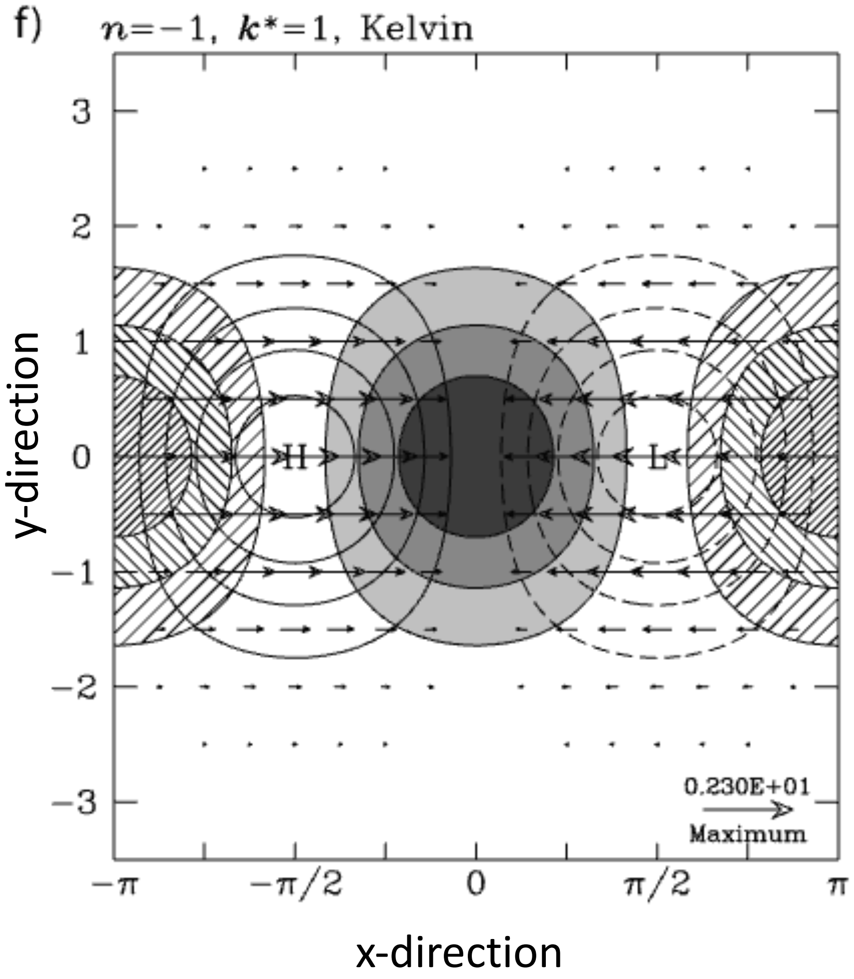

Kelvin waves zonal wind and height are symmetric with respect to the equator

$$(\hat{u}, \hat{v}, \hat{\eta}) = (1,\ 0,\ 1)e^{-\frac{y^2}{2c/\beta}}.$$

Kelvin waves are non-dispersive:

$c_p = c_g > 0$

P. L. Silva Dias
and T. Matsuno,
1986 (?) at
ICTP?

How to relate Matsuno's theory to an actual tropical atmosphere?

Linearized hydrostatic Boussinesq equations can be used to physically interpret Matsuno's SW solutions

The shallow water model introduced in the previous slides is the simplest setting to discuss equatorial waves, but it is not obvious to relate this model to an actual atmosphere. For instance, what would be the fluid depth (H) in this framework?

Linearized hydrostatic Boussinesq flow model

$$\partial_t u' = -\partial_x \phi + f v',$$
$$\partial_t v' = -\partial_y \phi' - f u',$$
$$0 = -\partial_z \phi' + b',$$
$$0 = \partial_x u' + \partial_y v' + \partial_z w',$$
$$\partial_t b' = -w' N^2.$$

We have introduced the buoyancy perturbation b', the geopotential ϕ' that can be interpreted as a perturbation to hydrostatic pressure, and and the buoyancy frequency $N^2 \equiv \partial_z \overline{b}$ with $\overline{b}(z)$ the buoyancy profile of the base state.

How to relate Matsuno's theory to an actual tropical atmosphere?

Linearized hydrostatic Boussinesq flow model

$$\partial_t u' = -\partial_x \phi + f v',$$
$$\partial_t v' = -\partial_y \phi' - f u',$$
$$0 = -\partial_z \phi' + b',$$
$$0 = \partial_x u' + \partial_y v' + \partial_z w',$$
$$\partial_t b' = -w' N^2.$$

$$\partial_t u_m' + \partial_x \phi_m - \beta y v'^{m} = 0$$
$$\partial_t v_m' + \partial_y \phi_m + \beta y u_m' = 0$$
$$\partial_t \phi_m' + c_m{}^2(\partial_x u_m + \partial_y v_m) = 0$$

$$\left(\frac{u'}{c_m}, \frac{v'}{c_m}, \frac{\phi'}{c_m^2}\right) = (u_m', v_m', \phi_m')e^{imz}, \quad c_m \equiv \frac{N}{|m|}.$$

How to relate Matsuno's theory to an actual tropical atmosphere?

Linearized hydrostatic Boussinesq flow model

$$\partial_t u' = -\partial_x \phi + f v',$$
$$\partial_t v' = -\partial_y \phi' - f u',$$
$$0 = -\partial_z \phi' + b',$$
$$0 = \partial_x u' + \partial_y v' + \partial_z w',$$
$$\partial_t b' = -w' N^2.$$

$$\partial_t u_m{}' + \partial_x \phi_m - \beta y v'_m = 0$$
$$\partial_t v_m{}' + \partial_y \phi_m + \beta y u_m{}' = 0$$
$$\partial_t \phi_m{}' + c_m{}^2 (\partial_x u_m + \partial_y v_m) = 0$$

$$\left(\frac{u'}{c_m}, \frac{v'}{c_m}, \frac{\phi'}{c_m^2}\right) = (u'_m, v'_m, \phi'_m) e^{imz}, \quad c_m \equiv \frac{N}{|m|}.$$

Dispersion relation:
$$\omega^2 - k^2 c^2 - \frac{\beta c^2 k}{\omega} = (2n+1)\,\beta c,$$

EW vertical propagation properties!

How to relate Matsuno's theory to an actual tropical atmosphere?

The concept of the equivalent height: The horizontal phase speed **c_m** of nonrotating hydrostatic Boussinesq waves with vertical wavenumber **m** can be interpreted in terms of an equivalent depth. This would be the depth of a shallow water model supporting similar horizontally propagating waves :

$$h_{eq} \equiv \frac{1}{g}\frac{N^2}{m^2}, \quad c_m = \sqrt{gh_{eq}}.$$

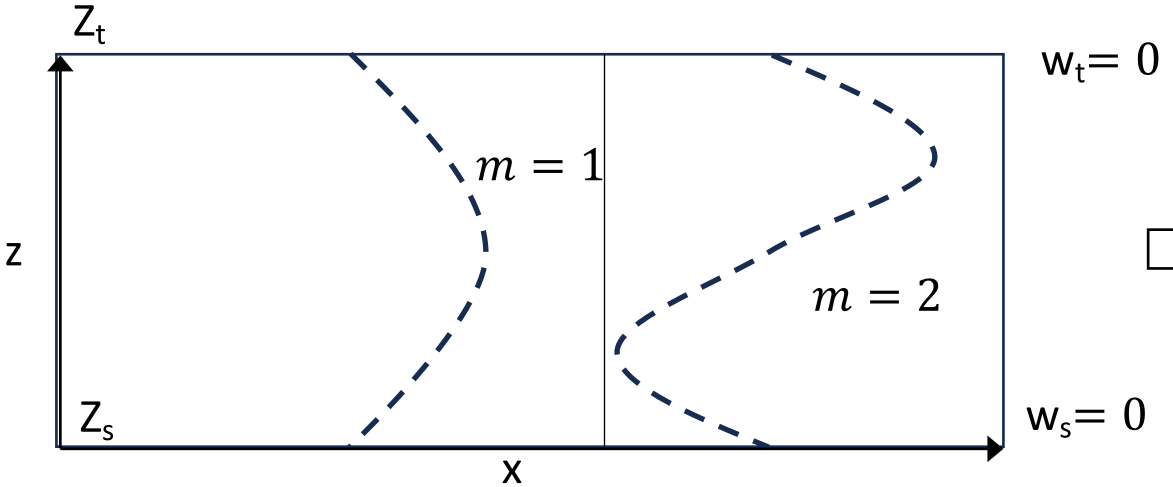

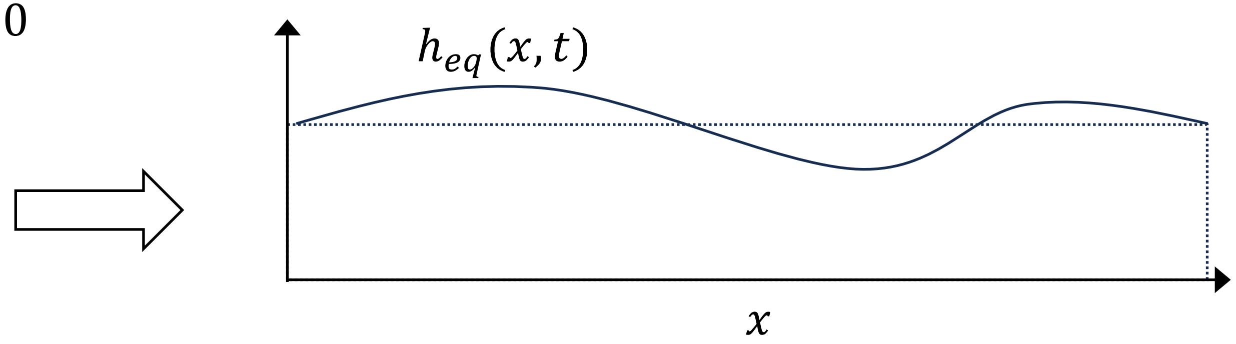

Matsuno-Gill solutions

$$\cancel{\frac{\partial}{\partial_t}\begin{pmatrix} u' \\ v' \\ \eta' \end{pmatrix}} = \mathcal{L}\begin{pmatrix} u' \\ v' \\ \eta' \end{pmatrix} + \begin{pmatrix} 0 \\ 0 \\ Q \end{pmatrix} - \alpha \begin{pmatrix} u' \\ v' \\ \eta' \end{pmatrix},$$

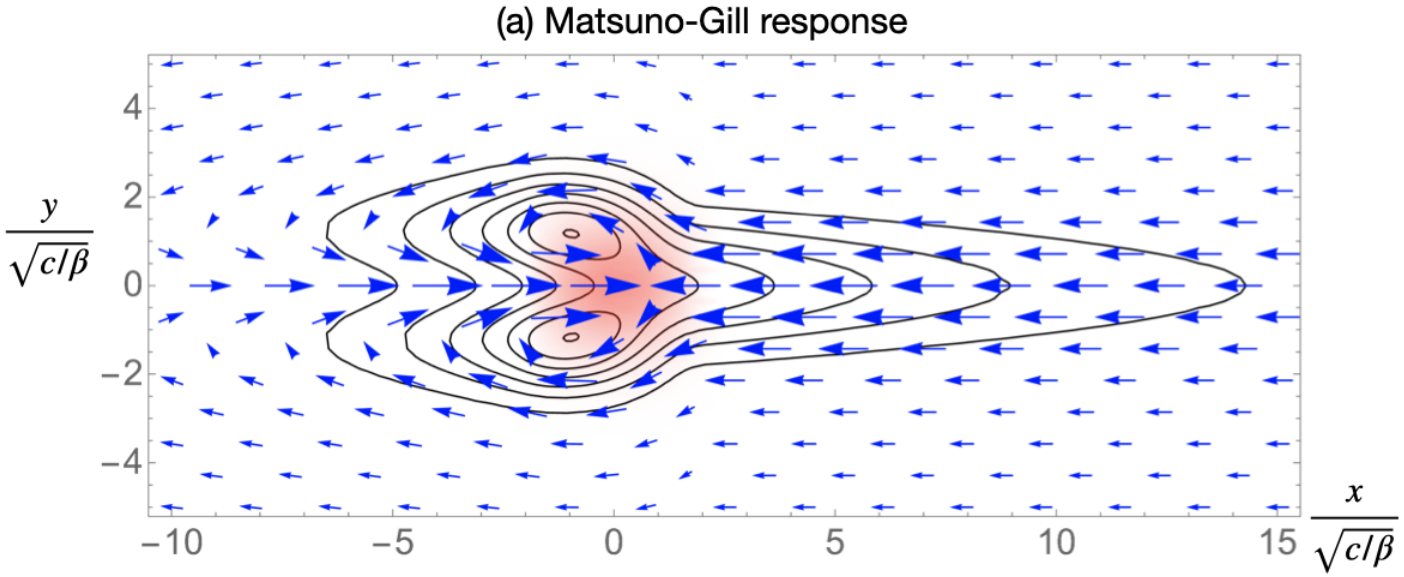

Figure 13.3. *a) Stationary response of linear shallow water model with frictional dissipation α and a localized mass loss term interpreted as a heat source (in red). Parameters are those used in (Vallis 2017). The contour lines represent the height*

What about convectively coupled equatorial waves?

The combination of weak rotation, stronger insolation and moisture availability in the tropics leads to two-way feedbacks between tropospheric equatorial waves and moist convection, which gives rise to what is known as convectively coupled equatorial waves.

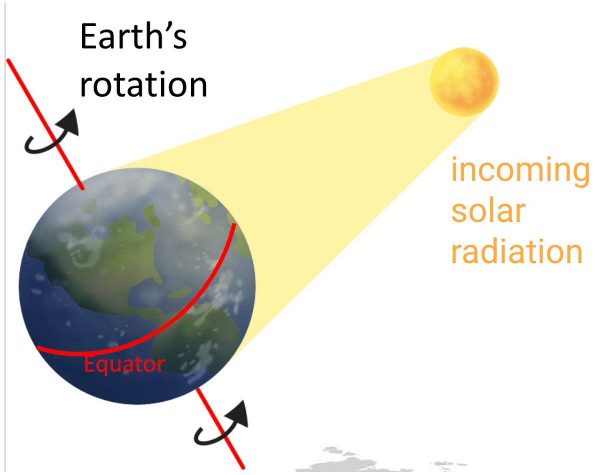

Free Equatorial Waves

$$\partial_t u' + \partial_x \phi \text{-} \beta y v' = 0$$

$$\partial_t v' + \partial_y \phi + \beta y u' = 0$$

$$\partial_t \phi' + \ c^2(\partial_x u + \partial_y v) = 0$$

Diabatic heating from moist convection might play a role in the initiation phase of the wave, but its maintenance is uncoupled from moist convection.

Convectively coupled equatorial waves

$$\partial_t u' + \partial_x \phi \text{-} \beta y v' = 0$$

$$\partial_t v' + \partial_y \phi + \beta y u' = 0$$

$$\partial_t \phi' + \ c^2(\partial_x u + \partial_y v) = Q1$$

$$D_t q' = -Q2$$

Moist convection and circulation co-evolve and interact

What about convectively coupled equatorial waves?

One primary observed impact of moisture on equatorial waves is to reduce their frequency inferred from Matsuno's theory. In turn, the lengthening of their time scale allows clouds and precipitation to organize into large-scale coherent structures that are consistent with the divergence fields of equatorial waves.

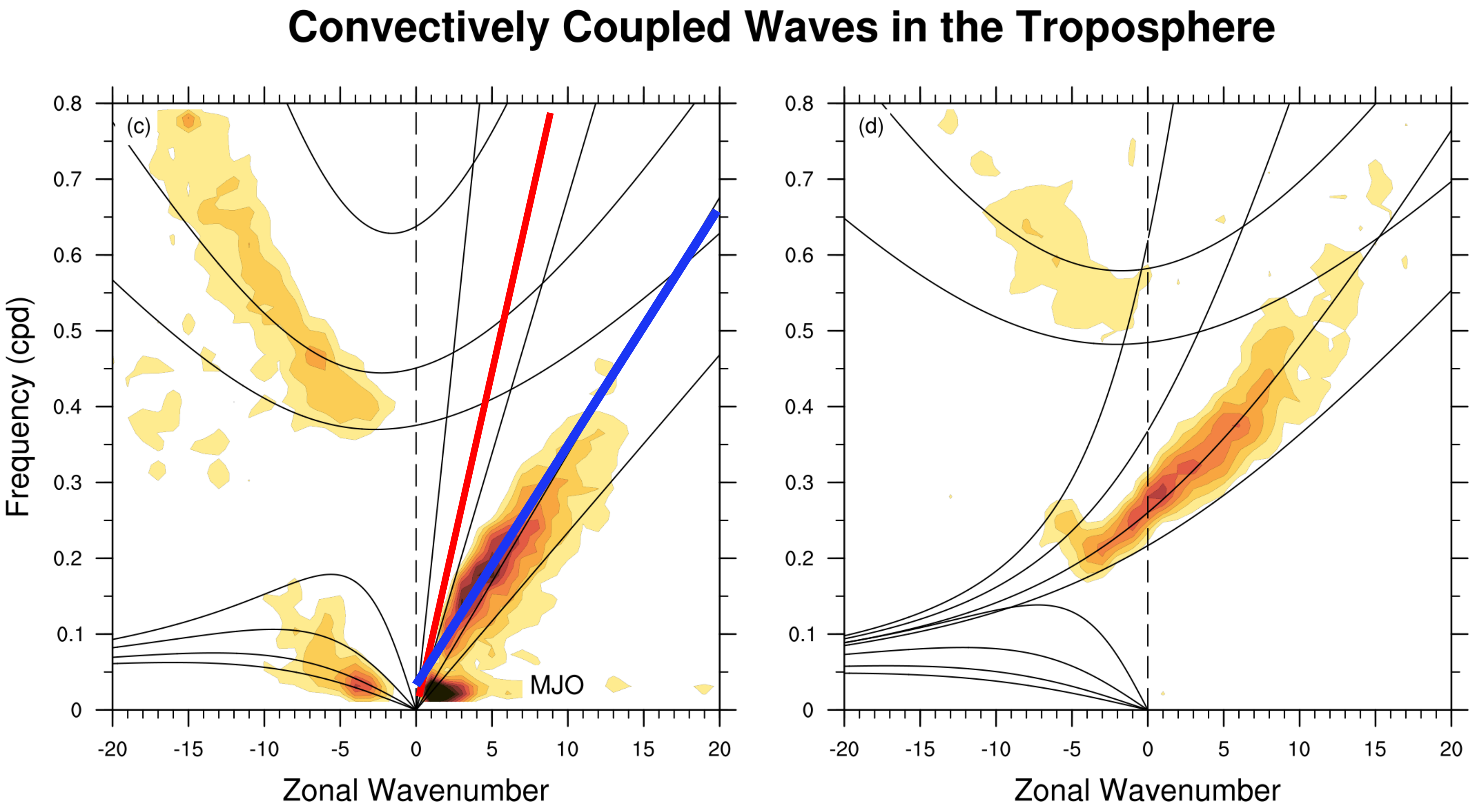

$h_{eq} \sim 250\text{m}$

$c_m = 50ms^{-1}$

$H = 15 \text{ km}$

$N = 10^{-2}\,\text{s}^{-1}$

$h_{eq} \sim 25\text{m}$

$c_m = 15ms^{-1}$

What about convectively coupled equatorial waves?

One primary observed impact of moisture on equatorial waves is to reduce their frequency inferred from Matsuno's theory. In turn, the lengthening of their time scale allows clouds and precipitation to organize into large-scale coherent structures that are consistent with the divergence fields of equatorial waves.

There are two main theories to explain how moisture is linked to the slowdown of convectively coupled equatorial waves in comparison to their dry counterparts:

Destabilization due to deep moist convection

The presence of moisture can destabilize a density profile that would be otherwise be stable in a dry atmosphere. (Emanuel *et al*. 1994).

$$N_{eff} = (1 - \alpha)N$$

The vertical wavenumber **m** is unchanged

$$\partial_t u_m' + \partial_x \phi_m - \beta y v'_m = 0$$

$$\partial_t v_m' + \partial_y \phi_m + \beta y u_m' = 0$$

$$\partial_t \phi_m' + c_m^2(\partial_x u_m + \partial_y v_m) = 0$$

$$h_{eq} \equiv \frac{1}{g}\frac{N_{eff}^2}{m^2}, \quad c_m = \sqrt{g h_{eq}}.$$

w~sin(mz)

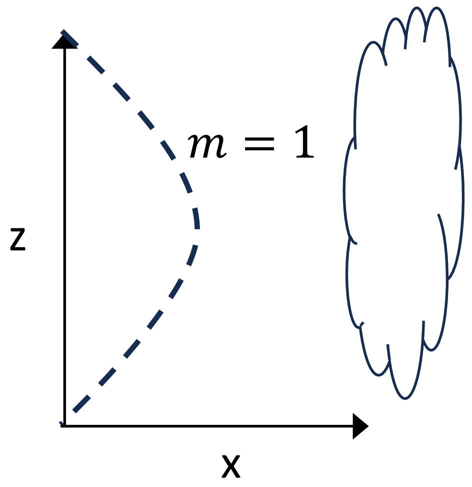

What about convectively coupled equatorial waves?

One primary observed impact of moisture on equatorial waves is to reduce their frequency inferred from Matsuno's theory. In turn, the lengthening of their time scale allows clouds and precipitation to organize into large-scale coherent structures that are consistent with the divergence fields of equatorial waves.

There are two main theories to explain how moisture is linked to the slowdown of convectively coupled equatorial waves in comparison to their dry counterparts:

Destabilization due to deep moist convection

The presence of moisture can destabilize a density profile that would be otherwise be stable in a dry atmosphere. (Emanuel *et al*. 1994).

$$N_{eff} = (1 - \alpha)N$$

The vertical wavenumber **m** is unchanged

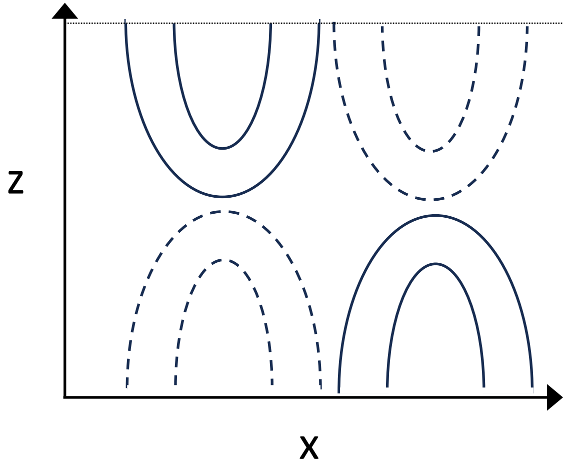

$u \sim \sin(mz)$

$m = 1$

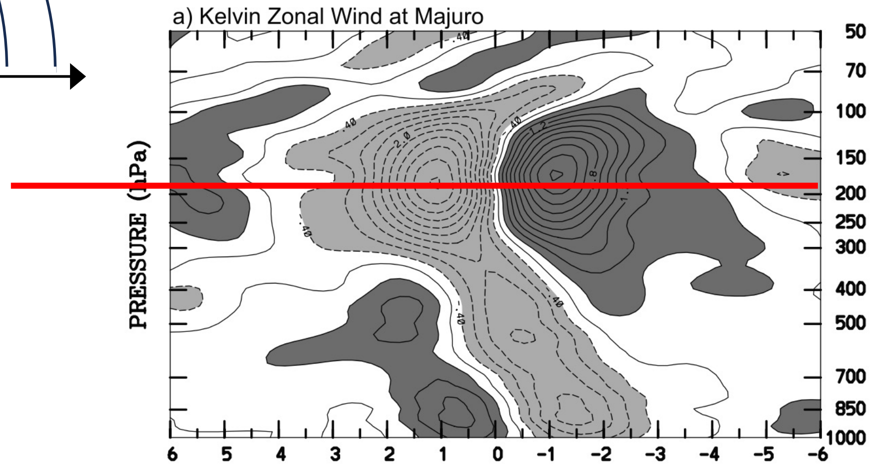

What about convectively coupled equatorial waves?

One primary observed impact of moisture on equatorial waves is to reduce their frequency inferred from Matsuno's theory. In turn, the lengthening of their time scale allows clouds and precipitation to organize into large-scale coherent structures that are consistent with the divergence fields of equatorial waves.

There are two main theories to explain how moisture is linked to the slowdown of convectively coupled equatorial waves in comparison to their dry counterparts:

Stratiform Instability

The equivalent height is set by latent heat release within the lower half of the troposphere (cumulus congestus clouds), which tends to precede the development of deep clouds, favoring a higher order vertical wavenumber m than would be expected from latent heating associated with deep convection.

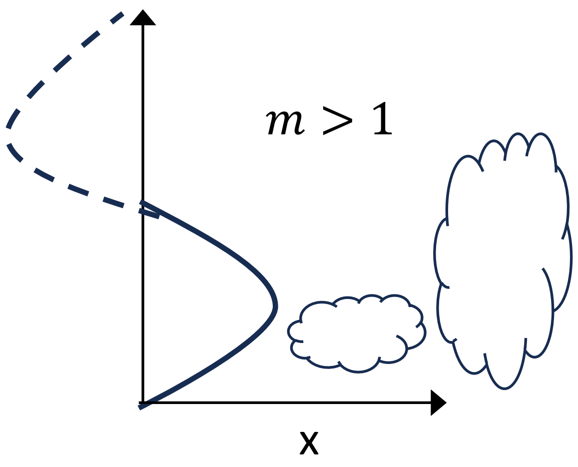

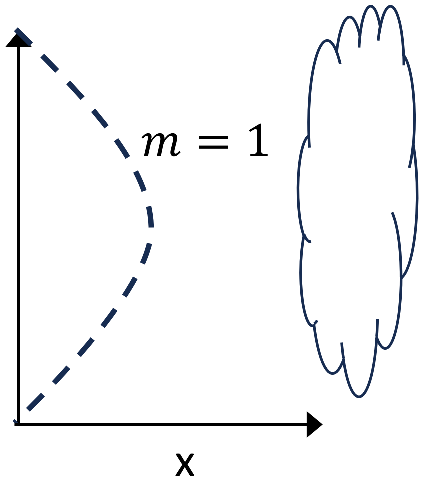

Mapes 2000, Majda and Shefter 2001, Johnson et. al 1999

What about convectively coupled equatorial waves?

One primary observed impact of moisture on equatorial waves is to reduce their frequency inferred from Matsuno's theory. In turn, the lengthening of their time scale allows clouds and precipitation to organize into large-scale coherent structures that are consistent with the divergence fields of equatorial waves.

There are two main theories to explain how moisture is linked to the slowdown of convectively coupled equatorial waves in comparison to their dry counterparts:

Stratiform Instability

The equivalent height is set by latent heat release within the lower half of the troposphere (cumulus congestus clouds), which tends to precede the development of deep clouds, favoring a higher order vertical wavenumber **m** than would be expected from latent heating associated with deep convection.

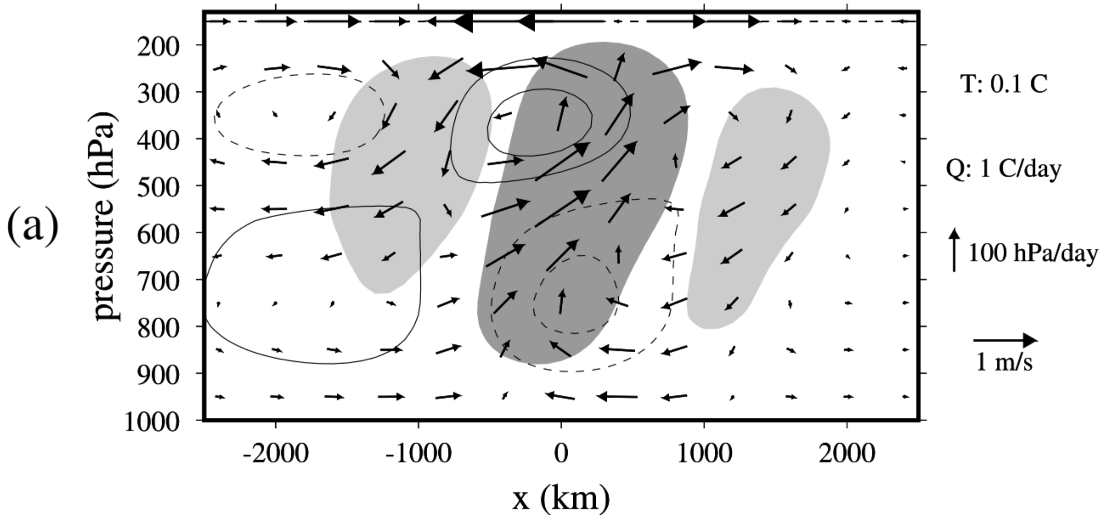

Superposition of m=1 and m=2 vertical modes from an idealized model (Kiladis 2009)

Mapes 2000, Majda and Shefter 2001, Johnson et. al 1999

Break!

MJO Theory (ies)?

- 40-50 day tropical oscillation seen in zonal winds, specific humidity, temperature, pressure and precipitation
- The convective active phase moves eastward from the Indian Ocean the Central Pacific

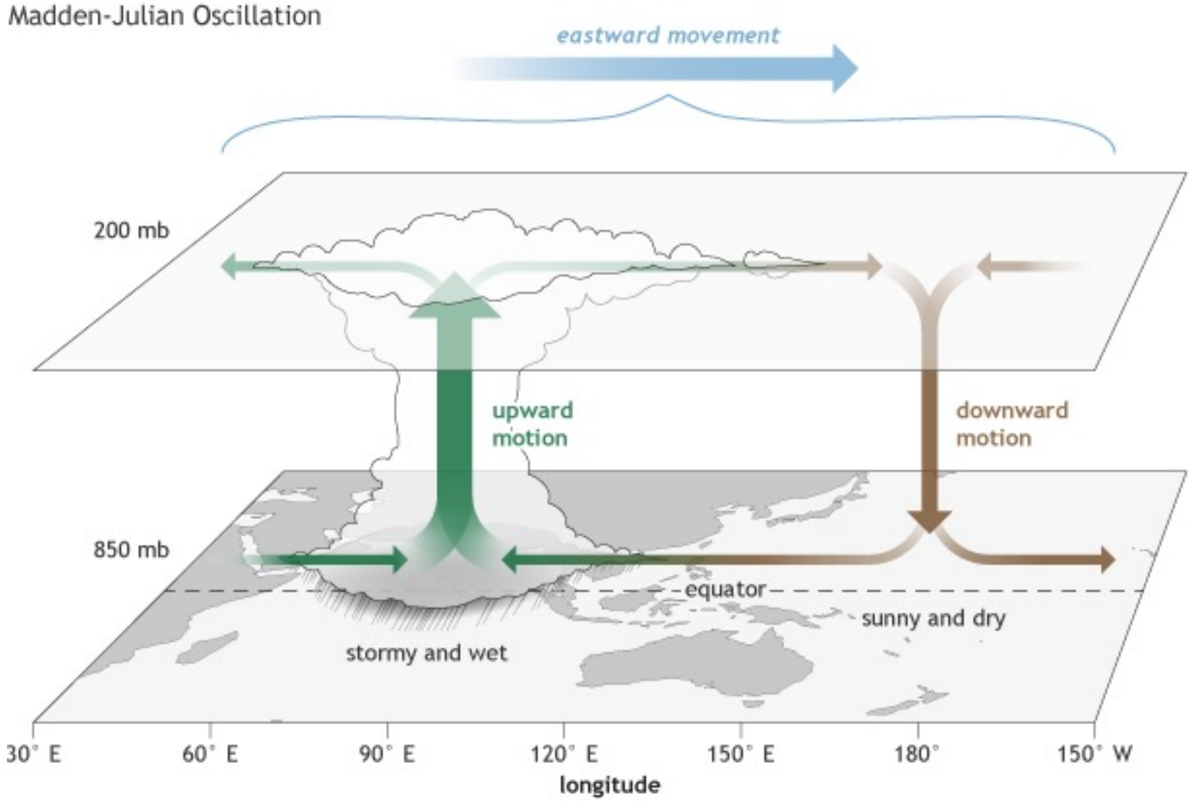

MJO Theory (ies)?

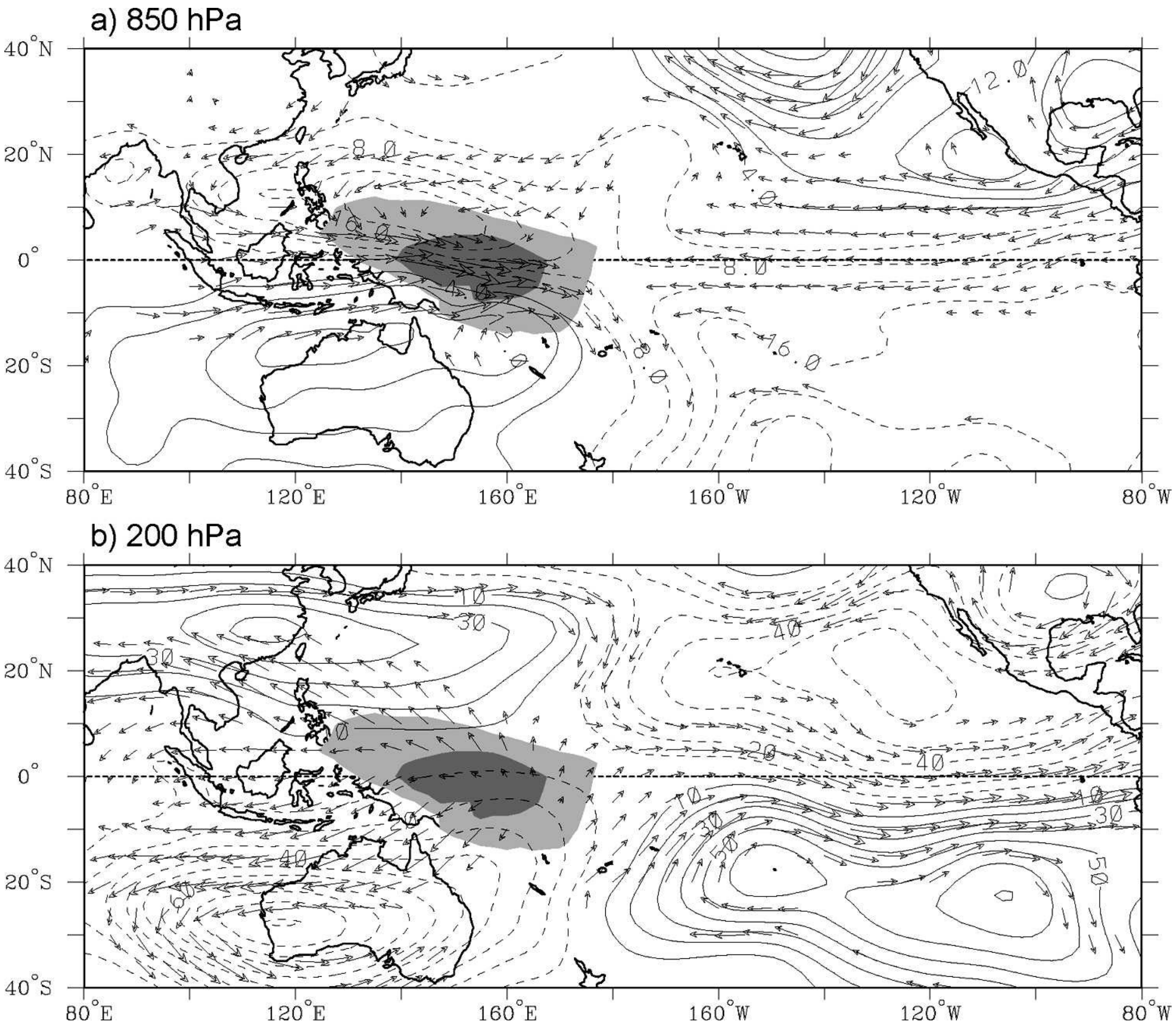

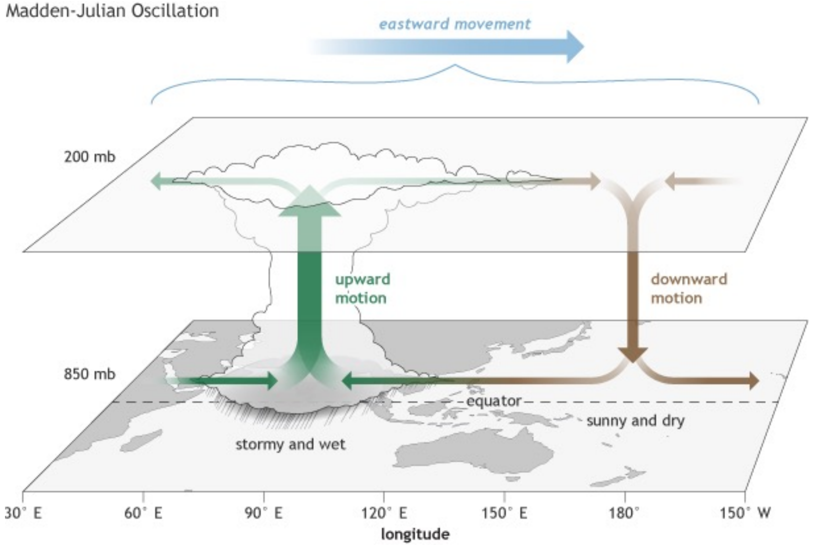

FIG. 2. Anomalous OLR and circulation from ERA-15 reanalysis on day 0 associated with a −40 W m^{-2} perturbation in MJO-filtered OLR at the equator, 155°E for the period 1979–93, all seasons included; (a) 850 and (b) 200 hPa. Dark (light) shading denotes OLR anomalies less than −32 W m^{-2} (−16 W m^{-2}). Streamfunction contour interval is (a) 4 3 10^5 m^2 s^{-1} and (b) 10 3 10^5 m^2 s^{-1}. Locally statistically significant wind vectors at the 95% level are shown. The largest vectors are about 2 m s^{-1} in (a) and around 5 m s^{-1} in (b).

from [Kiladis et al 2006]

MJO Theory (ies)?

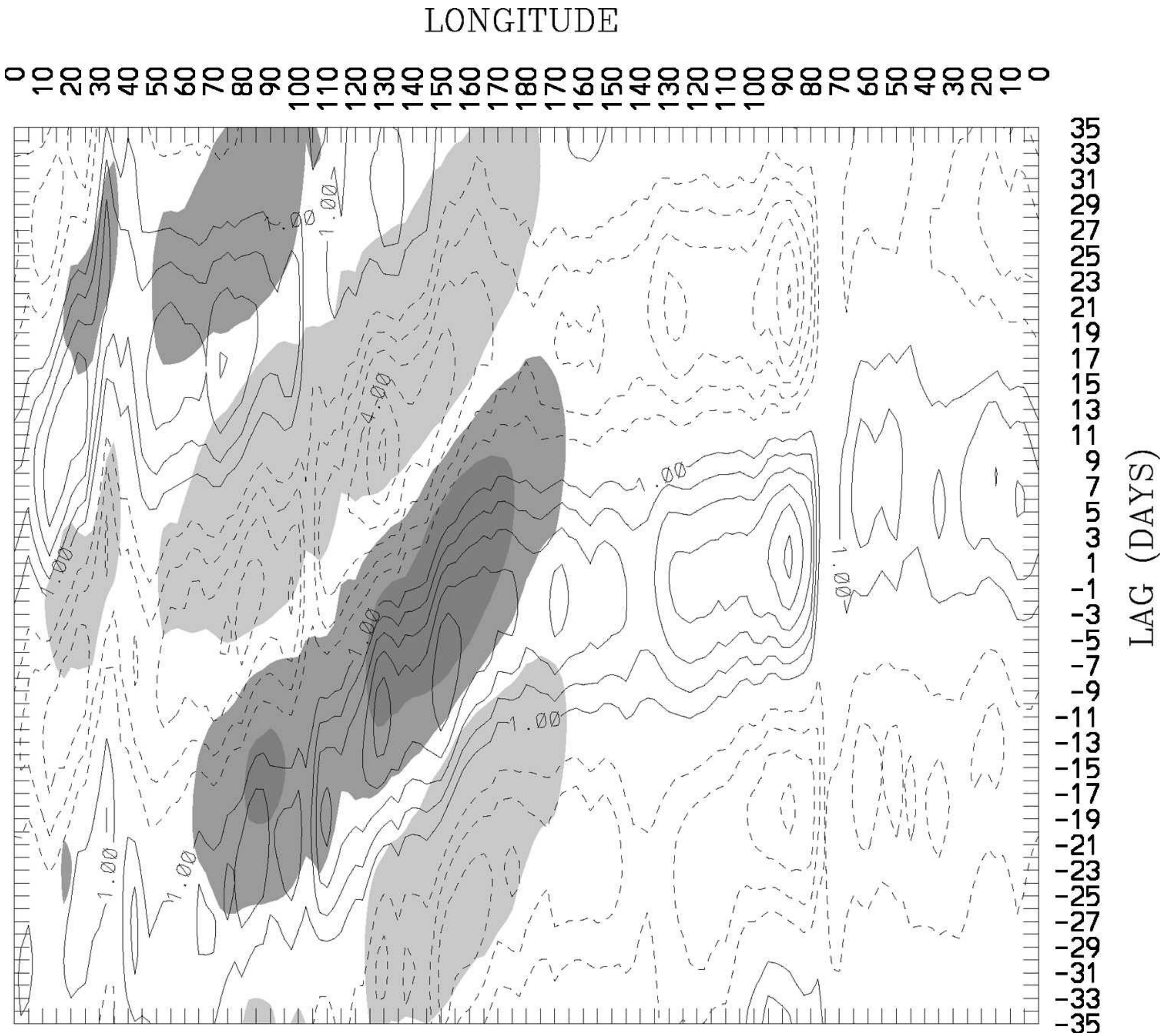

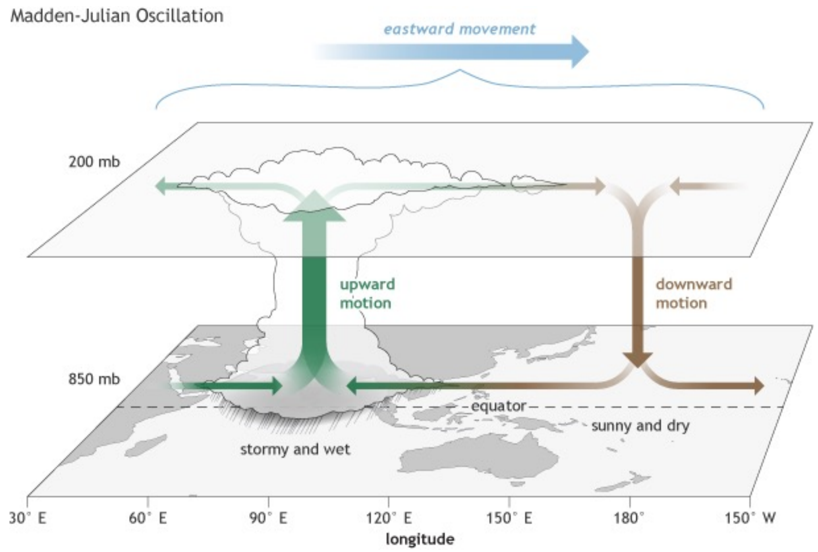

FIG. 11. Time–longitude diagram of anomalous 850-hPa specific humidity (contours, interval is 1 X 10^{-1} g kg^{-1}, negative dashed) and OLR [shading, dark (darkest) shading denotes OLR anomalies less than −16 W m^{-2} (-18 W m^{-2}), and light shading anomalies greater than +16 W m^{-2}] from day -35 through day +35 averaged from 10°S to 10°N, associated with a −40W m^{-2} perturbation in MJO-filtered OLR at the 0°, 155°E on day 0.

from [Kiladis et al 2006]

Why is the MJO important?

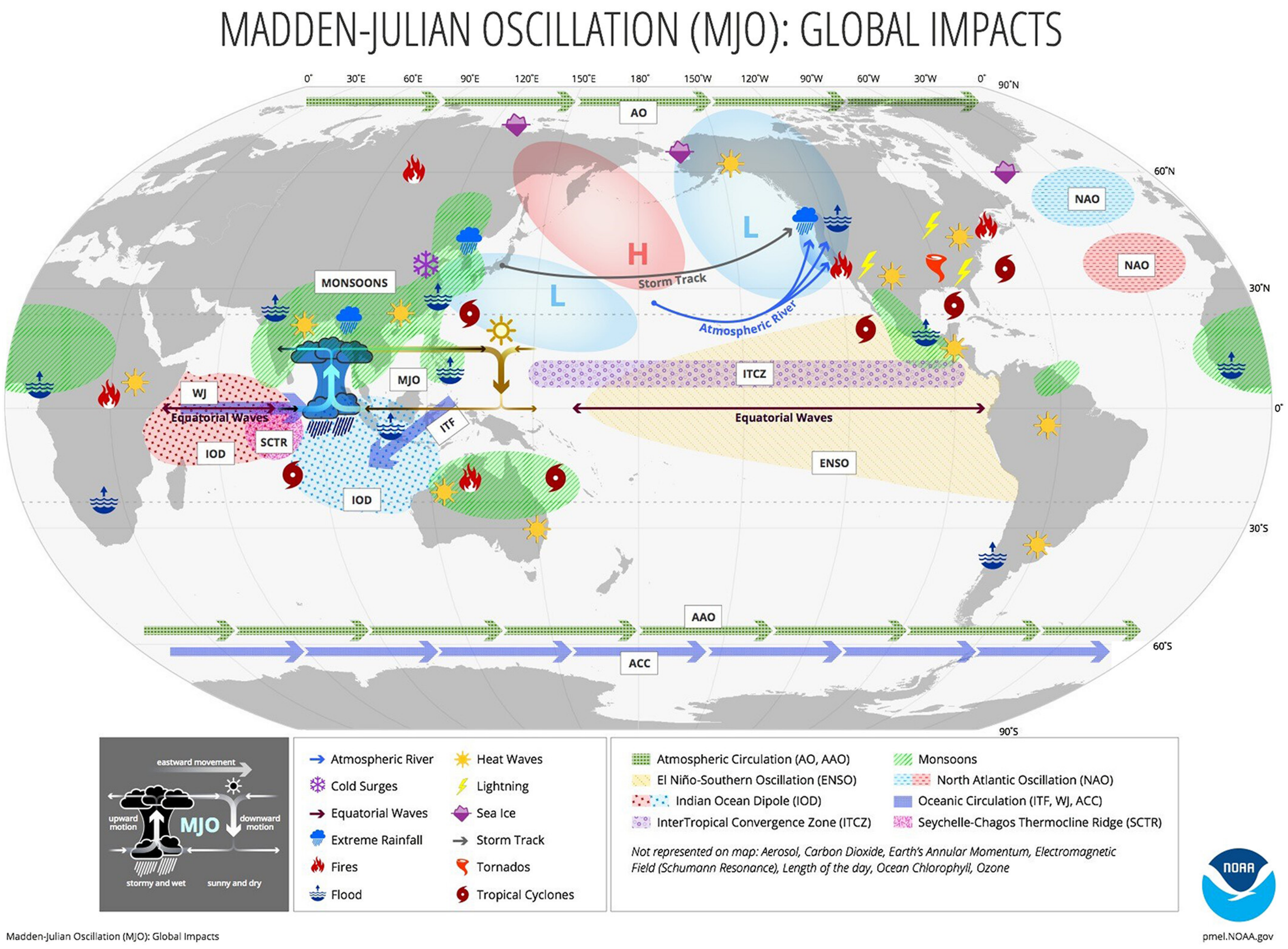

[Yoneyama, K. & Zhang, C. (2020)]

MJO propagation in CMIP3 (Lin 2005)

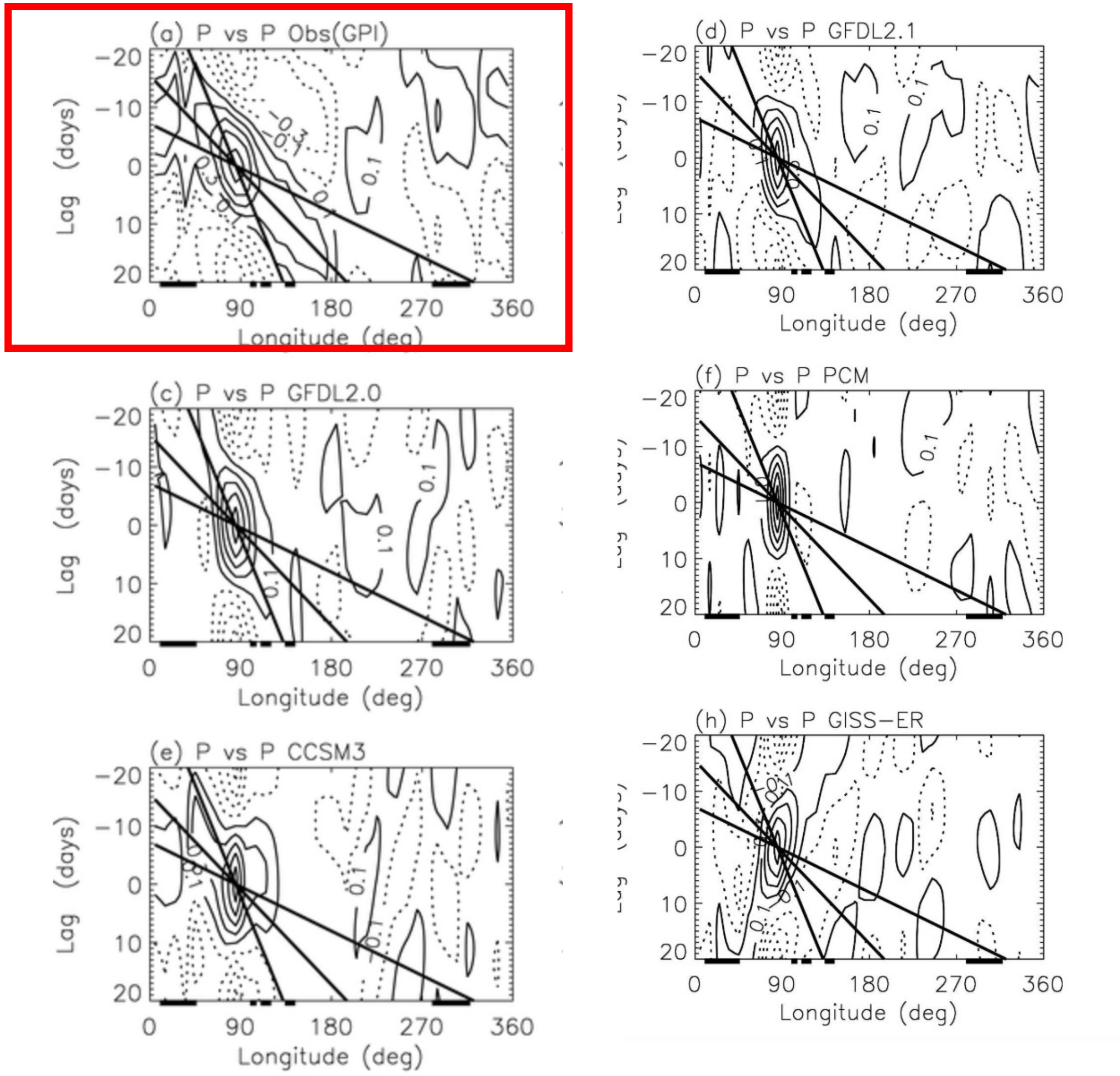

MJO propagation in CMIP3 ([Lin 2005](#))

MJO propagation in CMIP5/6 ([Chen et al. 2021](#))

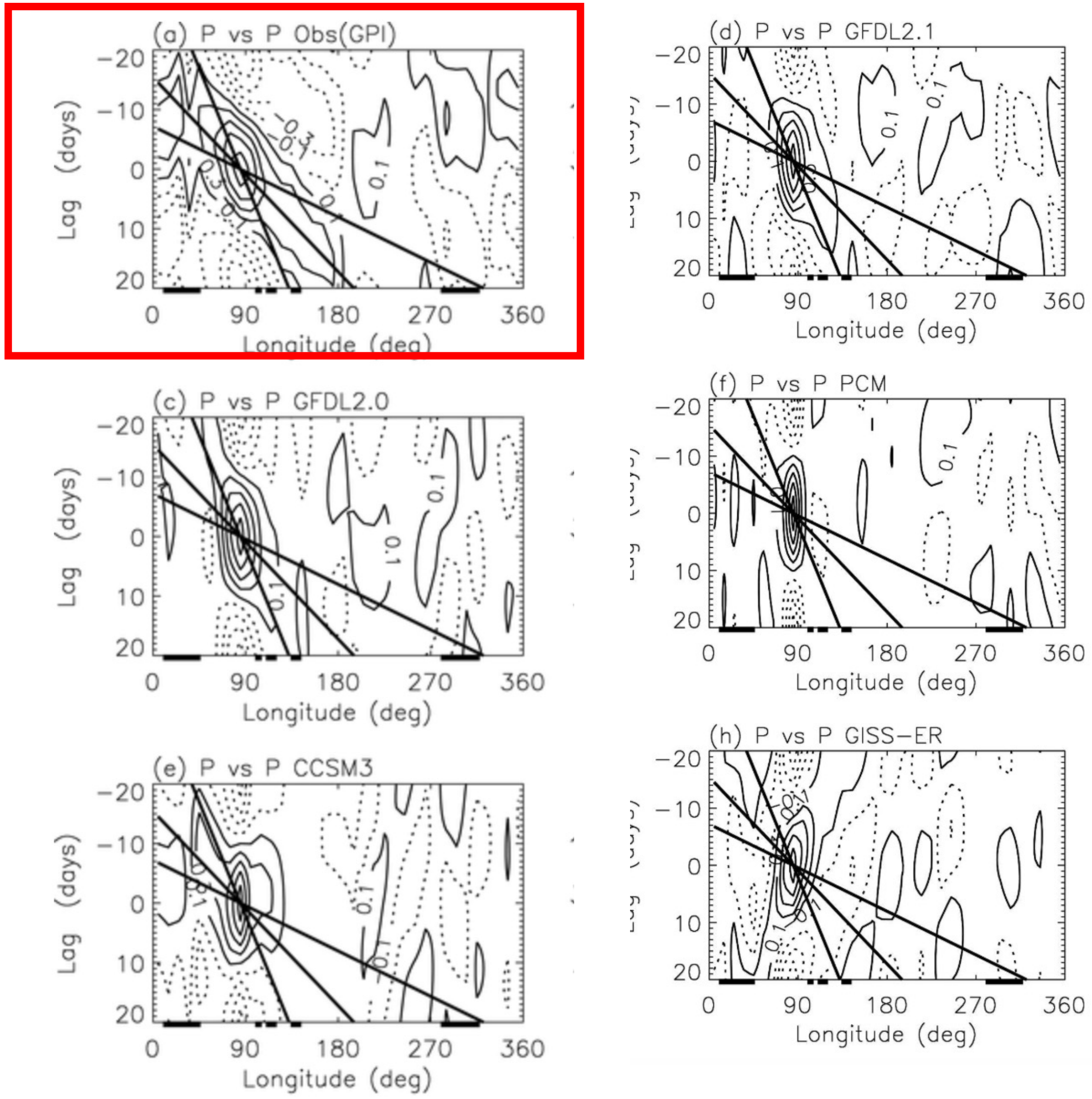

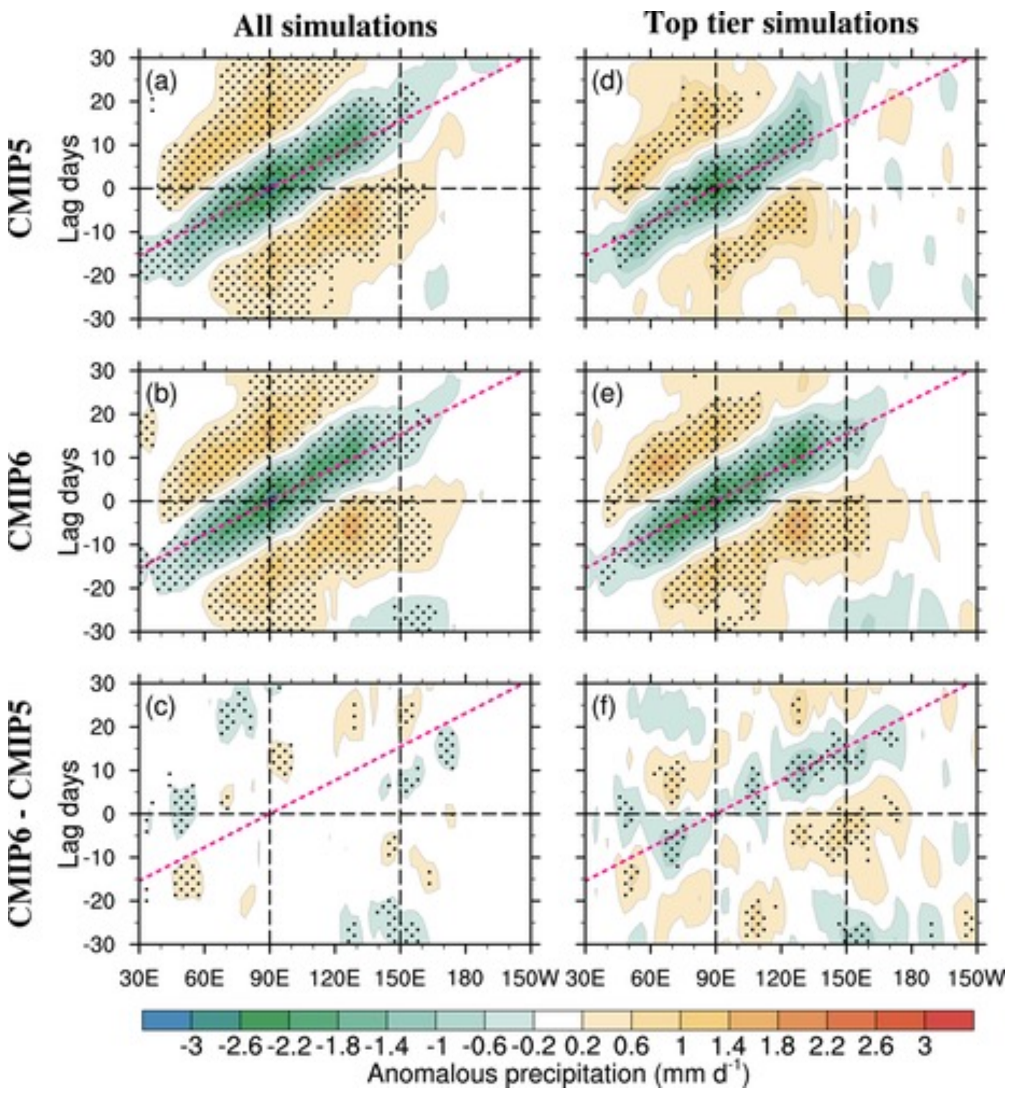

MJO amplitude in CMIP5/6

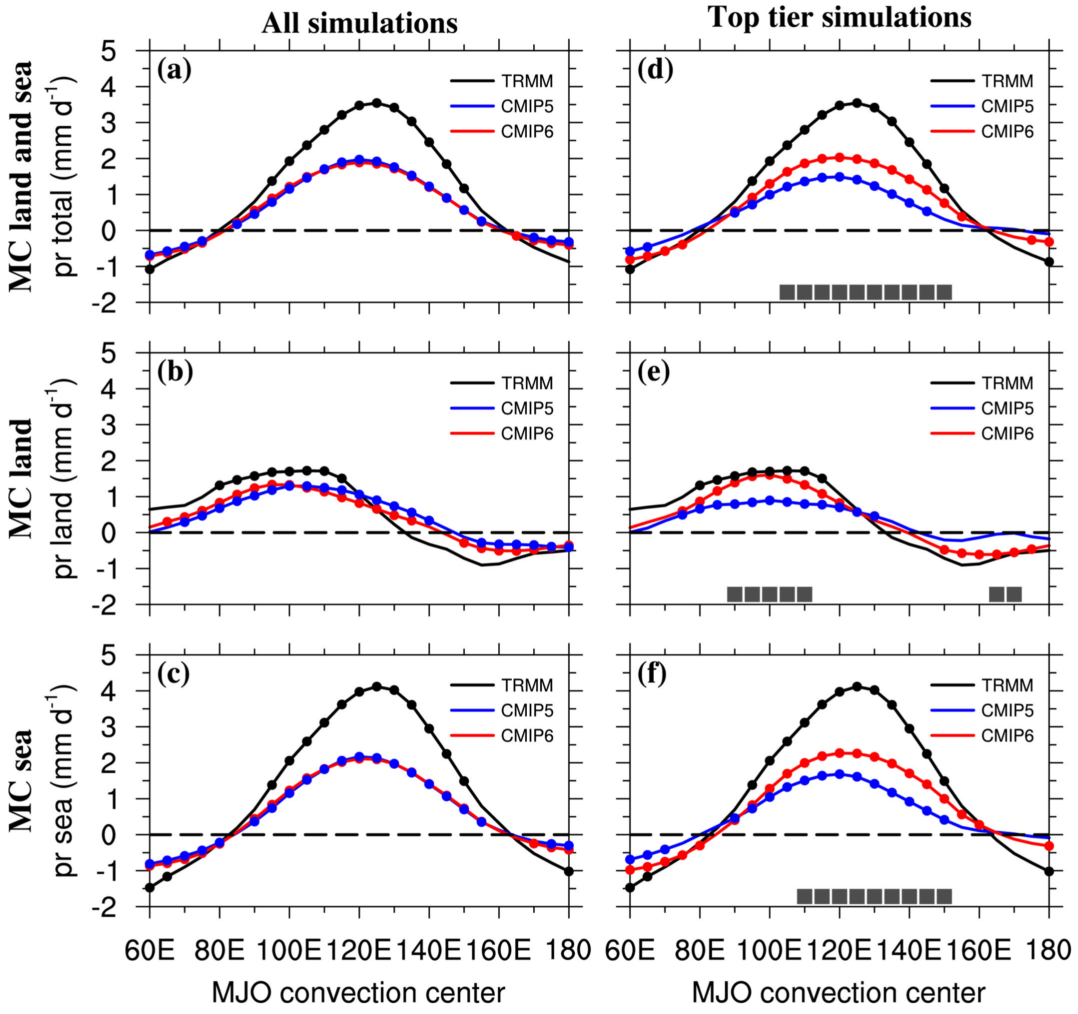

From Chen et al. 2021

MJO combined skill in CMIP5/6 --- “Spider Diagram”

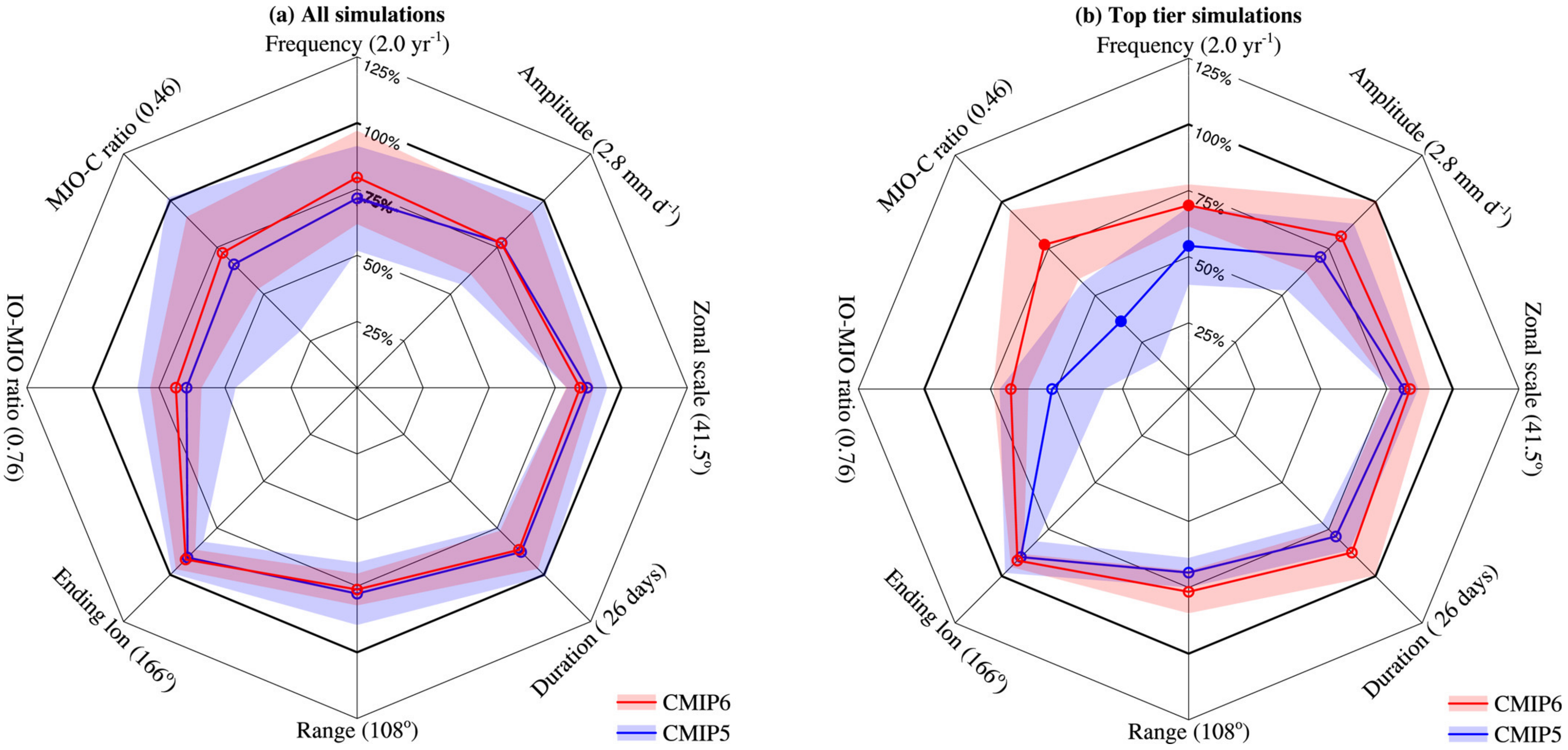

From Chen et al. 2021

MJO Theory (ies)?

A commonly agreed theory for the Madden Julian Oscillation still does not exist

Four Theories of the Madden-Julian Oscillation

C. Zhang[1], Á. F. Adames[2], B. Khouider[3], B. Wang[4], and D. Yang[5,6]

[1]NOAA Pacific Marine Environmental Laboratory, Seattle, WA, USA, [2]Department of Climate and Space Sciences and Engineering, University of Michigan, Ann Arbor, MI, USA, [3]Department of Mathematics and Statistics, University of Victoria, Victoria, British Columbia, Canada, [4]Department of Atmospheric Sciences, University of Hawaii, Honolulu, HI, USA, [5]Department of Land, Air and Water Resources, University of California, Davis, CA, USA, [6]Lawrence Berkeley National Laboratory, Berkeley, CA, USA

Abstract Studies of the Madden-Julian Oscillation (MJO) have progressed considerably during the past decades in observations, numerical modeling, and theoretical understanding. Many theoretical attempts have been made to identify the most essential processes responsible for the existence of the MJO. Criteria are proposed to separate a hypothesis from a theory (based on the first principles with quantitative and testable assumptions, able to predict quantitatively the fundamental scales and eastward propagation of the MJO). Four MJO theories are selected to be summarized and compared in this article: the skeleton theory, moisture-mode theory, gravity-wave theory, and trio-interaction theory of the MJO. These four MJO theories are distinct from each other in their key assumptions, parameterized processes, and, particularly, selection mechanisms for the zonal spatial scale, time scale, and eastward propagation of the MJO. The comparison of the four theories and more recent development in MJO dynamical approaches lead to a realization that theoretical thinking of the MJO is diverse and understanding of MJO dynamics needs to be further advanced.

from Zhang et al 2020

from Zhang et al 2020

MJO Theory (ies)?

2. Criteria and Desirable Functions of MJO Theories

In this section, we lay the ground necessary to distinguish a theory from a hypothesis of the MJO and specify what an MJO theory is expected to explain.

An MJO theory should satisfy the following criteria:

1. Its framework must be established from the Navier-Stokes equations or their simplified versions.
2. Its assumptions and approximations unique to the framework must be mathematically expressed. They should be testable against observations available currently or in the future.
3. It must be able to predict or explain quantitatively the most fundamental scales of the MJO in time (intra-seasonal) and space (planetary) and its eastward propagation.

from Zhang et al 2020

MJO Theory (ies)?

It is undoubtedly desirable that an MJO theory is able to reproduce and explain these vertical structures and many other observed features of the MJO:

1. Three-dimensional structure. There are pairs of low-level cyclonic (anticyclonic) vortices associated with the positive (negative) anomalies of MJO precipitation (reversed circulation at upper levels) (Hendon & Salby, 1994; Kiladis et al., 2005).
2. Seasonal cycle. The MJO migrates in latitude and peaks in the summer hemisphere (Salby & Hendon, 1994; Zhang & Dong, 2004). During boreal summer, the MJO propagates northeastward (Wang & Rui,). This complication of the MJO propagation is likely related to the background state of the Asian summer monsoon.
3. Irregularity. MJO events may occur in a group with one following another, known as successive MJO events (Matthews, 2000). Based on a simple visual inspection, one would find that the number of MJO events in a boreal winter season (December–February) can be 0–3. The interval between two adjacent MJO events can be 30–160 days (Zhang, 2005).
4. Multiscale structure (e.g., embedded waves). Within the convection envelope of the MJO, there is a rich spectrum of higher-frequency perturbations (Chen et al., 1996; Nakazawa, 1988; Roundy, 2008). Some of these disturbances belong to the family of equatorial waves, others do not.
5. Modulation by other phenomena (e.g., Indian Ocean Dipole (IOD), El Niño–Southern Oscillation (ENSO), quasi-biennial oscillation (QBO), and extratropical perturbations). The number, strength, and longitudinal location of the MJO vary with lower-frequency climate variability (Son et al., 2017).
6. Air-sea interaction. Through its strong surface wind, rainfall, and cloudiness, the MJO modulates the ocean mixed-layer structure and near surface current of the underneath ocean. Oceanic feedback to the MJO is subtle in observations, although its effects are evident in numerical simulation and prediction (DeMott et al., 2015). It has been studied theoretically (Wang & Xie, 1998).

The common base for the four MJO theories from Zhang et al 2020

- *MJO as an atmospheric internal mode with the first baroclinic vertical structure,*
- *an equatorial beta plane,*
- *linear and hydrostatically balanced large-scale*

$$\frac{\partial u}{\partial t} - \beta y v = -\frac{\partial \phi}{\partial x} - \epsilon u$$

$$\frac{\partial v}{\partial t} + \beta y u = -\frac{\partial \phi}{\partial y} - \epsilon v$$

$$\frac{\partial \phi}{\partial t} + H\left(\frac{\partial u}{\partial x} + \frac{\partial v}{\partial y}\right) = Q_1 - \mu\phi$$

$$\frac{Dq}{Dt} = -Q_2$$

1) Skeleton theory
2) Moisture-mode theory
3) Gravity-wave theory
4) Trio-interaction theory

Q_1 and Q_2 are the apparent heating and moisture sink
("Johnson et al., 2015; Yanai et al., 1973 "

where H is the equivalent depth, and μ a coefficient for thermal damping, commonly known as Newtonian cooling. This is the commonly known dry shallow-water system (Equations 2a–2c) with a moisture equation (Equation 2d). This system is the base for the four theories. However, (Equation 2d) is not included in the gravity-wave theory (section 6).

Each MJO theory from Zhang et al 2020 invokes unique sets of parametrizations, closures, parameters and constants

Table 2
Main Parameterization and Closure Assumptions

	Skeleton	Moisture Mode	Gravity Wave	Trio-interaction
Precipitation (convective heating)	Proportional to lower-tropospheric humidity and wave activity	Proportional to column moisture	Triggered by geopotential minimum	Betts-Miller Bretherton Kuo
Cloud radiation feedback		Proportional to precipitation, decaying exponentially with zonal wavenumber		Constant or as in the moisture-mode theory
Wave activity	Oscillating against lower-tropospheric moisture			
Moisture advection parameter A_{KR}		Sum of meridional and zonal wind moistening processes		

Table 3
Main Parameters and Constants

	Skeleton	Moisture mode	Gravity wave	Trio-interaction
Convective timescale	relaxation (through Γ) (5 hr)	Relaxation (13 hr)	Duration of storm events (6 hr)	Relaxation (12 hr)
Momentum damping		0.3 day^{-1}		0.06 day^{-1}
Newtonian cooling		0.3 day^{-1}		0.12 day^{-1}
Background diabatic heating	1 K day^{-1}	2 K day^{-1}		
Background moisture vertical gradient	1.19 g kg^{-1} km^{-1}	1.26 g kg^{-1} km^{-1}		Exponentially decrease with a scale height of 2.2 km
number density of storms			1 per 1,000 km^2 day^{-1}	

Skeleton theory

$$\boxed{\frac{\partial a}{\partial t} = \Gamma q(\overline{a} + a)}$$

q is lower troposphere moisture and **a** is the meso- and synoptic wave activity

$$Q_1 = \overline{H}(\overline{a} + a) - S_\theta$$

$$Q_2 = \overline{H}(\overline{a} + a) - S_q$$

$$S_\theta = S_q$$

Apparent heating and moisture sink balance each other

Skeleton theory

$$\frac{\partial a}{\partial t} = \Gamma q(\bar{a} + a)$$

q is lower troposphere moisture and **a** is the meso- and synoptic wave activity

$$Q_1 = \overline{H}(\bar{a} + a) - S_\theta$$

$$Q_2 = \overline{H}(\bar{a} + a) - S_q$$

$$S_\theta = S_q$$

Apparent heating and moisture sink balance each other

Variables are projected in the vertical onto the first baroclinic mode and in the meridional direction onto the equatorially trapped Kelvin and first Rossby wave modes

$$K_t + K_x = -\frac{1}{\sqrt{2}}\bar{H}A.$$

$$Rt - \frac{1}{3}Rx = -\frac{2\sqrt{2}}{3}\bar{H}\,A$$

$$Q_t + \frac{1}{\sqrt{2}}\bar{Q}\,R_x\left(-1 + \frac{1}{6}\bar{Q}\right)\left(\bar{H}A\right)$$

$$A_t = \Gamma Q(\bar{a} + A)$$

Skeleton theory

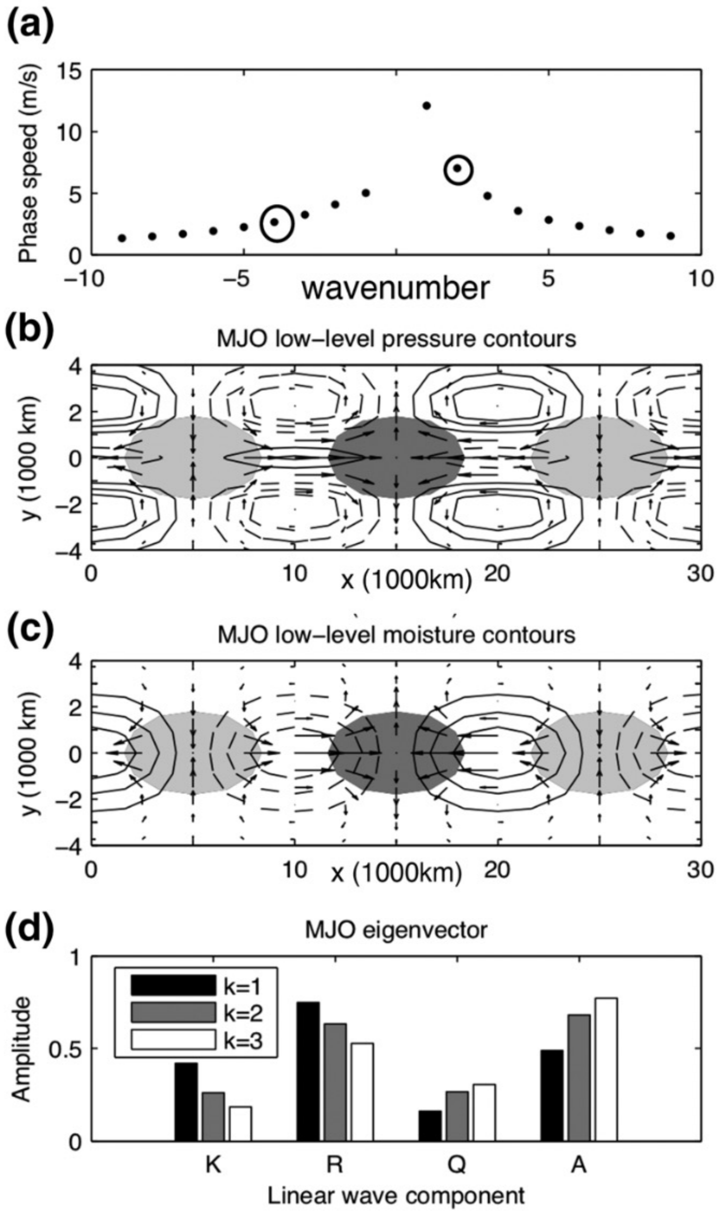

- Solutions are stable
- Planetary-scale eastward modes have structures consistent with the MJO
- Slow eastward modes group velocity is nearly zero
- Convective heating and low level moisture anomalies are out of phase

"The key motivating idea for the skeleton theory is that, in an appropriate parameter regime, lower-tropospheric moisture and convective activity are set to oscillate on the intraseasonal scale, against each other as in a predator-and-prey model. "

Moisture mode theory

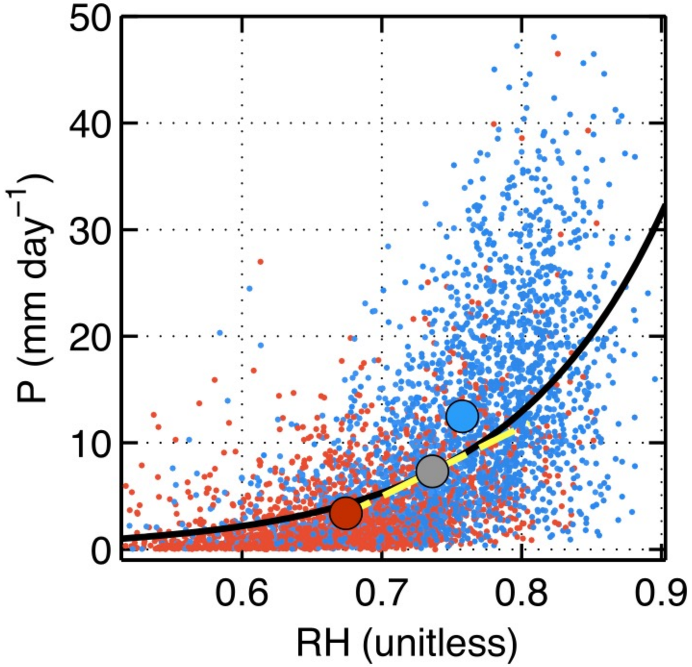

$$\frac{\partial P_r{}'}{\partial t} = \frac{1}{\tau_c}\left(-\langle \mathbf{V}\cdot\nabla q\rangle' + \left\langle \alpha\frac{Q_R'}{L_v}\right\rangle - \left\langle (1-\alpha)\frac{Q_c'}{L_v}\right\rangle + E'\right)$$

$$P_r = P_0 \exp(aRH)$$

P_0 and a are best fit coefficients.

$$P_r{}' = \frac{\langle q' \rangle}{\tau_c}, \quad \tau_c = \frac{\langle q_s \rangle}{a\bar{P_r}}$$

$$(RH = \langle q \rangle / \langle q_s \rangle,$$

Moisture mode theory

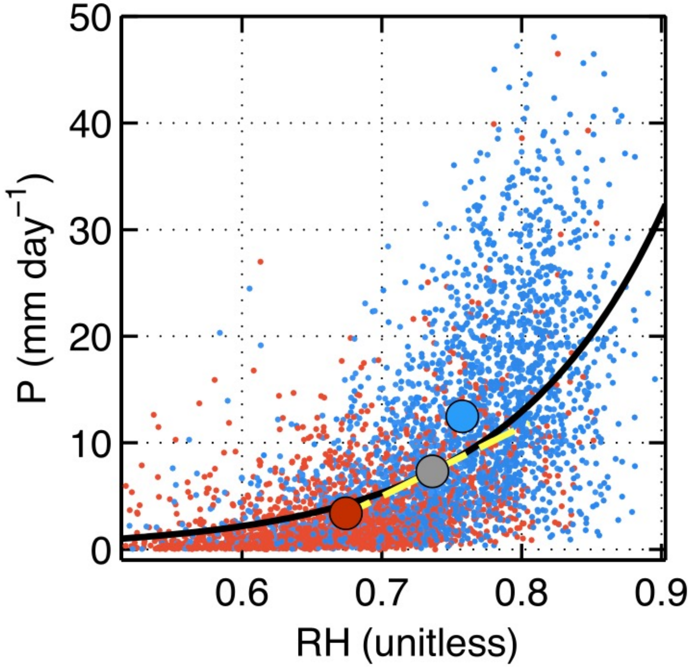

$$P_r = P_0 \exp(aRH)$$

P_0 and a are best fit coefficients.

$$P_r{}' = \frac{\langle q' \rangle}{\tau_c}, \quad \tau_c = \frac{\langle q_s \rangle}{a\bar{P_r}}$$

$$(RH = \langle q \rangle / \langle q_s \rangle,$$

$$\frac{\partial P_r{}'}{\partial t} = \frac{1}{\tau_c}\left(-\langle \mathbf{V}\cdot\nabla q\rangle' + \left\langle \alpha \frac{Q_R'}{L_v} \right\rangle - \left\langle (1-\alpha)\frac{Q_c'}{L_v} \right\rangle + E'\right)$$

Vertical velocity is inferred from Q1 (Weak Temperature Gradient approximation)

$$(\omega \partial_p s)' = Q_1',$$

The anomalous wind field is in steady-state balance with the apparent heating as predicted by the Matsuno-Gill model

$$\frac{\partial P_r{}'}{\partial t} = \frac{1}{\tau_c}\left(-u'\delta \bar{q}_u - nv'\frac{\partial \bar{q}}{\partial y} - \widetilde{M}_{eff} P_r{}'\right)$$

$$\widetilde{M}_{eff} = \widetilde{M}(1+r) - r$$

Moisture mode theory

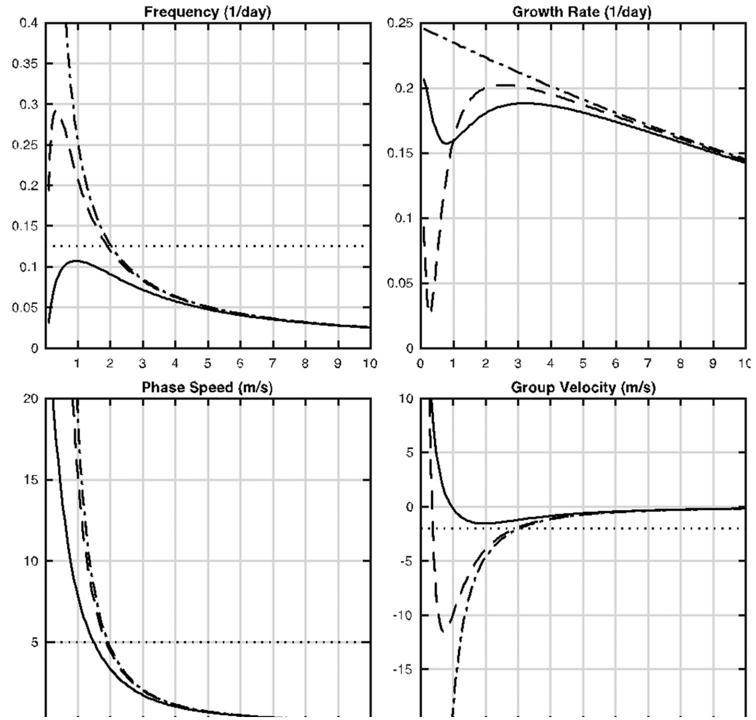

- The longwave cloud-radiation feedback plays a key role in generating instability;
- the spatial-scale selection is through the wide-spread nature of the cloud-radiative feedback;
- precipitation and moisture are in phase;

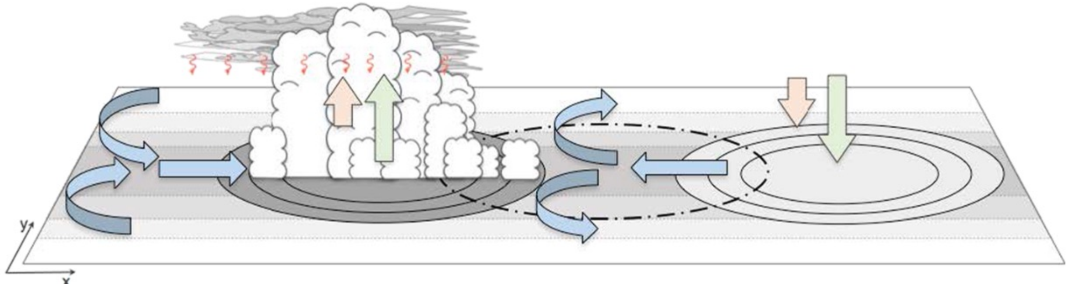

The has been studies using reanalysis and climate models that support the moisture mode theory. But there have also been studies that challenge the moisture-mode view of the MJO

Gravity wave theory

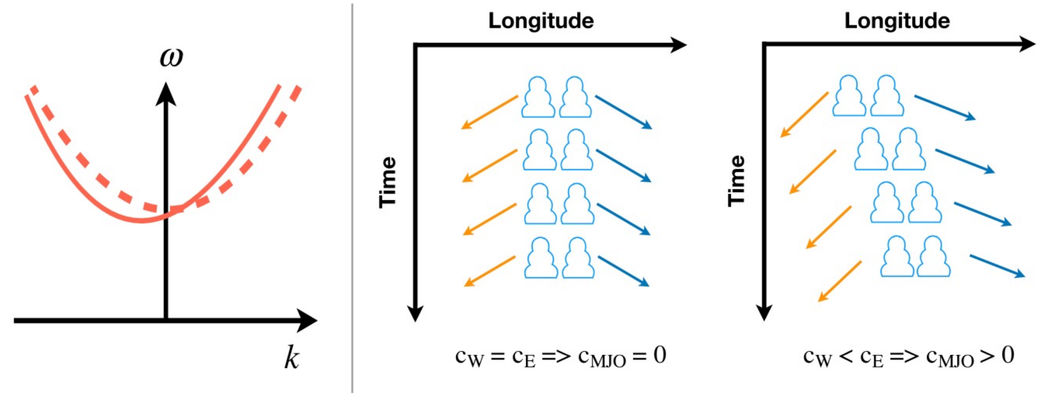

Figure 13. Propagation mechanism of the MJO in the gravity-wave theory. Left: Dispersion relation of inertia-gravity waves. The dashed line represents the dispersion relation symmetric about east and west: $\omega(-k) = \omega(k)$. The solid line represents the dispersion relation with an eastward tilt, as in Earth's tropical atmosphere. Middle: Standing waves when $c_W = c_E$. Right: Eastward propagating wave envelopes when c_W %3C c_E.

Linear shallow water system

+ trigger convection

Q_1

$$Q = \begin{cases} \dfrac{Q_0}{\tau_c A_c}\left[1 - \left(\dfrac{\Delta t - \tau_c/2}{\tau_c/2}\right)^2\right]\left(1 - \dfrac{L^2}{R_c^2}\right) & \text{where } \phi < \phi_c,\ 0 < \Delta t < \tau_c,\ L^2 < R_c^2 \\ 0 & \text{otherwise} \end{cases}. \tag{13}$$

where

ϕ_c	is the threshold for geopotential to trigger convection,
$c \equiv \sqrt{\phi_c}$	is the gravity-wave phase speed,
Q_o	is the convective heating amplitude per event,
τ_c	is the duration of individual convective storms (different from that in section 5),
Δt	is the period of time since convection is triggered,
A_c	is the area of convective storms,
R_c	is the radius of individual convective storms, and
$L = (\Delta x^2 + \Delta y^2)^{1/2}$	is the distance from the convective center, where Δx and Δy are zonal and meridional distances from the convective center, respectively.

Gravity wave theory

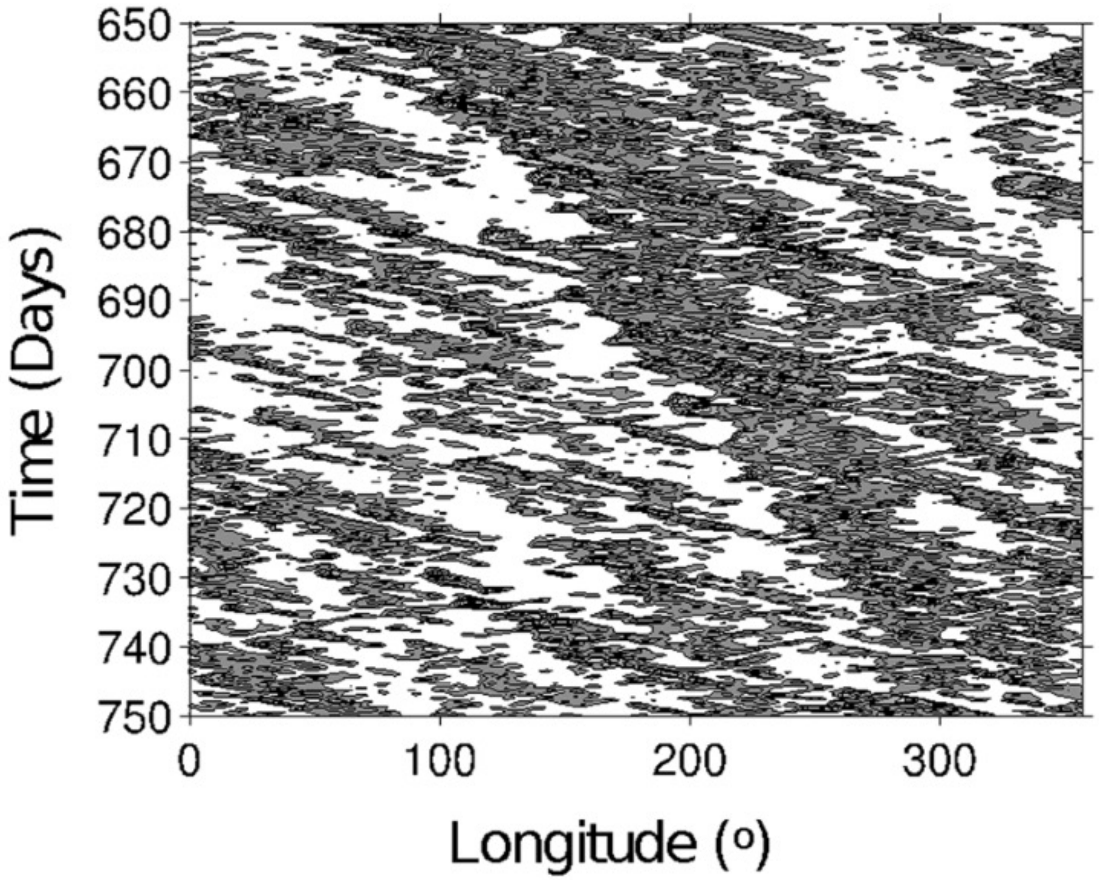

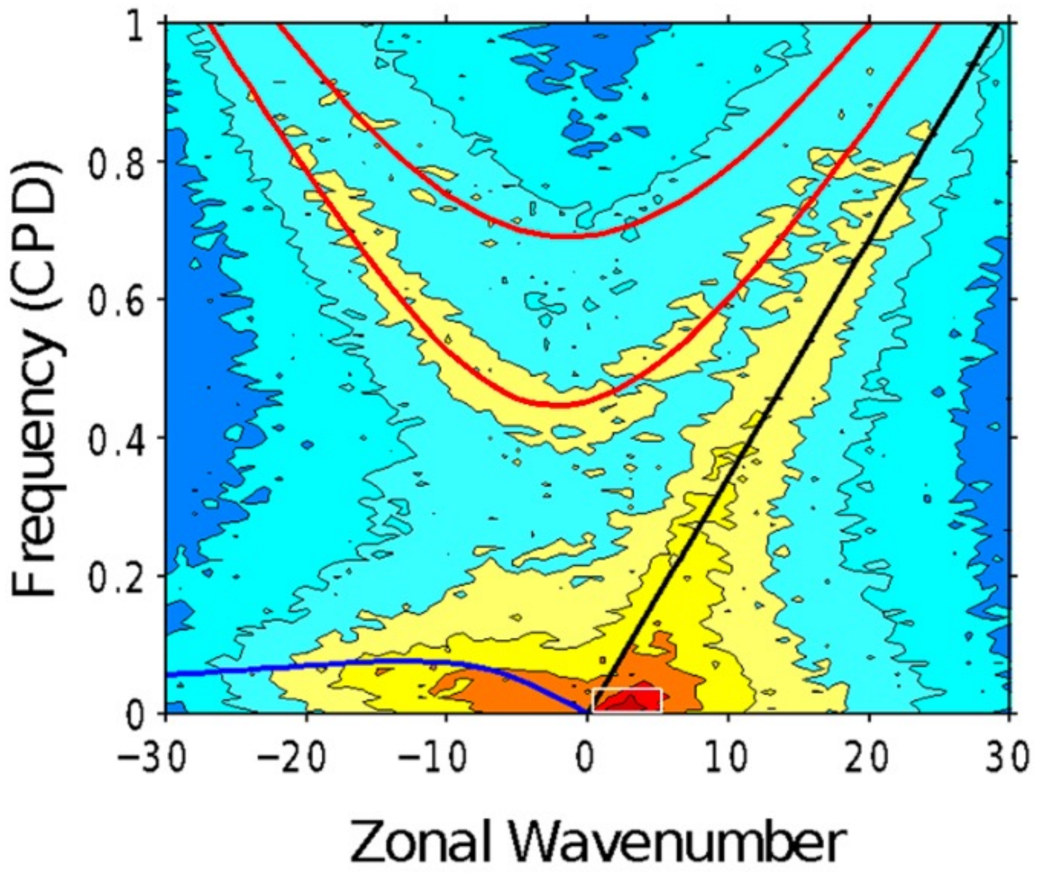

- Envelopes of EIG and WIG make up the “MJO”
- There is no prognostic moisture equation.

Trio interaction theory

7.1. Essence

The most critical component of this theory is the convectively coupled Kelvin-Rossby wave structure and the phase lead of BL convergence to convective heating. In consequence,

1. the fundamental MJO physics is rooted in the feedbacks between the dynamics (frictionally driven BL convergence and equatorial wave dynamics), moisture, and diabatic heating from convection and radiation;
2. the BL feedback is responsible for the selection of the zonal scale and eastward propagation of the MJO;
3. the eastward propagation speed of the MJO is determined by the basic state moist static energy, the moisture feedback, and the coupling of Kelvin and Rossby waves, and
4. the BL feedback and the cloud-radiative feedback produce the instability for the growth of the MJO.

7.2. Assumptions

1. The BL dynamics can be represented by a barotropic prognostic equation.
2. The BL depth is constant in time and space.
3. The long-wave (semigeostrophic) approximation is applied to the free troposphere but not the BL.
4. Total moisture convergence is due to the sum of BL and lower free tropospheric convergence of mean moisture by the anomalous winds.
5. And BL convergence is determined by the lower-tropospheric geopotential anomaly.

7.3. Uniqueness

This trio-interaction theory integrates four major possesses proposed in the existing theoretical MJO frameworks developed over the past three decades. It can accommodate a variety of simplified convective schemes. Among the MJO theories discussed in this article, this is the only one in which the BL convergence feedback plays an essential role in generating eastward propagation, planetary-scale instability, and the coupled Kelvin-Rossby wave structure of the MJO.

Trio interaction theory

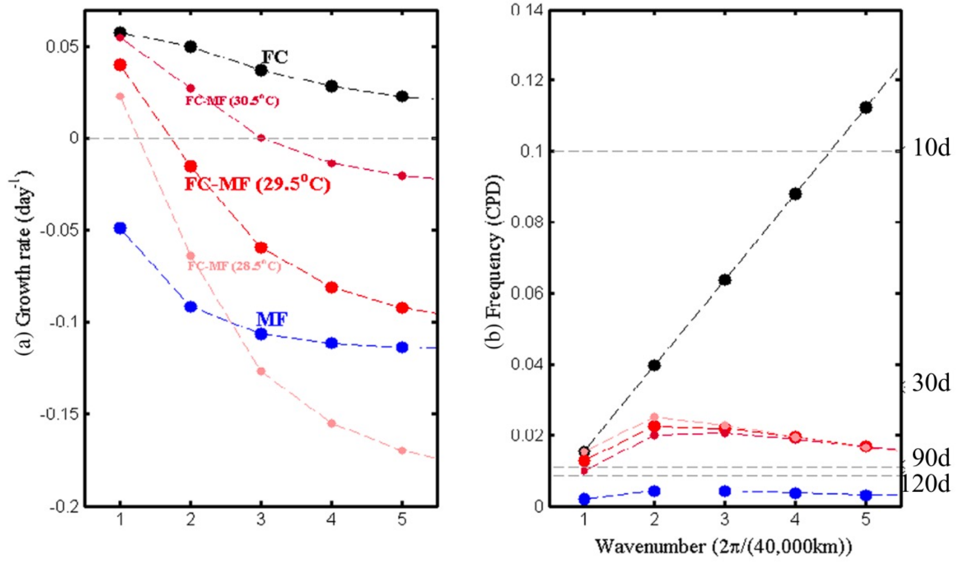

Figure 20. Comparison of (left panel) the growth rate (day^{-1}), and (right) frequency (cycle per day) as functions of wavenumber obtained from three theoretical models, namely, the frictional coupled K-R model (FC; black), the moisture-mode model (MF; blue), and the combined FC-MF or trio-interaction model (red). The basic state SST of 29.5°C is uniform. The results from the trio-interaction theory with a warmer SST of 30.5°C and a cooler SST of 28.5°C are also shown for comparison. Adopted from Liu and Wang (2017).

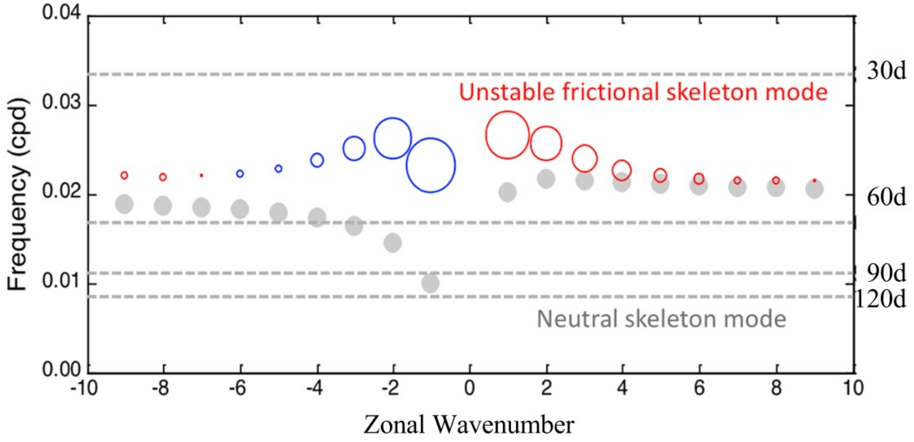

Figure 23. Comparison of results from the skeleton theory (section 4.4) and a frictional skeleton model (Liu & Wang, 2012) in terms of frequency (period) as a function of wavenumber. Gray dots denote neutral skeleton mode from the skeleton theory without the BL effect. Colored circles denote unstable frictional skeleton mode derived from the frictional skeleton model. Red (Blue) colored circles denote growing (damping) modes. The diameters of the circles represent the magnitude of growth rates with maximum growth rate being 0.11 day^{-1}. Adopted from Liu and Wang (2012).

How do these theories explain

1. MJO selection of planetary scale?
2. MJO selection of eastward propagation?
3. MJO slow propagation speed?

MJO selection of planetary scale

Skeleton theory	Moisture-mode theory	Gravity-wave theory	Trio-interaction theory
The zonal scale of the MJO is selected when the predicted horizontal structure of the MJO matches the observed. In its stochastic version, the selection is through stochastic damping of small scales	The zonal scale is selected by the vertical motion imparted by anomalous radiative heating that is stronger for larger scales	the horizontal scale is determined by the travel distance of gravity waves and intensity of precipitation	The trio-interaction theory selects the zonal scale through instability generated by BL convergence and damping of small scales by tropospheric moisture feedback.

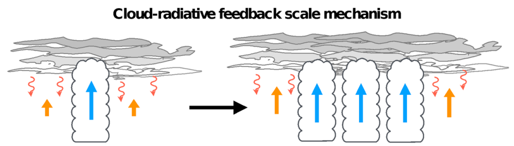

Figure 8. Schematic describing the mechanism in which the interactions between convection and radiation lead to planetary scale selection. In a moist atmosphere, upper-tropospheric clouds expand far away from a region of precipitation (clouds with blue arrows). This region reduces the outgoing longwave radiation, effectively warming the troposphere. Upward motions (orange arrows) result in order to maintain the WTG balance. These upward motions advect moisture upward and reduce GMS, moistening the troposphere.

MJO selection of eastward propagation

Skeleton theory	Moisture-mode theory	Gravity-wave theory	Trio-interaction theory
produces neutral solutions that propagate both east-ward and westward. At planetary scales, the eastward propagating solutions match the observed features of the MJO.	the eastward propagation is caused by advection of moisture by the wind anomalies.	the MJO propagates eastward because EIG travels faster than WIG due to the β effect.	the BL moisture convergence generates positive moisture and heating anomalies to the east of an MJO convection center, leading to its eastward propagation.

MJO slow propagation speed

Skeleton theory	Moisture-mode theory	Gravity-wave theory	Trio-interaction theory
the key factor for the speed is the wave activity parameter (*Γ*)	the dry static stability, the strength of moisture advection, and convective moisture adjustment timescale determine the propagation speed.	The small difference between the speeds of EIG and WIG gives rise to the MJO speed in the gravity-wave theory	Propagation speed is determined by three factors: (a) the basic state MSE, which affects the heating intensity and effective static stability, (b) moisture feedback which enhances the Rossby wave component and slows down the eastward propagation, and (c) the coupling of Kelvin and Rossby waves.

Roles of MJO feedbacks

Table 5
Roles of Different Feedbacks

MJO mechanisms	BL Feedback	Moisture Feedback	K-R Wave Feedback	Cloud-Radiation Feedback	Gravity Wave Feedback	Wave-activity feedback
Planetary scale selection	Trio-interaction		Skeleton	Moisture-mode	Gravity-wave	Skeleton
Eastward propagation	Moisture-mode Trio-interaction	Skeleton moisture-mode	Skeleton		Gravity-wave	Skeleton
Propagation speed	Trio-interaction	Trio-interaction	Trio-interaction		Gravity-wave	
Instability	Trio-interaction	Moisture-mode Trio-interaction	Trio-interaction	Moisture-mode Trio-interaction		Stochastic skeleton

This is the effect of BL frictional moisture convergence on convection

"the degree to which the observed BL moisture convergence is caused by BL friction and other processes (i.e., cloud heating and large-scale eddies) need to be quantified "

Roles of MJO feedbacks

Table 5
Roles of Different Feedbacks

MJO mechanisms	BL Feedback	Moisture Feedback	K-R Wave Feedback	Cloud-Radiation Feedback	Gravity Wave Feedback	Wave-activity feedback
Planetary scale selection	Trio-interaction		Skeleton	Moisture-mode	Gravity-wave	Skeleton
Eastward propagation	Moisture-mode Trio-interaction	Skeleton moisture-mode	Skeleton		Gravity-wave	Skeleton
Propagation speed	Trio-interaction	Trio-interaction	Trio-interaction		Gravity-wave	
Instability	Trio-interaction	Moisture-mode Trio-interaction	Trio-interaction	Moisture-mode Trio-interaction		Stochastic skeleton

This is the effect of evolving tropospheric moisture on convection

“This fundamental discrepancy can be pushed to an extreme as to whether the MJO is a dry mode”

Roles of MJO feedbacks

Table 5
Roles of Different Feedbacks

MJO mechanisms	BL Feedback	Moisture Feedback	K-R Wave Feedback	Cloud-Radiation Feedback	Gravity Wave Feedback	Wave-activity feedback
Planetary scale selection	Trio-interaction		Skeleton	Moisture-mode	Gravity-wave	Skeleton
Eastward propagation	Moisture-mode Trio-interaction	Skeleton moisture-mode	Skeleton		Gravity-wave	Skeleton
Propagation speed	Trio-interaction	Trio-interaction	Trio-interaction		Gravity-wave	
Instability	Trio-interaction	Moisture-mode Trio-interaction	Trio-interaction	Moisture-mode Trio-interaction		Stochastic skeleton

This represents the role of the Kelvin-Rossby dynamics in the MJO..

horizontal moisture convergence?
horizonal moisture advection?
slow eastward propagation ?
growth rate for planetary waves?
and not included in the gravity-wave theory!

Roles of MJO feedbacks

Table 5
Roles of Different Feedbacks

MJO mechanisms	BL Feedback	Moisture Feedback	K-R Wave Feedback	Cloud-Radiation Feedback	Gravity Wave Feedback	Wave-activity feedback
Planetary scale selection	Trio-interaction		Skeleton	Moisture-mode	Gravity-wave	Skeleton
Eastward propagation	Moisture-mode Trio-interaction	Skeleton moisture-mode	Skeleton		Gravity-wave	Skeleton
Propagation speed	Trio-interaction	Trio-interaction	Trio-interaction		Gravity-wave	
Instability	Trio-interaction	Moisture-mode Trio-interaction	Trio-interaction	Moisture-mode Trio-interaction		Stochastic skeleton

This is the enhancement of total diabatic heating by large-scale cloud radiative heating.

*In the moisture-mode theory, it provides the main mechanism for the horizonal moisture advection.

Roles of MJO feedbacks

Table 5
Roles of Different Feedbacks

MJO mechanisms	BL Feedback	Moisture Feedback	K-R Wave Feedback	Cloud-Radiation Feedback	Gravity Wave Feedback	Wave-activity feedback
Planetary scale selection	Trio-interaction		Skeleton	Moisture-mode	Gravity-wave	Skeleton
Eastward propagation	Moisture-mode Trio-interaction	Skeleton moisture-mode	Skeleton		Gravity-wave	Skeleton
Propagation speed	Trio-interaction	Trio-interaction	Trio-interaction		Gravity-wave	
Instability	Trio-interaction	Moisture-mode Trio-interaction	Trio-interaction	Moisture-mode Trio-interaction		Stochastic skeleton

It represents the role of synoptic-scale gravity waves in the MJO

"Whether gravity waves are essential to the MJO needs to be supported by evidence of their coherence in space and time."

Roles of MJO feedbacks

Table 5
Roles of Different Feedbacks

MJO mechanisms	BL Feedback	Moisture Feedback	K-R Wave Feedback	Cloud-Radiation Feedback	Gravity Wave Feedback	Wave-activity feedback
Planetary scale selection	Trio-interaction		Skeleton	Moisture-mode	Gravity-wave	Skeleton
Eastward propagation	Moisture-mode Trio-interaction	Skeleton moisture-mode	Skeleton		Gravity-wave	Skeleton
Propagation speed	Trio-interaction	Trio-interaction	Trio-interaction		Gravity-wave	
Instability	Trio-interaction	Moisture-mode Trio-interaction	Trio-interaction	Moisture-mode Trio-interaction		Stochastic skeleton

"It remains to be confirmed whether interaction between synoptic and large-scale convective activities can be represented in such a simple form "

This is the planetary-scale envelope of synoptic-scale and mesoscale convective heating that interacts with large-scale moisture only in the skeleton theory, where it is used to parametrize large-scale convective heating of the MJO.

Summary of MJO theories

The theories presented in Zhang et al 2020 are the result of combined efforts and feedback among the modeling, observing and theory communities .

But yes, there are lots of discrepancies among theories, unexplained MJO behavior, and simulation deficiencies…

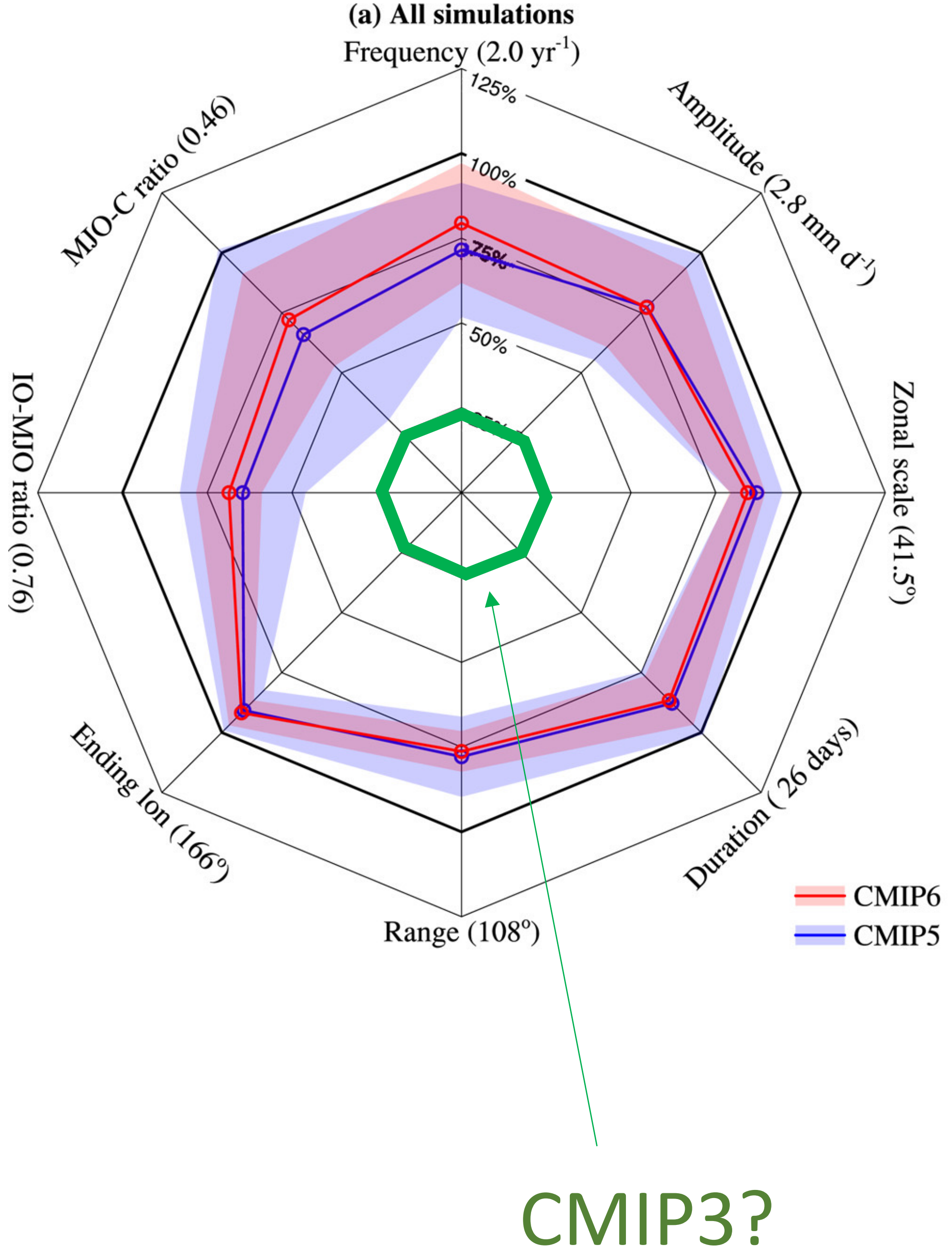

From Chen et al. 2021

Key takeaways:

- Planetary waves are trapped along the equator due to the change in the Coriolis parameter’s sign.
- The equatorial wave spectrum includes fast-oscillating inertia-gravity waves and low frequency Rossby waves, with mixed Rossby-gravity wave branch and an eastward-propagating equatorial Kelvin wave filling the frequency gap.
- Linear theory works well to interpret observations, providing mechanistic insights into the global scale atmospheric response to tropical convective heating.
- Important questions remain about the role of moisture in convectively coupled

equatorial waves and the Madden-Julian Oscillation (MJO).

Part 2: Observations of Tropical Waves

1. Brief history of observations
2. Identification of tropical waves
3. Beyond space-time spectral analysis
4. Example: Observed structure of CCEWs

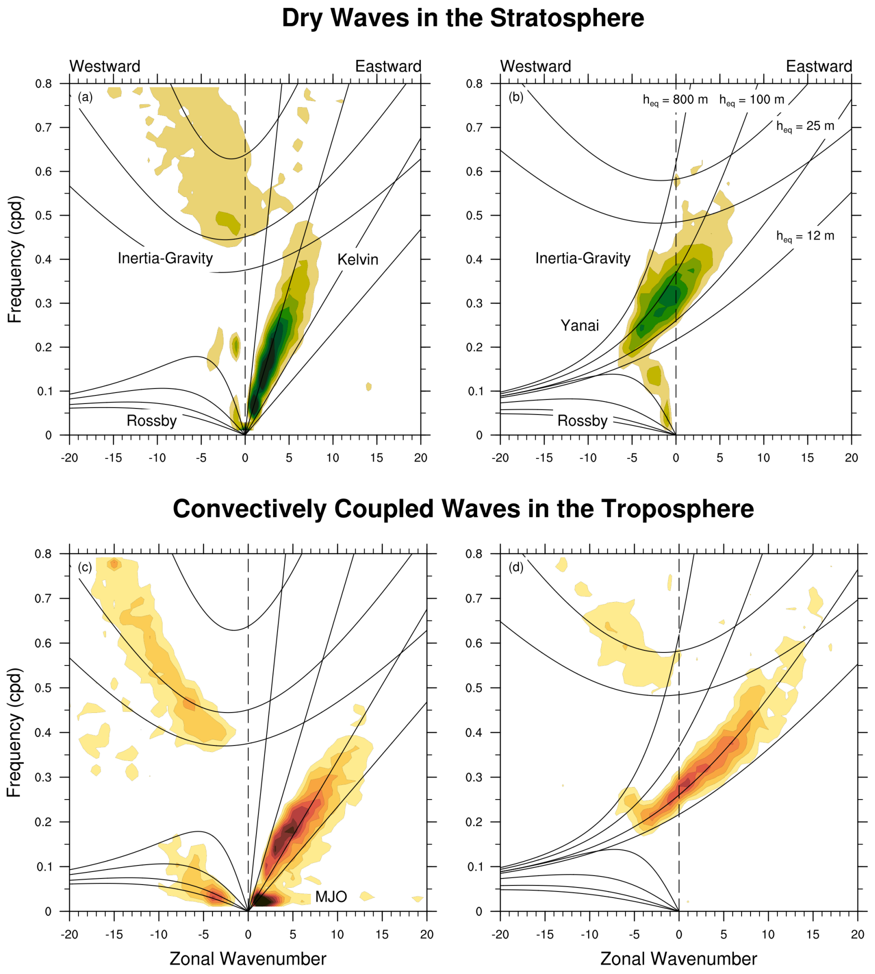

Figure 13.4. Wave number-frequency power spectrum of equatorial data averaged. from 15 S to 15 N displayed as the ratio between the raw and smoothed red noise background spectrum (details in Wheeler and Kiladis 1999). The top panel demonstrates dry waves in the stratosphere as power spectra of zonal wind at 50 hPa from ERA5 reanalysis. The bottom panel shows convectively coupled waves in the troposphere as spectra of brightness temperature from satellite observation. In both panels, the data are decomposed into symmetric (left) and antisymmetric (right) components. Contours start at 1.2 with an interval of 0.4 at the top panels and begin at 1.1 with an increase of 0.1 at the bottom. Dispersion curves are overlaid for equivalent depths of 12, 25, 100, and 800 m.

Brief history of observations of tropical waves

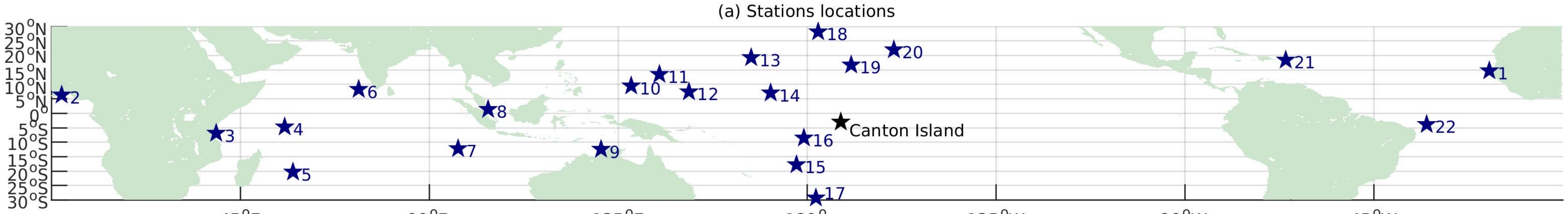

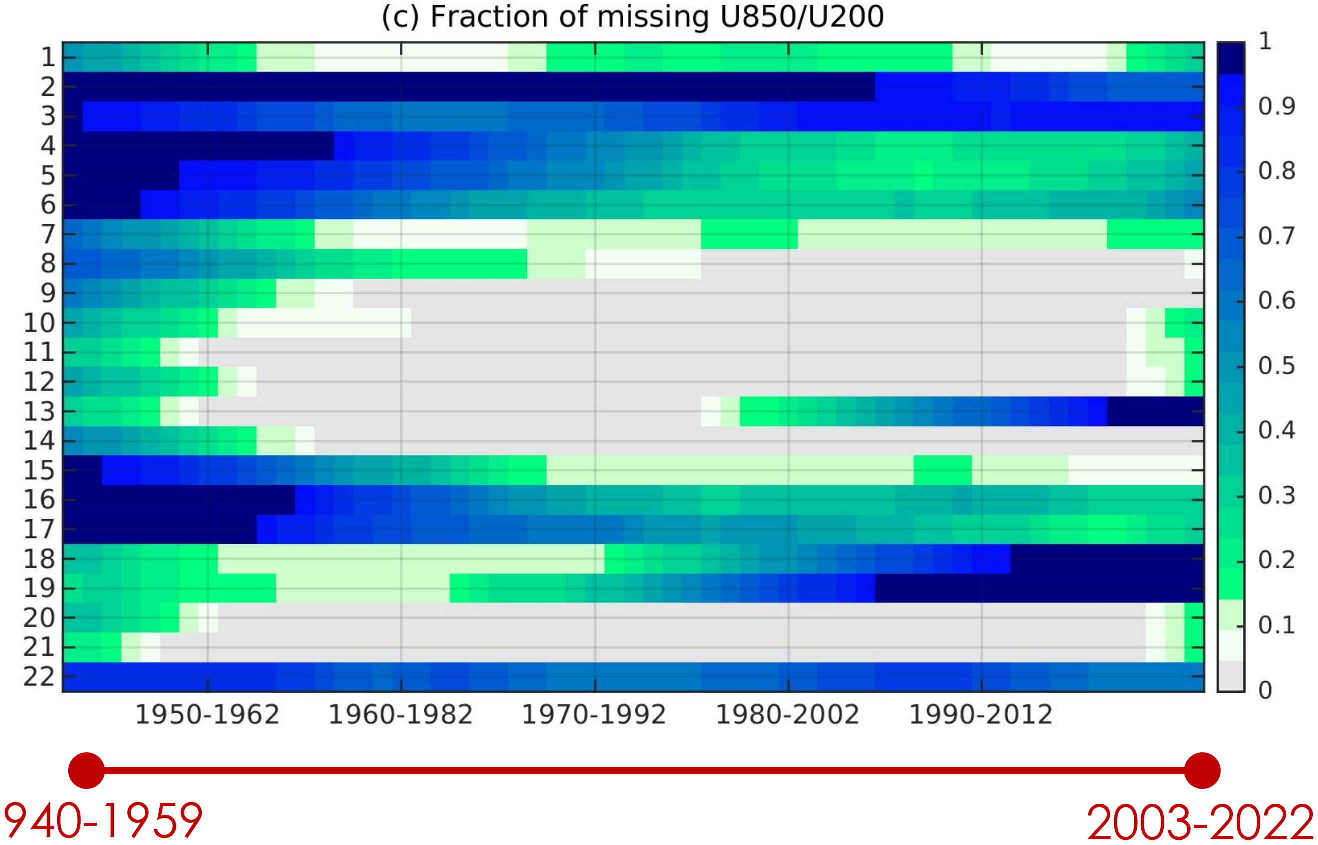

NOAA/NCEI Integrated Global Radiosonde Archive (IGRA)

Discovery of Yanai and Kelvin Waves

The discovery of equatorial waves in observations was based on sounding data over tropical stations and was motivated by Matsuno's theoretical work.

Stratospheric Wave Disturbances Propagating over the Equatorial Pacific*

M. Yanai and T. Maruyama

Geophysical Institute, Tokyo University, Tokyo

(Manuscript received 19 July 1966)

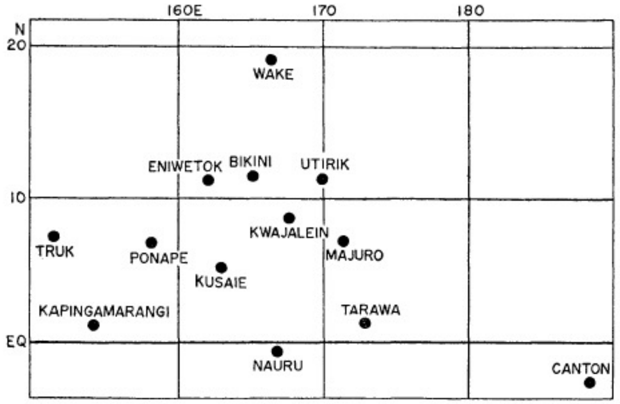

Fig. 1. Upper-air stations in the central equatorial Pacific during March-July 1958.

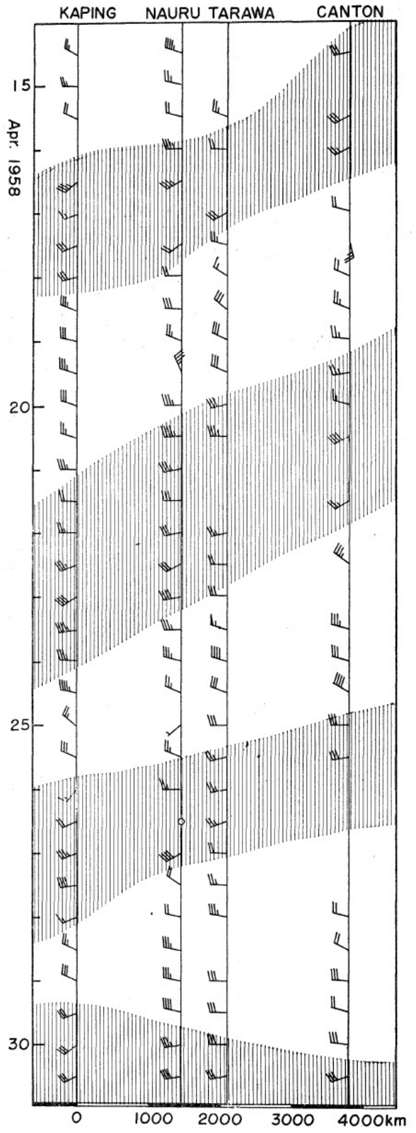

Fig. 4. Time series of 70,000 ft (or 21 km) winds at Kapingamarangi, Nauru, Tarawa and Canton Island for 15-30 April 1958. Winds with southerly components are shaded.

Discovery of Yanai and Kelvin Waves

The discovery of equatorial waves in observations was based on sounding data over tropical stations and was motivated by Matsuno's theoretical work.

Observational Evidence of Kelvin Waves in the Tropical Stratosphere[1]

JOHN M. WALLACE AND V. E. KOUSKY

University of Washington, Seattle

(Manuscript received 1 February 1968, in revised form 25 March 1968)

ABSTRACT

This study of synoptic-scale wave motions in the equatorial stratosphere is based on the analysis of six months of radiosonde data from three tropical stations. Fluctuations in the zonal wind with an average period of 15 days and amplitudes in the order of 8–12 m sec^{-1} are noted. Corresponding fluctuations are found in the temperature field with amplitudes of 3–5C and a phase lead of $\frac{1}{4}$ cycle with respect to the zonal wind. These wave motions which propagate phase downward do not appear to involve the meridional wind component.

The observed fluctuations resemble Kelvin waves, which represent one of the solutions of the wave equation on an equatorial beta plane. One of the notable features of this type of wave is that it produces an upward flux of westerly momentum. The observations indicate that this flux is large enough to account for the westerly accelerations associated with the quasi-biennial oscillation.

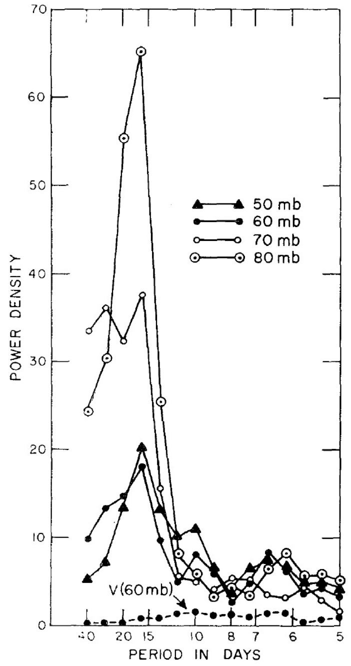

FIG. 8. Power spectra of zonal wind fluctuations at 80, 70, 60 and 50 mb shown together with the spectrum for the meridional wind fluctuations at 60 mb. Zonal wind data are prewhitened by means of a procedure described in the text.

Discovery of the MJO

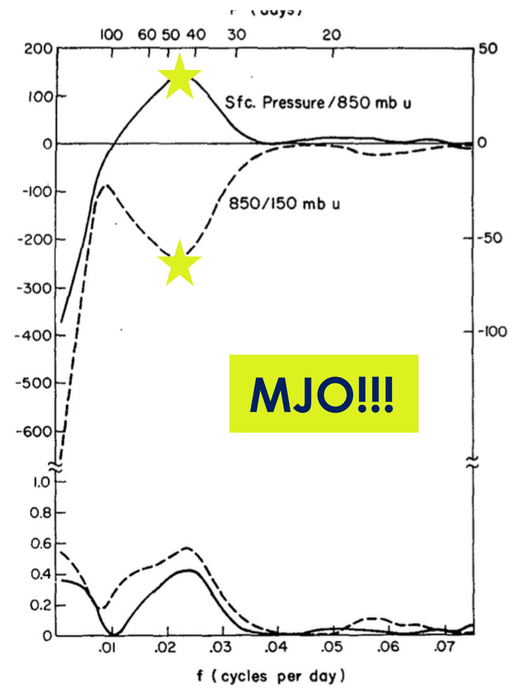

FIG. 1. (Top) The co-spectrum of the 850- and 150-mb zonal wind (u) (dashed, and left ordinate values) together with the co-spectrum of the station (sfc) pressure and the 850-mb zonal wind (solid, and right ordinate values) for Canton Island, June 1957 through March 1967. The ordinate is co-spectral density normalized to unit bandwidth (m^2 sec^{-2} day). (Bottom) The coherence-squared statistic for the 850- and 150-mb zonal wind and the station pressure and 850-mb u-series. The 0.1% prior (~6% *a posteriori*) confidence level on the null hypothesis of no association is 0.25. In this and the remaining spectra only the frequency range 0 to 0.075 day^{-1} is shown.

Detection of a 40–50 Day Oscillation in the Zonal Wind in the Tropical Pacific

ROLAND A. MADDEN AND PAUL R. JULIAN

Discovery of the MJO

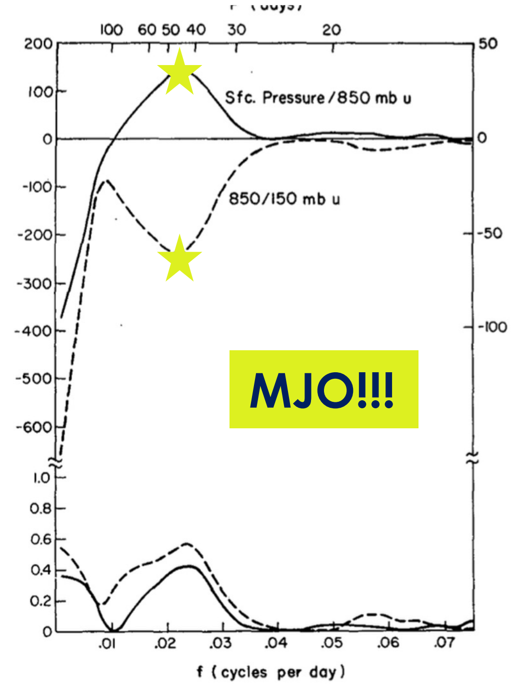

FIG. 1. (Top) The co-spectrum of the 850- and 150-mb zonal wind (u) (dashed, and left ordinate values) together with the co-spectrum of the station (sfc) pressure and the 850-mb zonal wind (solid, and right ordinate values) for Canton Island, June 1957 through March 1967. The ordinate is co-spectral density normalized to unit bandwidth (m² sec⁻² day). (Bottom) The coherence-squared statistic for the 850- and 150-mb zonal wind and the station pressure and 850-mb u-series. The 0.1% prior (~6% *a posteriori*) confidence level on the null hypothesis of no association is 0.25. In this and the remaining spectra only the frequency range 0 to 0.075 day⁻¹ is shown.

Detection of a 40–50 Day Oscillation in the Zonal Wind in the Tropical Pacific

ROLAND A. MADDEN AND PAUL R. JULIAN

Description of Global-Scale Circulation Cells in the Tropics with a 40–50 Day Period

ROLAND A. MADDEN AND PAUL R. JULIAN

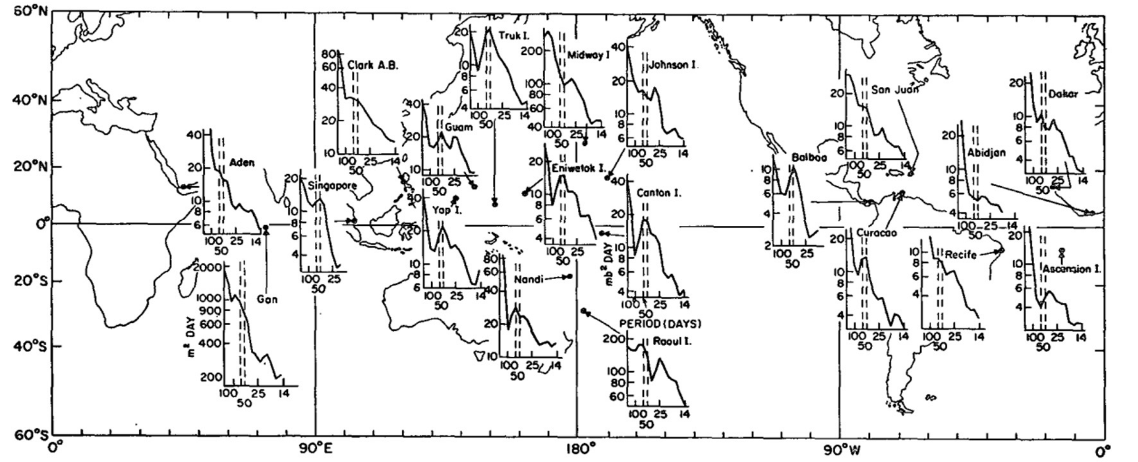

FIG. 1. Variance spectra for station pressures at several locations. Units for ordinates (mb² day) and abscissas (period in days) are indicated on spectrum for Canton Island. Ordinates are logarithmic and abscissas are linear with respect to frequency. The 40–50 day period range is indicated by the dashed vertical lines.

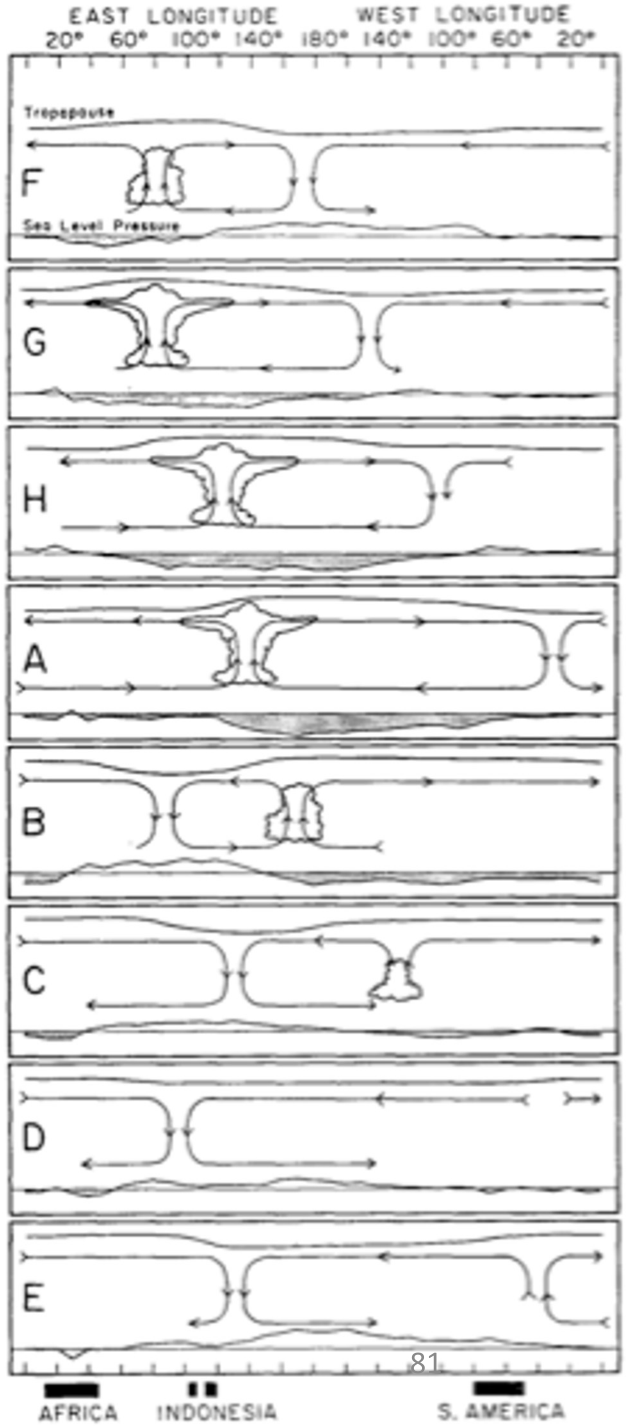

Cross-spectral analysis across tropical islands indicated that the 40-50 Day peaks are a planetary scale phenomena that moves to east

Analysis of satellite data

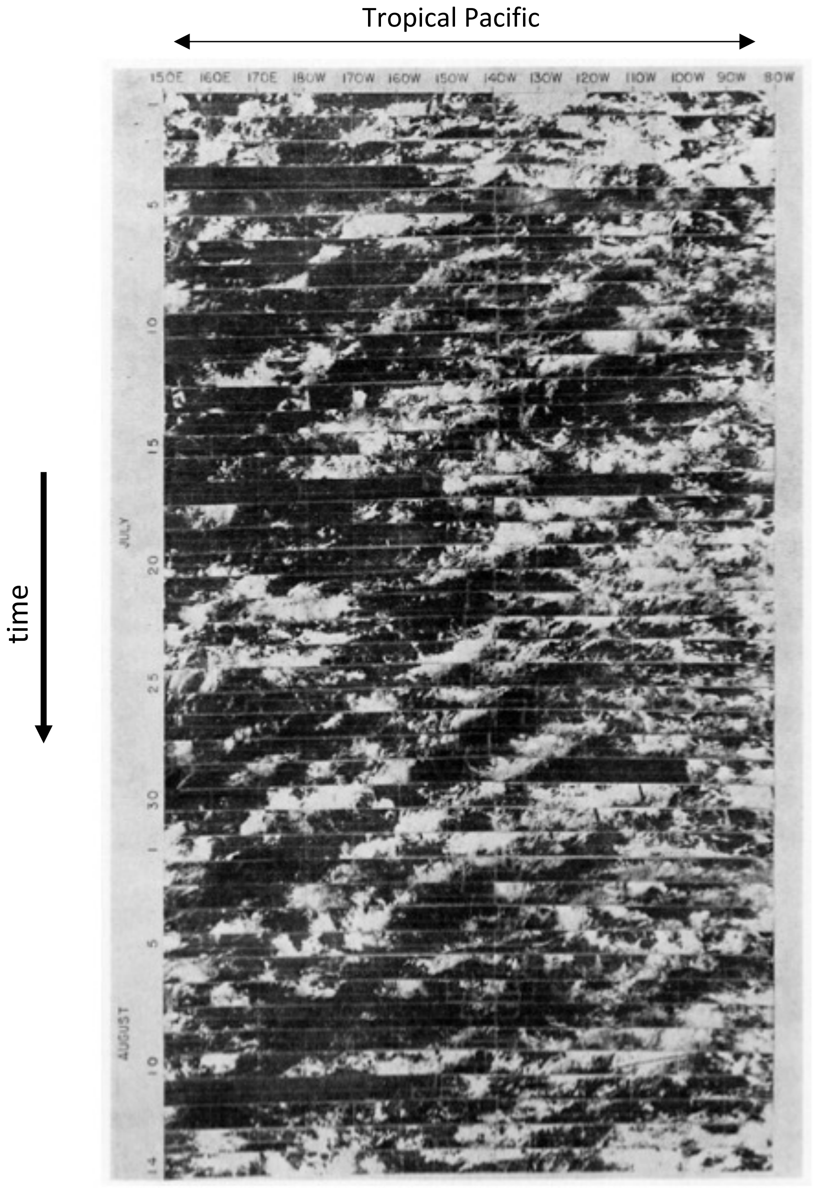

FIG. 1. Time-longitude section of satellite photographs of the period 1 July–14 August 1967 for the 5–10N latitude band in the Pacific. The following data are missing: 4 July (150E–155W), 17 July (150E–150W, 130W-100W), 29 July (130W–100W), 11 August (150E–150W).

Chang 1970 analyzed hovemullers of tropical satellite images and Hayashi 1981

Space-Time Spectral Analysis and its Applications to Atmospheric Waves

By Yoshikazu Hayashi

Geophysical Fluid Dynamics Laboratory/NOAA, Princeton University
Princeton, New Jersey 08540, U.S.A.
(Manuscript received 19 September, 1981)

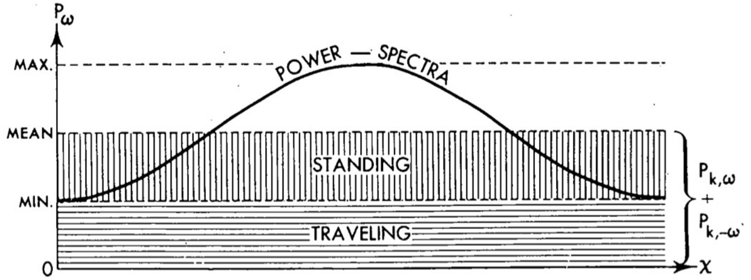

Fig. 7 Spacial distribution of the time power spectra (solid curve) of disturbances composed of eastward and westward moving waves with a single wavenumber and the same frequencies. The

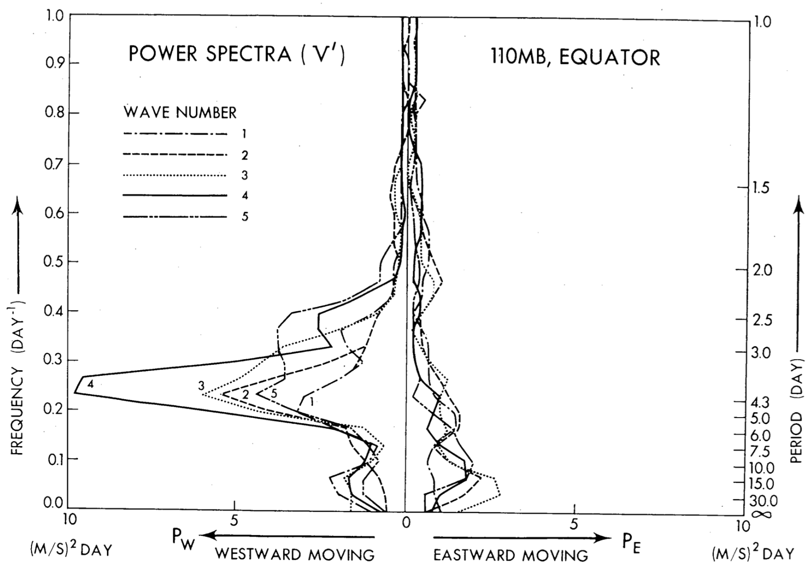

Fig. 8 Space-time power spectra of the grid model's meridional component at 110 mb over the equator during the period July August.

Analysis of satellite data

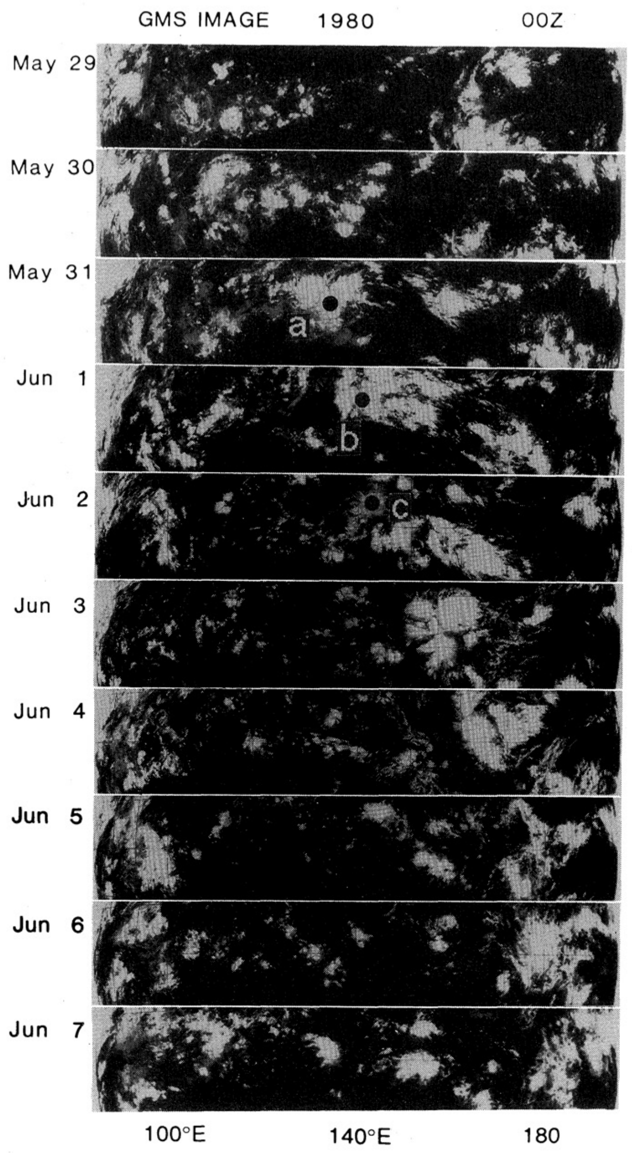

Nakazawa, 1986, 1987

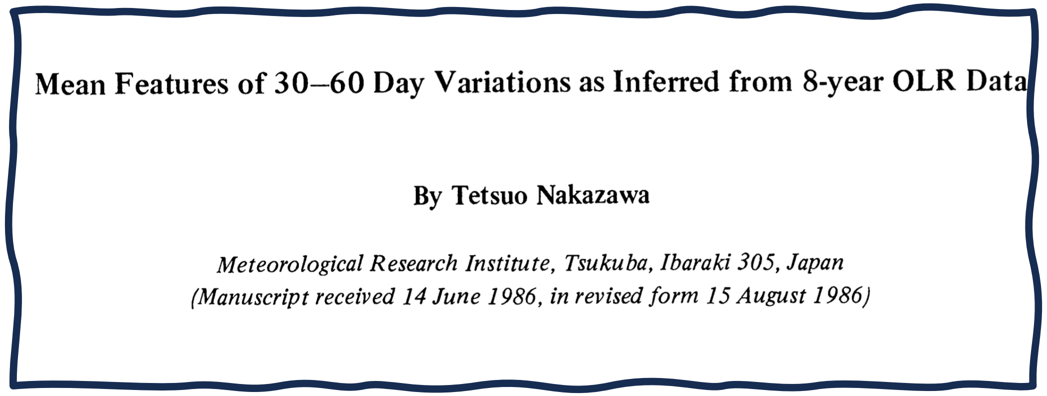

Mean Features of 30–60 Day Variations as Inferred from 8-year OLR Data

By Tetsuo Nakazawa

Meteorological Research Institute, Tsukuba, Ibaraki 305, Japan
(Manuscript received 14 June 1986, in revised form 15 August 1986)

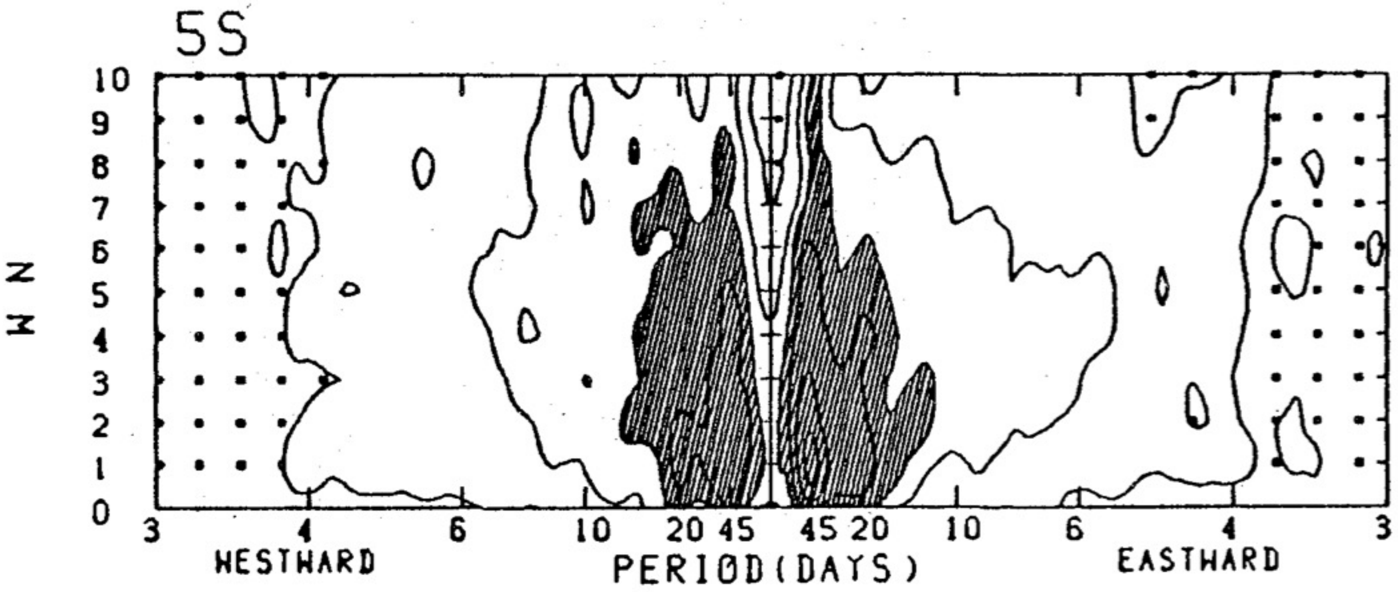

Analysis of satellite data

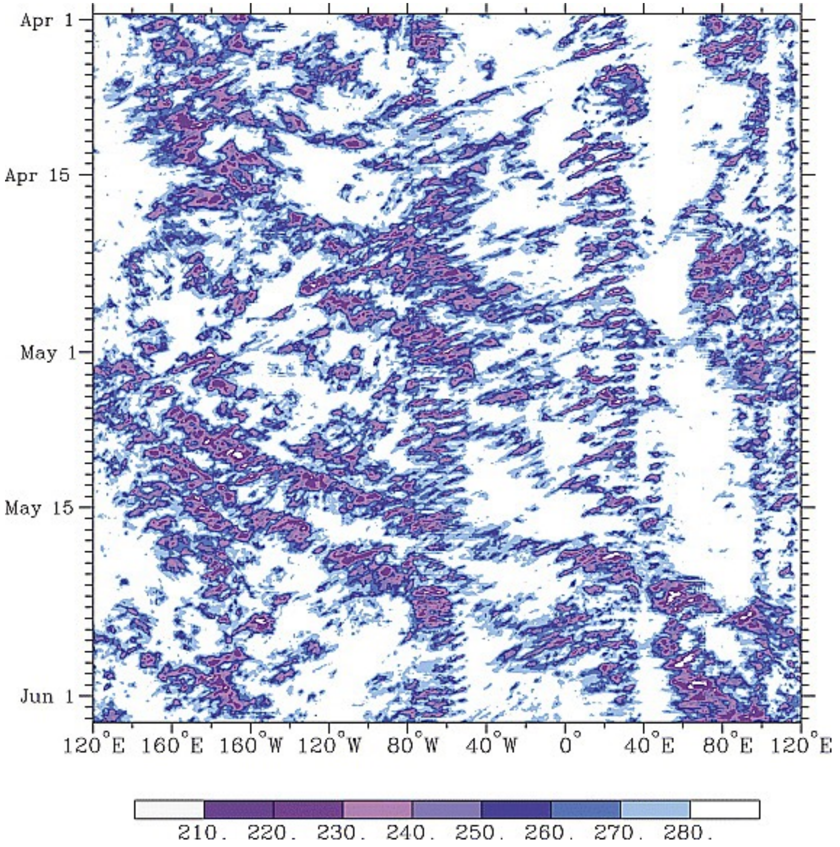

Chang 1970 started looking at satellite images -> Takayabu 1994, -> Wheeler and Kiladis 1999

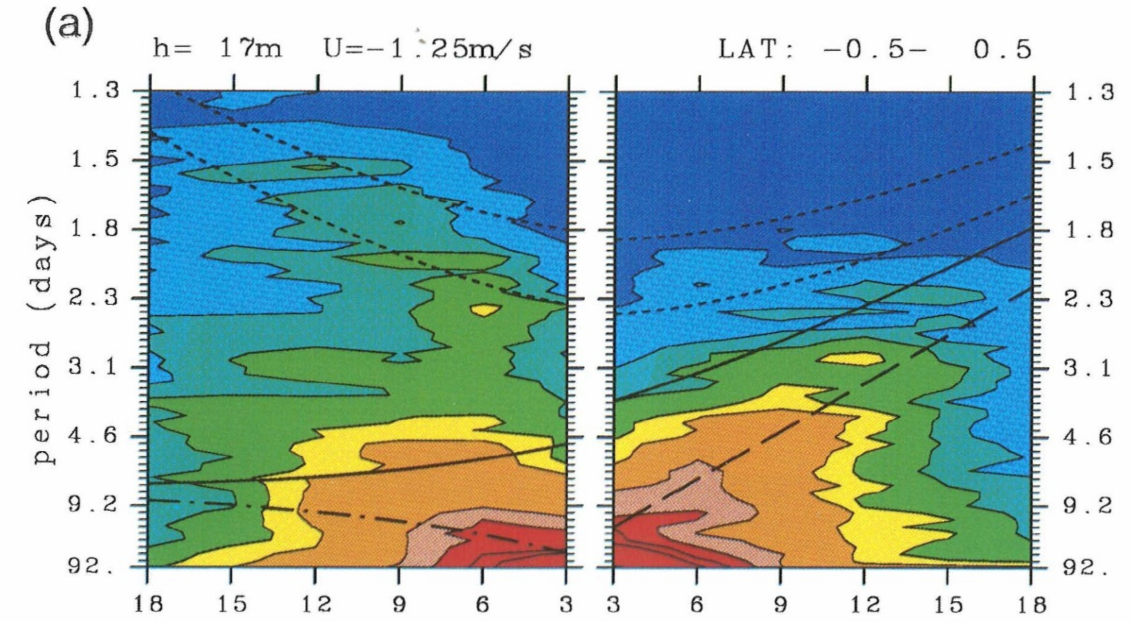

Convectively Coupled Waves in the Troposphere

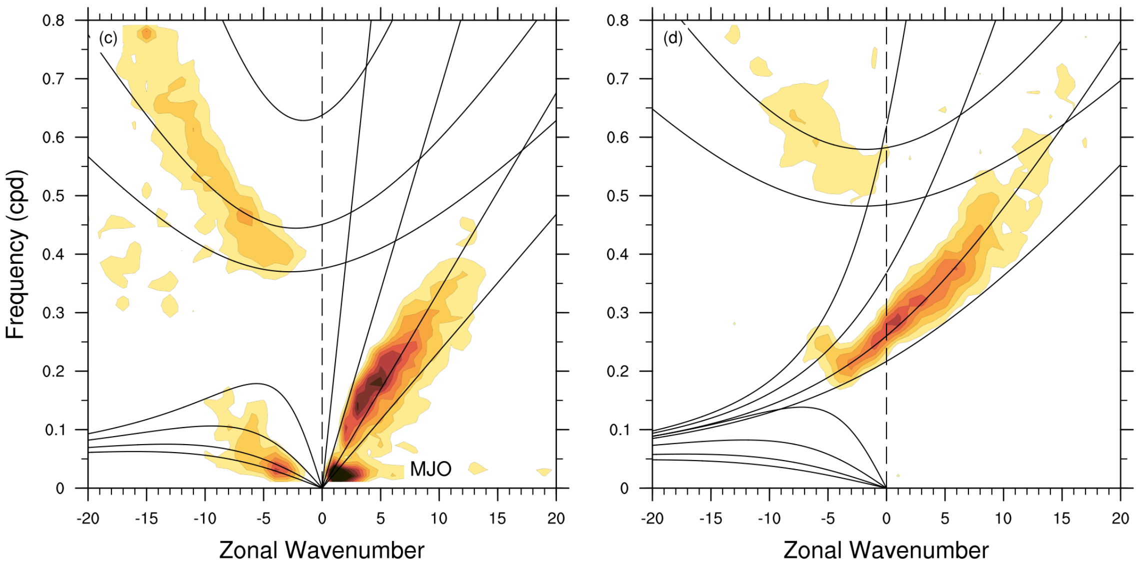

Wheeler and Kiladis 1999

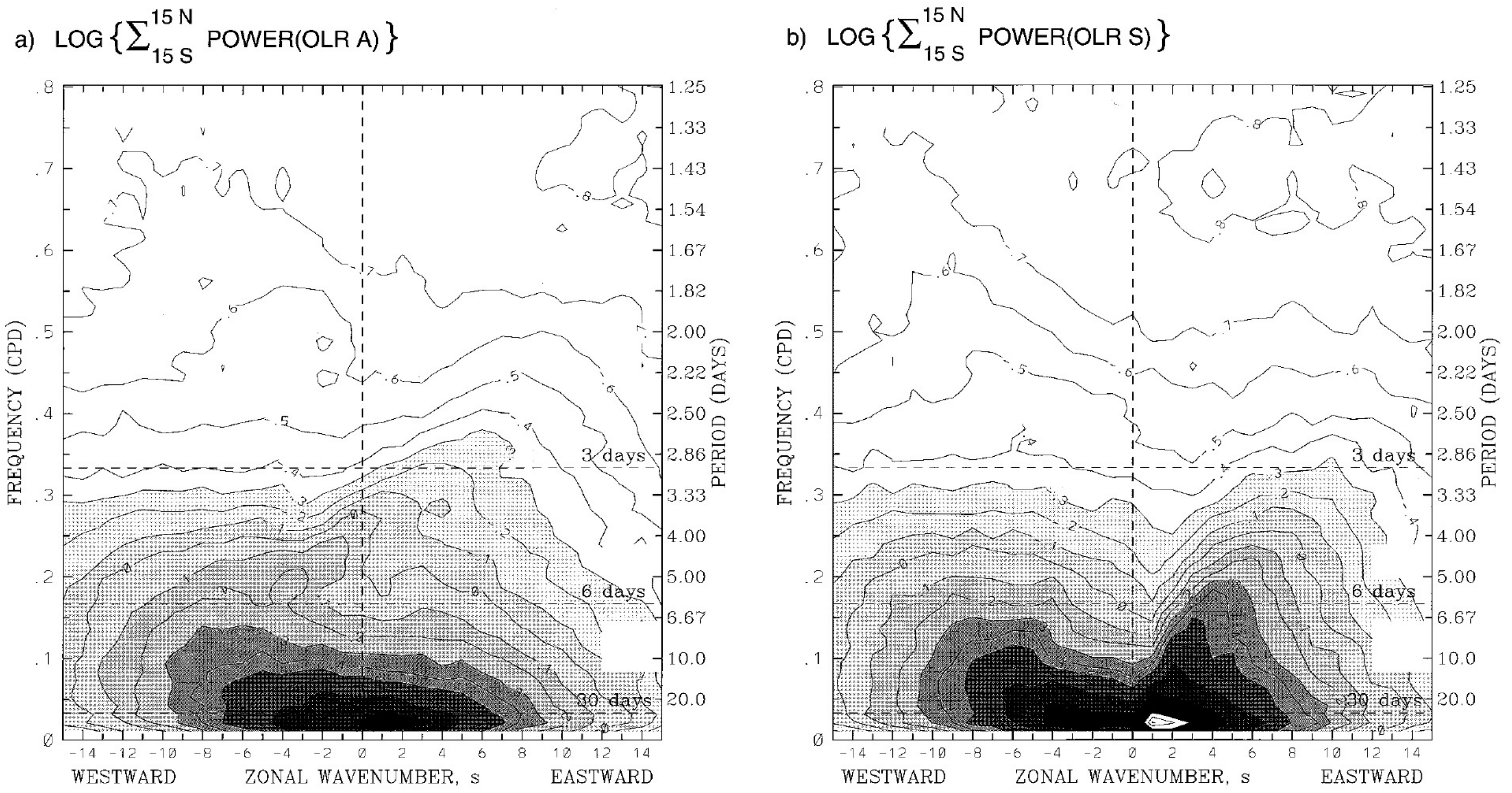

FIG. 1. Zonal wavenumber-frequency power spectra of the (a) antisymmetric component and (b) symmetric component of OLR, calculated for the entire period of record from 1979 to 1996. For both components, the power has been summed over 15°S–15°N lat, and the base-10 logarithm taken for plotting. Contour interval is 0.1 arbitrary units (see text). Shading is incremented in steps of 0.2. Certain erroneous spectral peaks from artifacts of the satellite sampling (see text) are not plotted.

Wheeler and Kiladis 1999

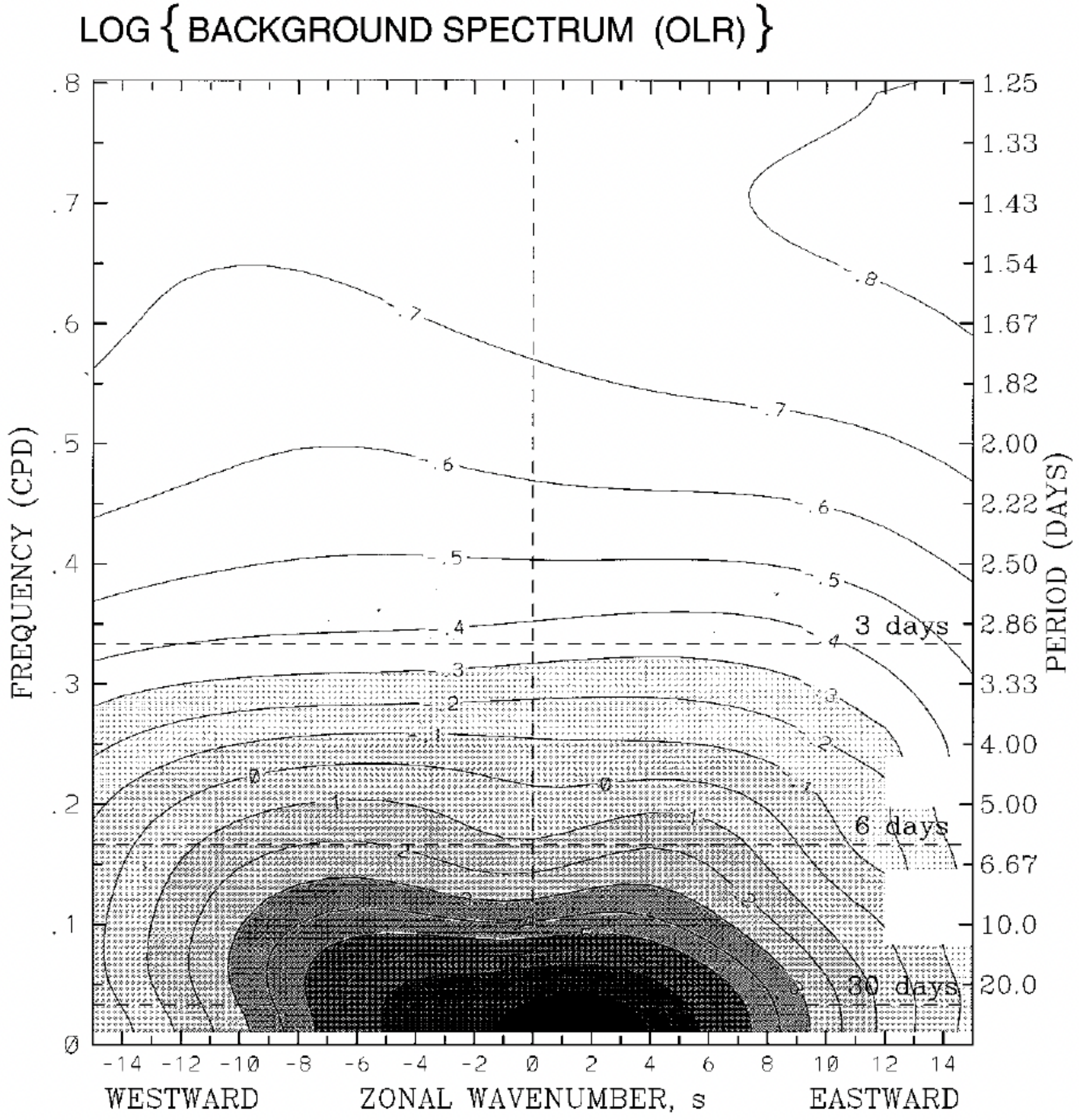

FIG. 2. Zonal wavenumber-frequency spectrum of the base-10 logarithm of the ''background'' power calculated by averaging the individual power spectra of Figs. 1a and 1b, and smoothing many times with a 1-2-1 filter in both wavenumber and frequency. The contour interval and shading are the same as in Fig. 1.

Wheeler and Kiladis 1999

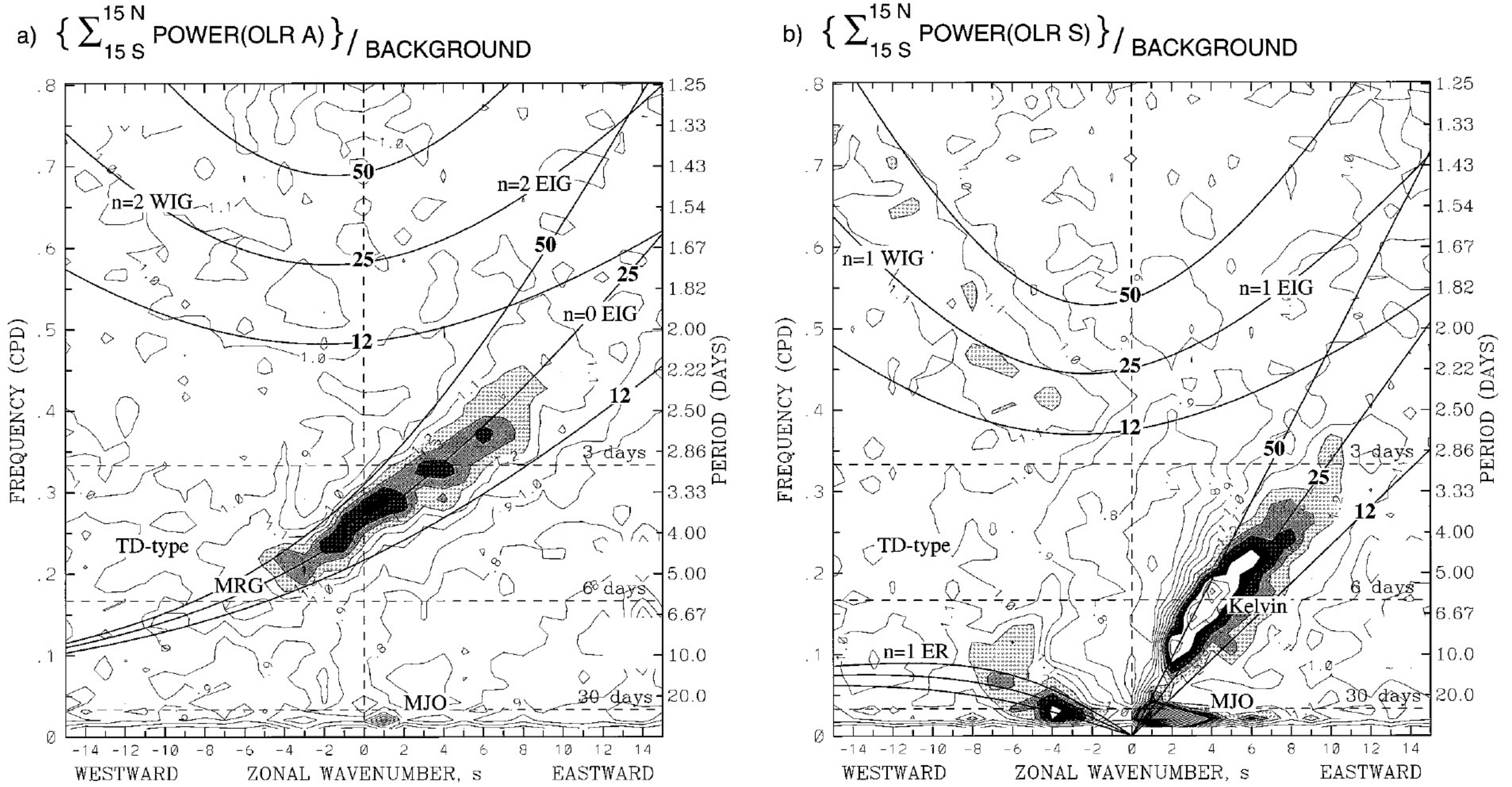

FIG. 3. (a) The antisymmetric OLR power of Fig. 1a divided by the background power of Fig. 2. Contour interval is 0.1, and shading begins at a value of 1.1 for which the spectral signatures are statistically significantly above the background at the 95% level (based on 500 dof). Superimposed are the dispersion curves of the even meridional mode-numbered equatorial waves for the three equivalent depths of h = 12, 25, and 50 m. (b) Same as in panel a except for the symmetric component of OLR of Fig. 1b and the corresponding odd meridional mode-numbered equatorial waves. Frequency spectral bandwidth is 1/96 cpd.

Space-Time Coherence and Phase diagrams
U850xPR and U200xPR

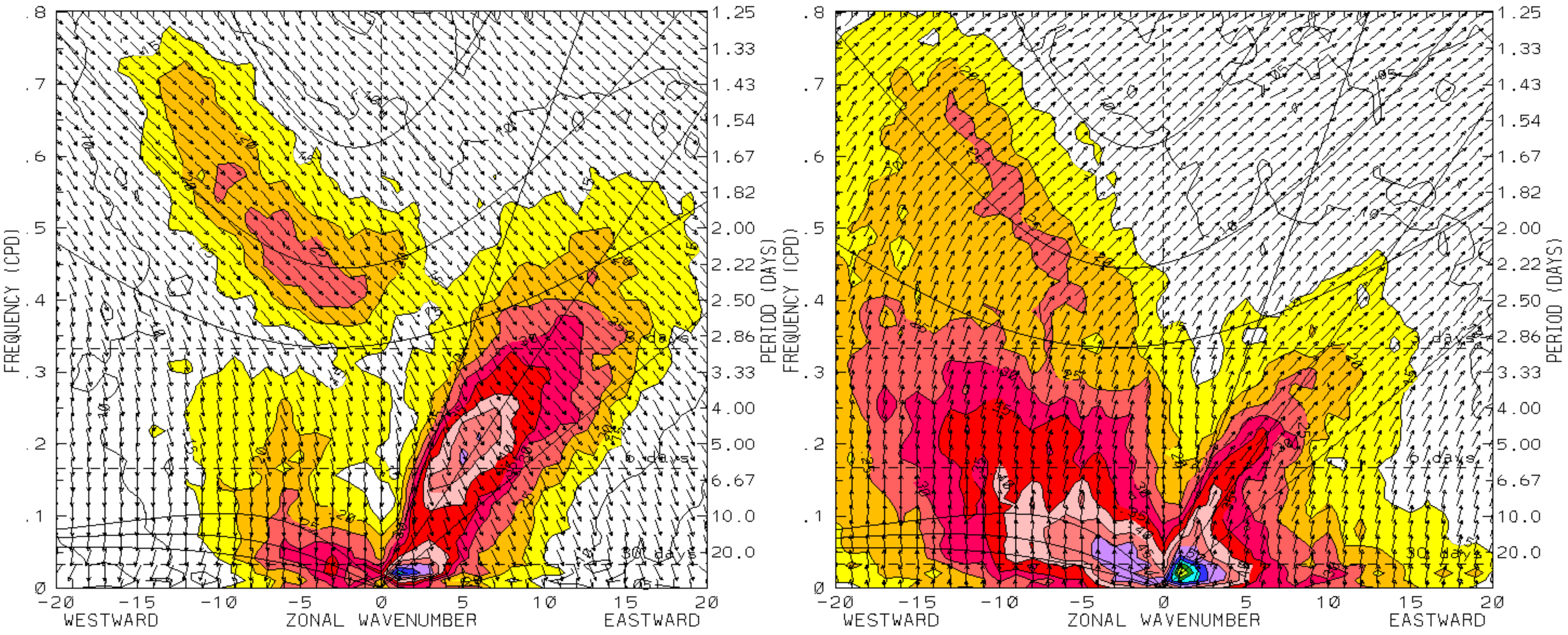

Localized Space-Time Spectra

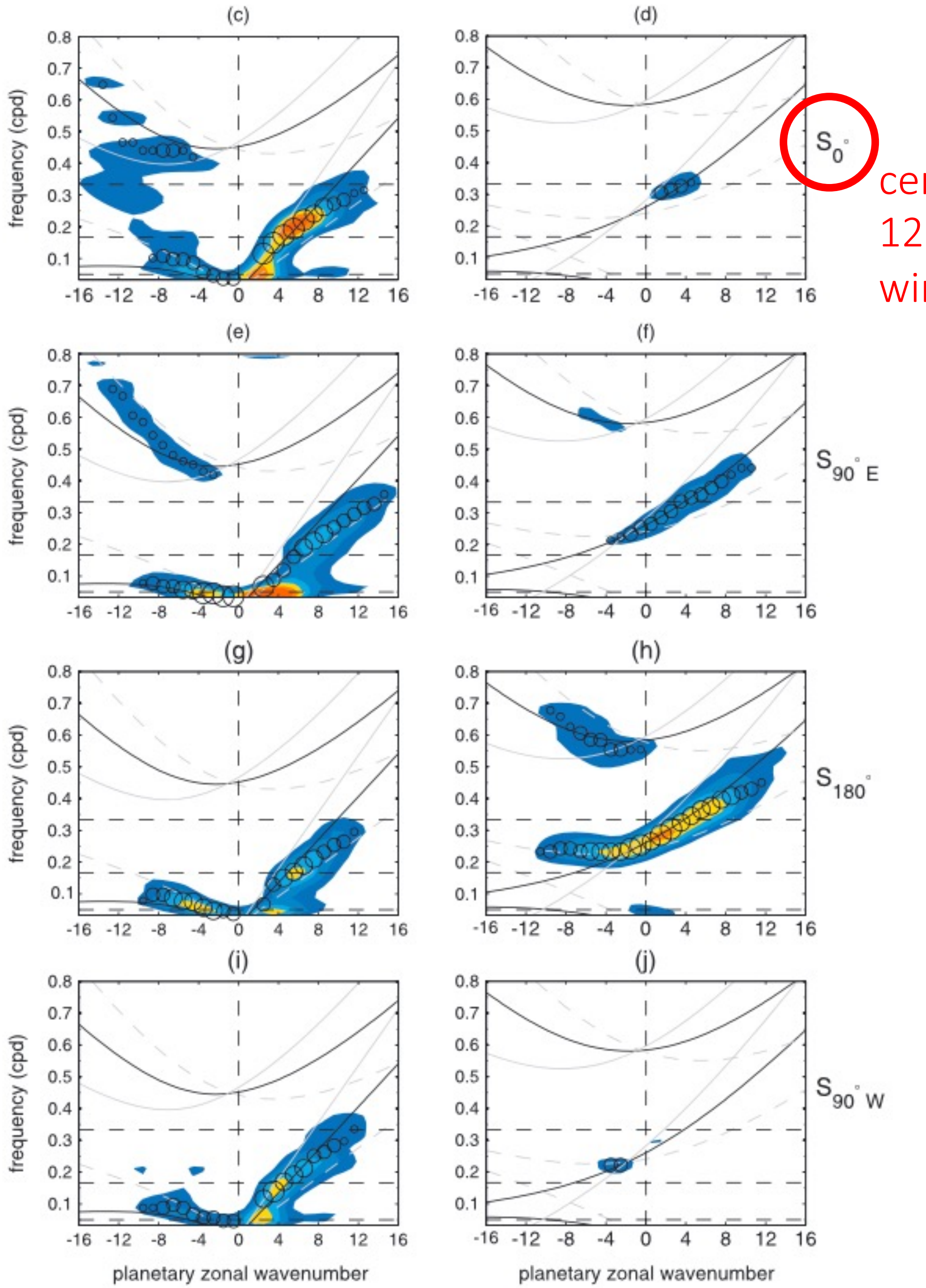

center of 120º window

Glonbal Space-Time Spectra

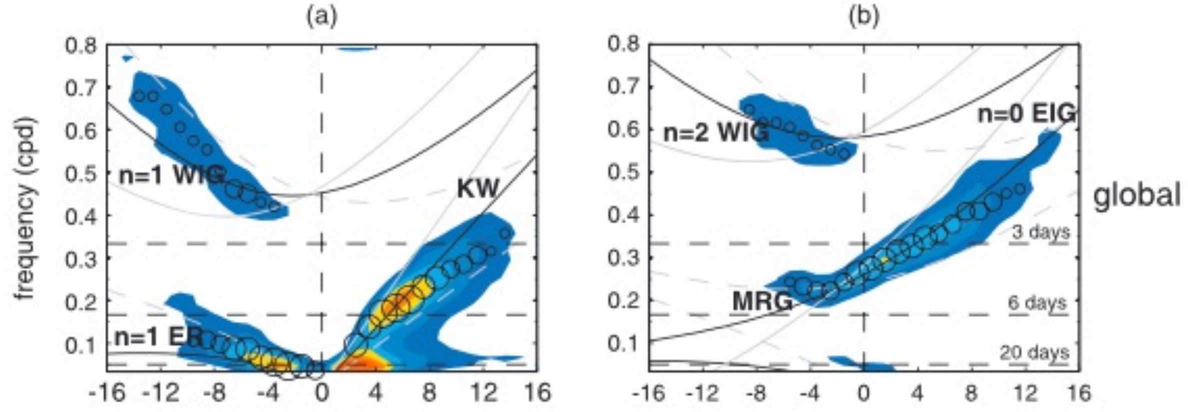

Figure 1. Space-time spectra of CLAUS T_b where each panel shows the total power above the background (shading). Rows correspond to the (a, b) global spectra and the regional spectra for sectors centered at (c, d) 0°, (e, f) 90°E, (g, h) 180°, and (i, j) 90°W. Figures 1a, 1c, 1e, 1g, and 1i display the symmetric (antisymmetric) components. Symbols correspond to the weighted frequency calculated using (2) where the size of the symbol is proportional to the amount of power above the background (the smallest circle represents 10% of power above the background). Shading interval is 0.1, starting at 1.1. The dispersion curves are shown for H_{eq} = 25 m with U = 0 m s^{-1} (black), U = 5 m s^{-1} (solid gray), and U = −5 m s^{-1} (dashed gray).

Identification of tropical waves: spectral filtering

[Kiladis 2009](#)
[Knippertz 2022](#)

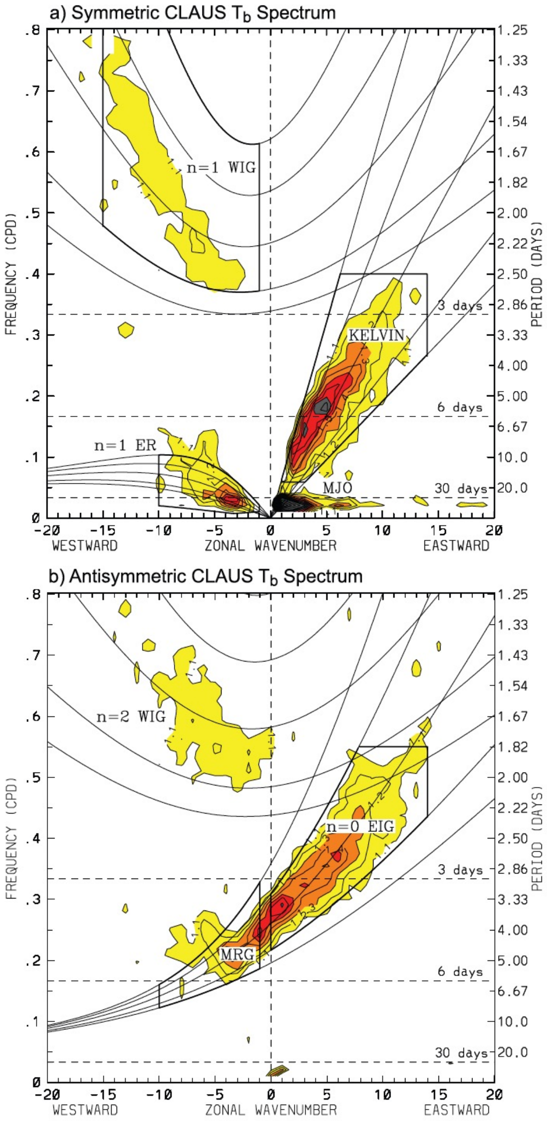

Figure 1

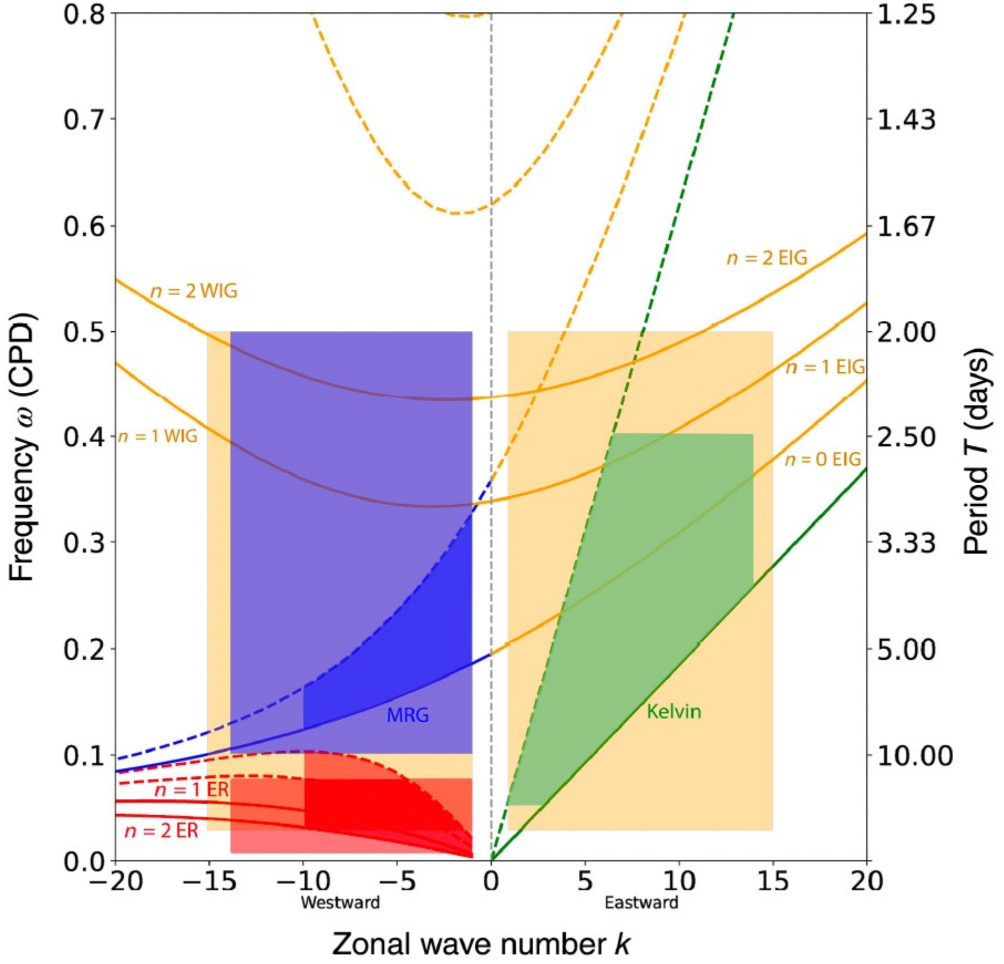

spectral peaks guide the definition of the spectral regions used for filtering (i.e. spectral coeficients are zeroed outside of those regions)

Identification of tropical waves: spectral filtering

Knippertz 2022

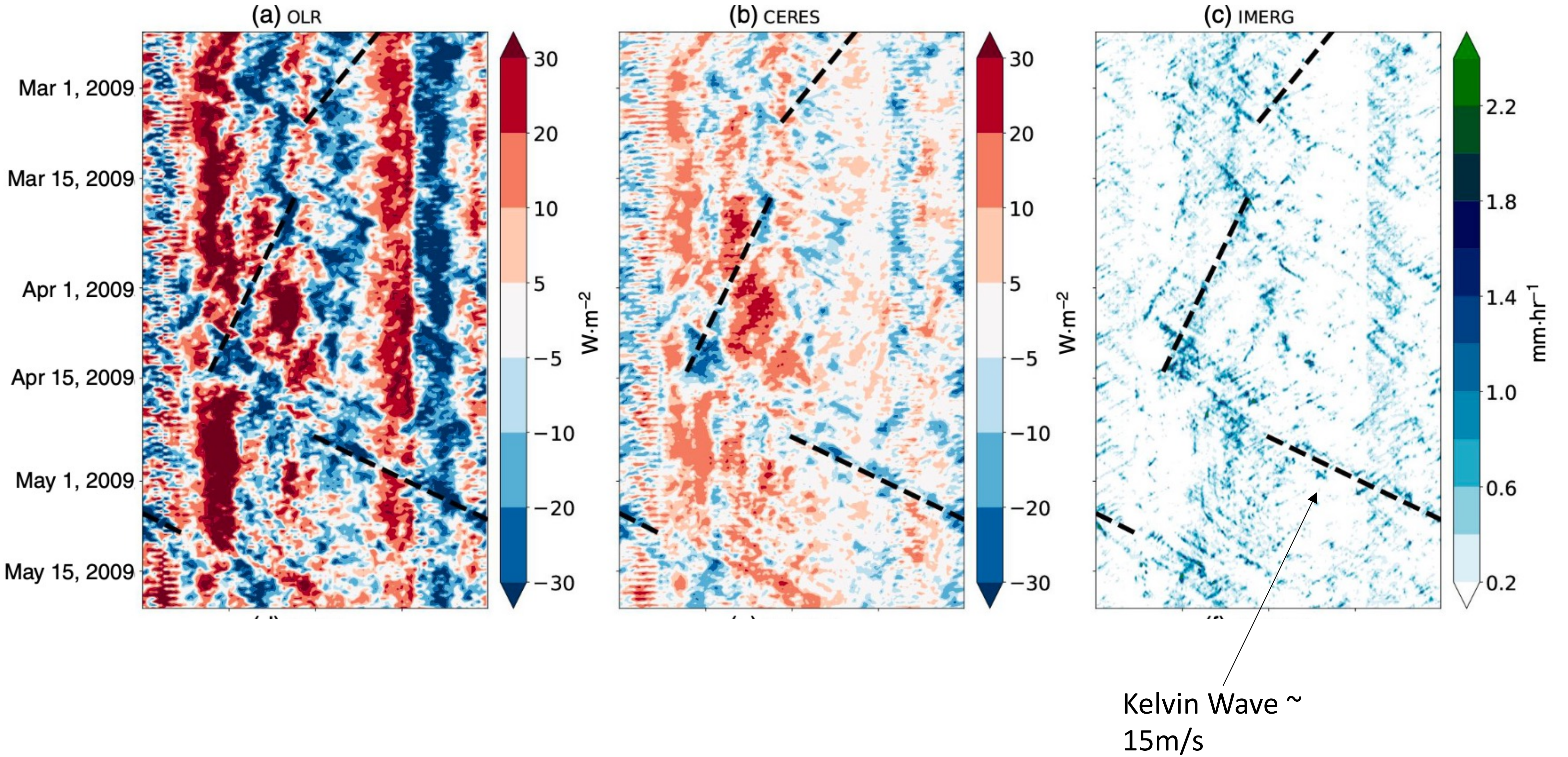

Identification of tropical waves: spectral filtering

Knippertz 2022

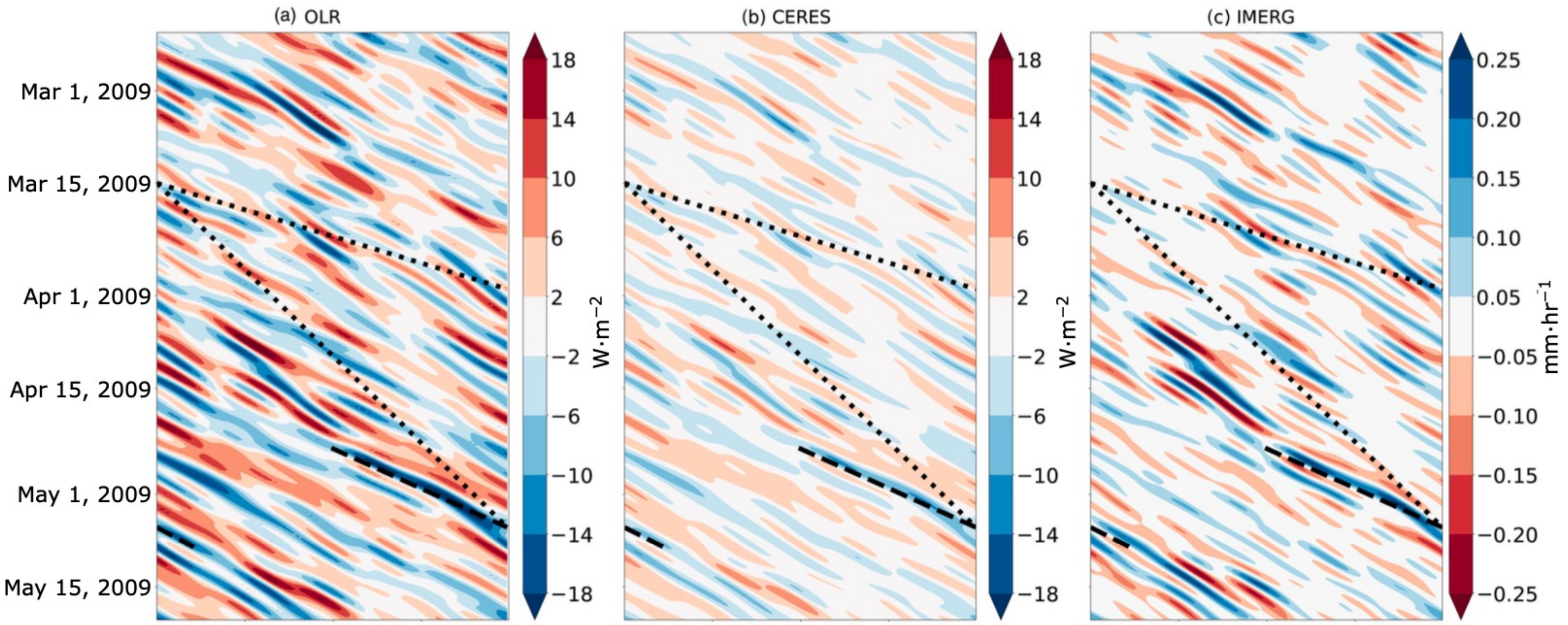

Identification of tropical waves: spectral filtering

Knippertz 2022

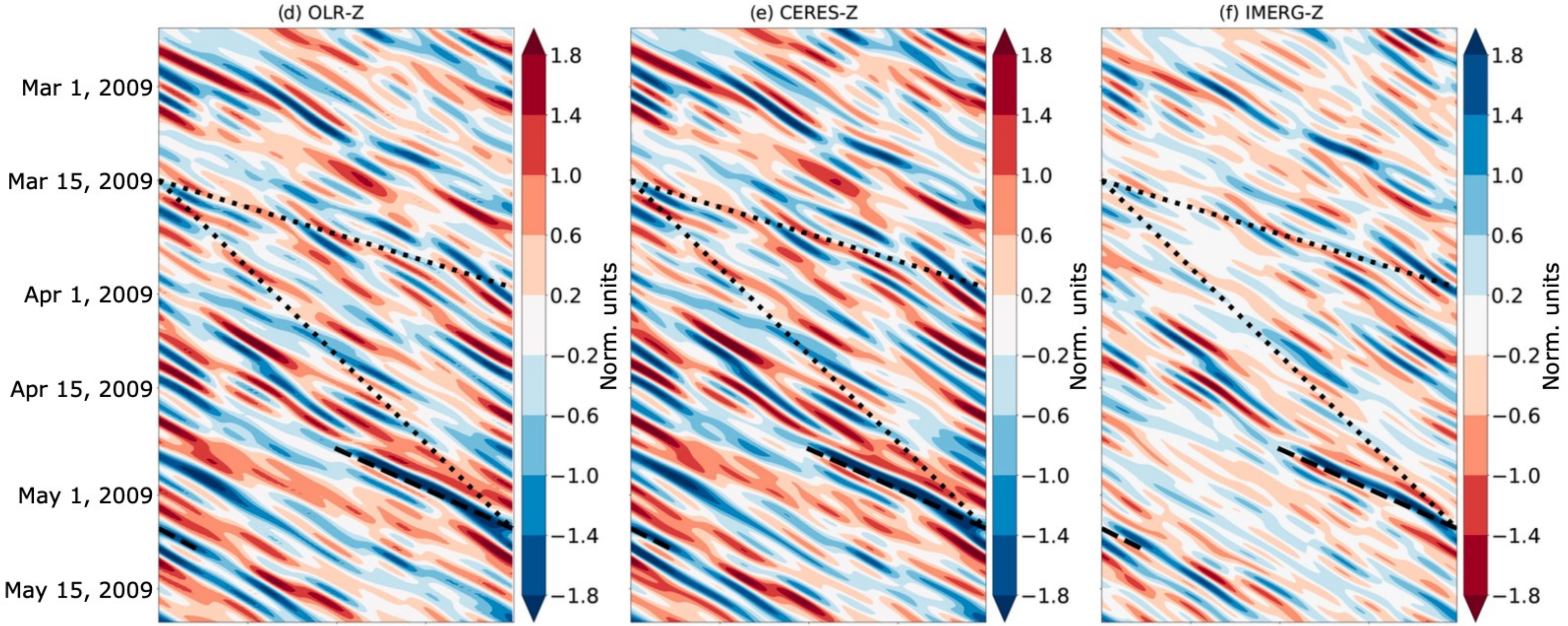

Identification of tropical waves: spectral filtering

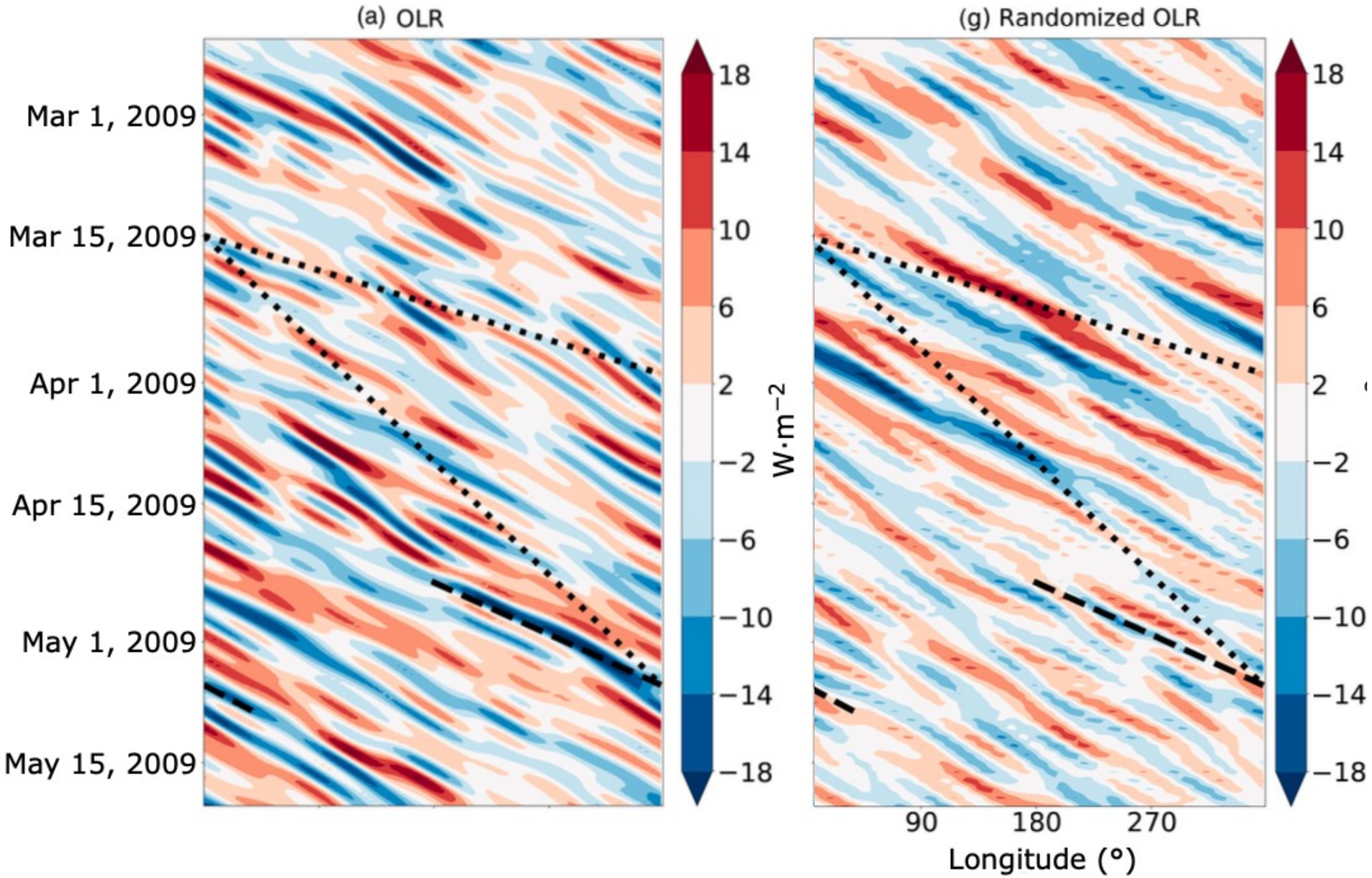

Randomized OLR fields still look like Kelvin Waves after filtering

Identification of tropical waves: spectral filtering

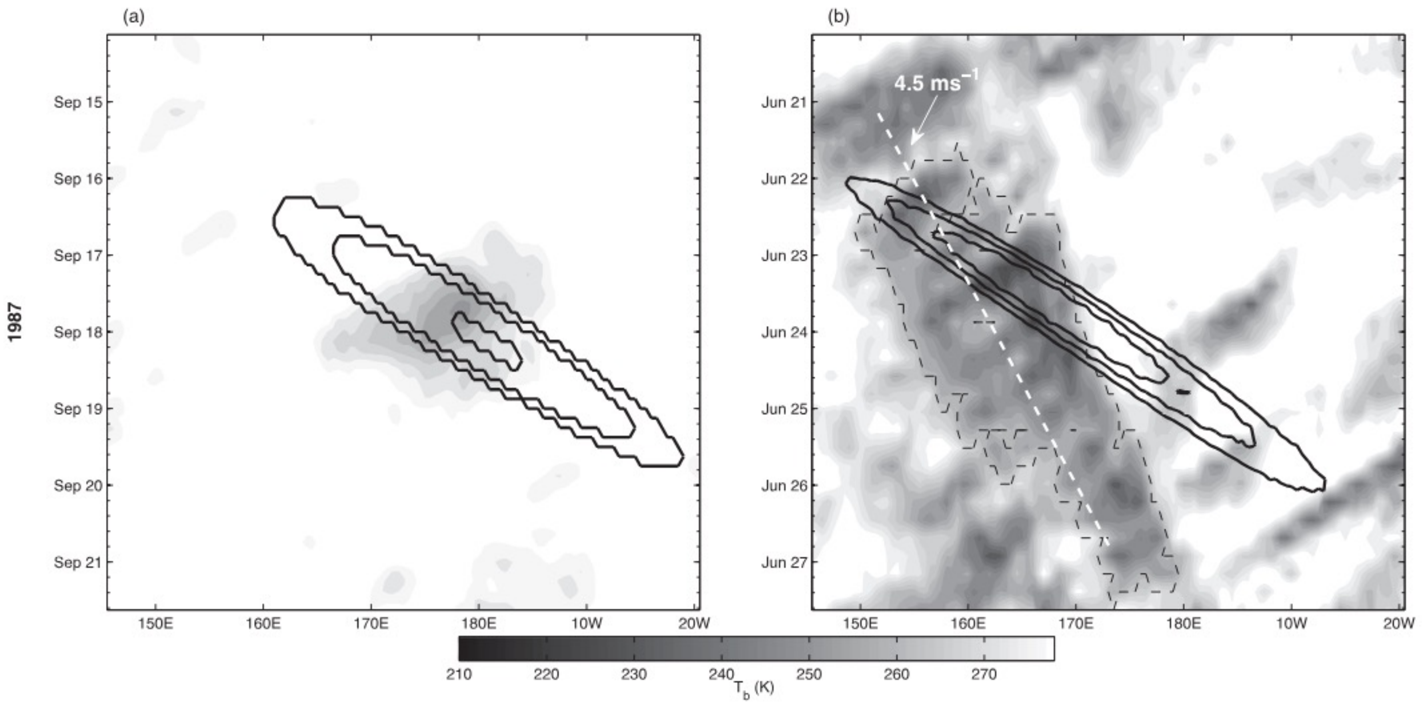

FIG. 1. Time–longitude sections of raw CLAUS T_b data (shading) during (a) September and (b) June 1987 averaged from 7.5°S to 7.5°N, overlaid with Kelvin-filtered T_b (black contours). The dashed contour in (b) is at 245 K.

An Object-Based Approach to Assessing the Organization of Tropical Convection

JULIANA DIAS

Physical Sciences Division, NOAA/Earth System Research Laboratory, Boulder, Colorado

STEFAN N. TULICH

CIRES, University of Colorado, and Physical Sciences Division, NOAA/Earth System Research Laboratory, Boulder, Colorado

GEORGE N. KILADIS

Physical Sciences Division, NOAA/Earth System Research Laboratory, Boulder, Colorado

Identification of tropical waves: spectral filtering

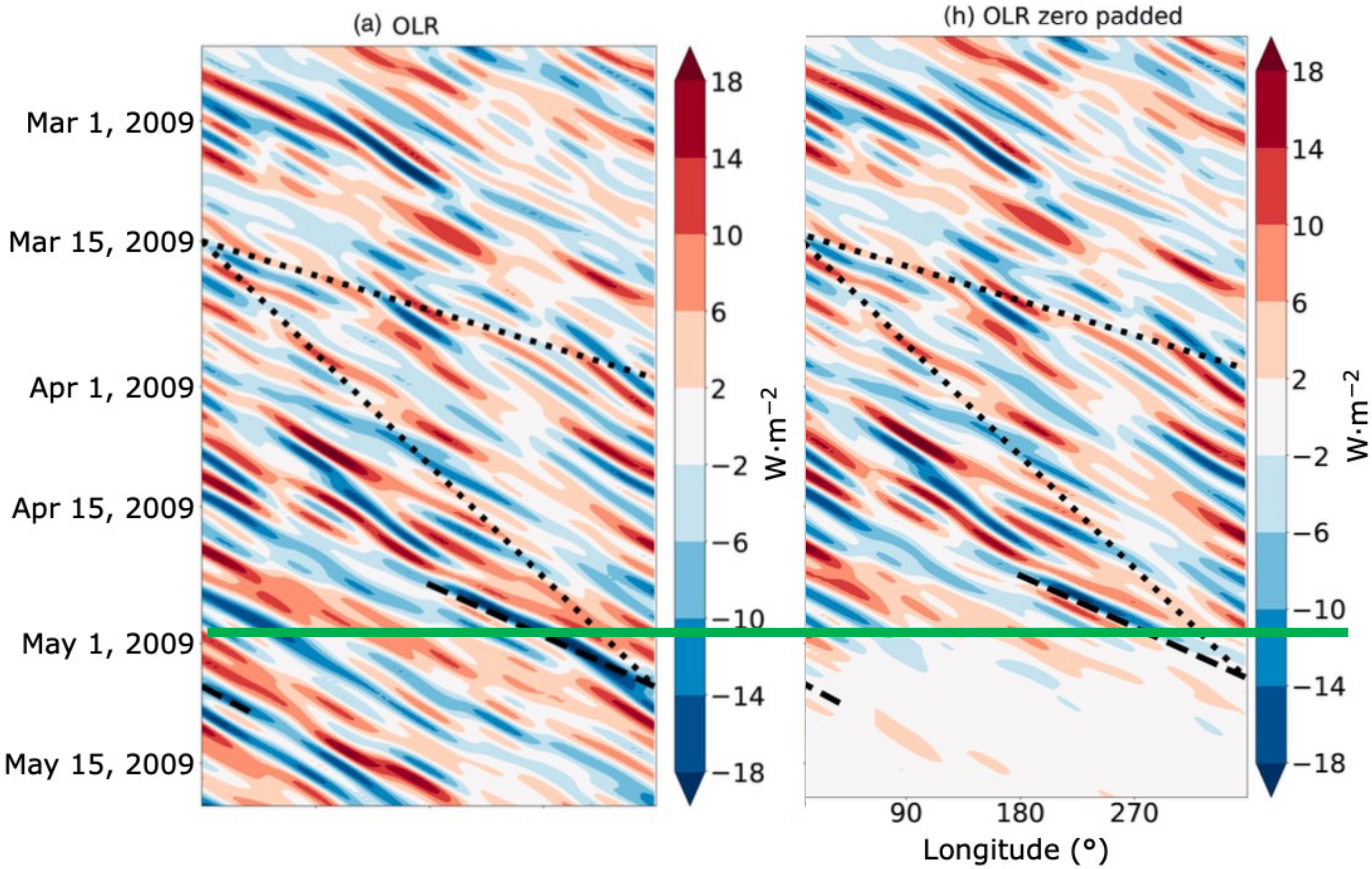

The method *can* be used in real - time applications, and even for short-range forecasts!

What about other methods?

The intricacies of identifying equatorial waves

Peter Knippertz[1] | Maria Gehne[2] | George N. Kiladis[2] | Kazuyoshi Kikuchi[3] | Athul Rasheeda Satheesh[1] | Paul E. Roundy[4] | Gui-Ying Yang[5] | Nedjeljka Žagar[6] | Juliana Dias[2] | Andreas H. Fink[1] | John Methven[7] | Andreas Schlueter[8] | Frank Sielmann[6] | Matthew C. Wheeler[9]

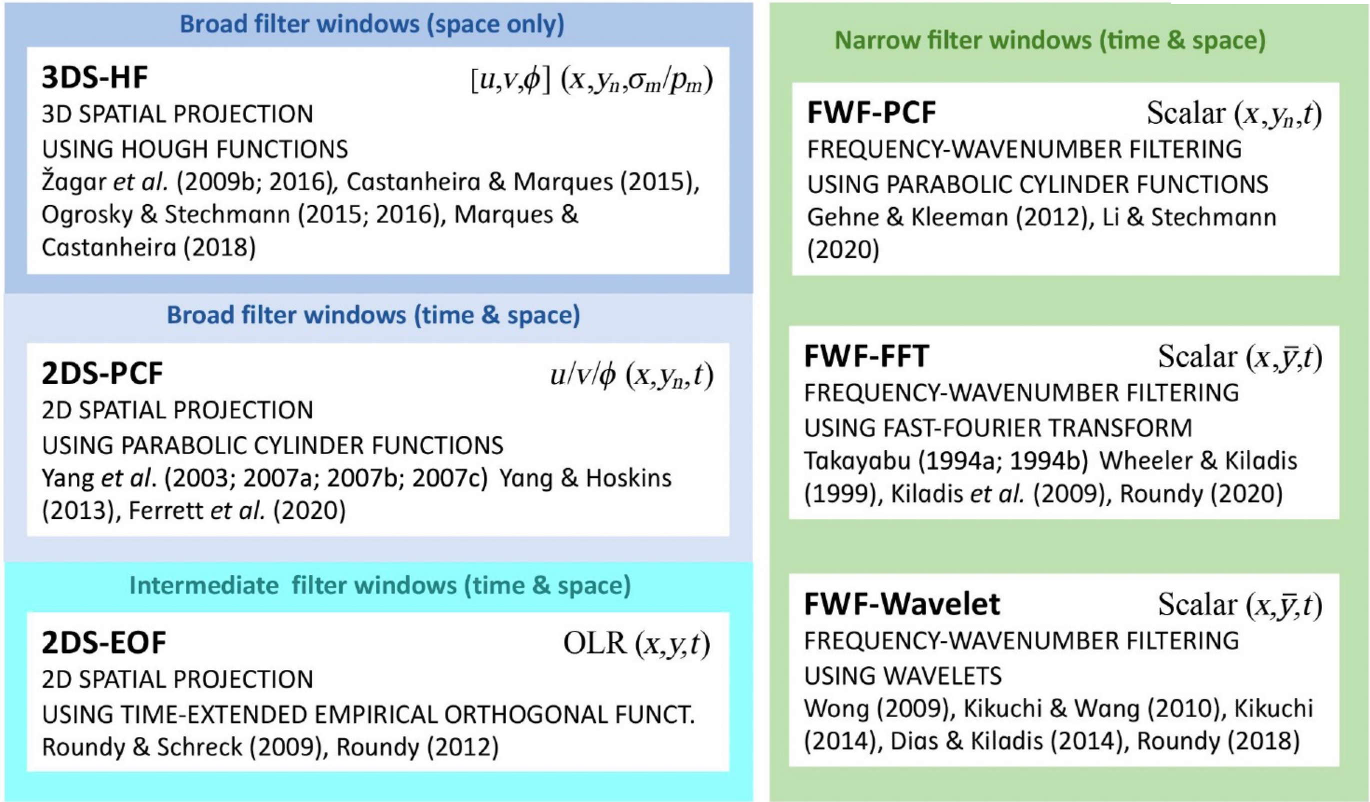

Knippertz 2022

FIGURE 3 Identification methods investigated in this paper. Each method is given with its full name and abbreviation, as well as a list of key publications. The top right corner of each box provides information about the input fields used with each method, together with the coordinates employed. Subscripts n and m stand for meridional and vertical modes, respectively; an overbar indicates a latitudinal average. OLR, outgoing long-wave radiation, u, zonal wind; v, meridional wind; ϕ, geopotential; p, pressure, σ, terrain-following coordinate. The frequency–wave-number methods can, in principle, be applied to any two-dimensional scalar field (OLR, u, v, and ϕ, but also divergence and rainfall). The methods are grouped according to the size of the filters used to identify EWs. For more details, see Section 3 [Colour figure can be viewed at wileyonlinelibrary.com]

The intricacies of identifying equatorial waves

Peter Knippertz[1] | Maria Gehne[2] | George N. Kiladis[2] | Kazuyoshi Kikuchi[3] | Athul Rasheeda Satheesh[1] | Paul E. Roundy[4] | Gui-Ying Yang[5] | Nedjeljka Žagar[6] | Juliana Dias[2] | Andreas H. Fink[1] | John Methven[7] | Andreas Schlueter[8] | Frank Sielmann[6] | Matthew C. Wheeler[9]

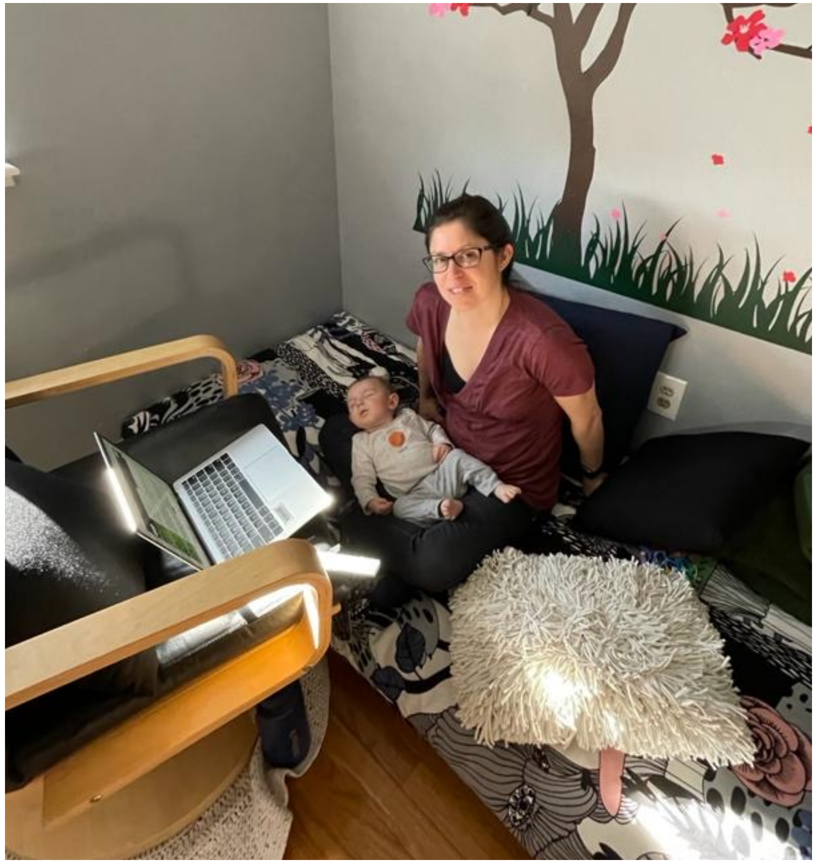

+

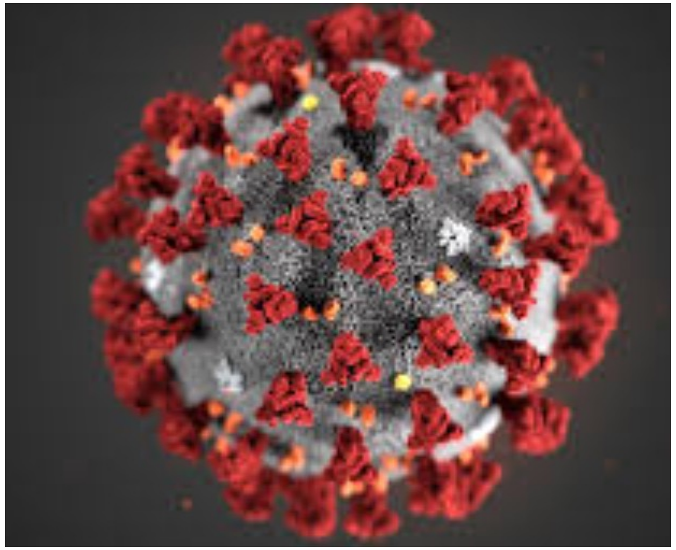

=

?

Knippertz 2022

What about other methods?

Broad filter windows (time & space)

2DS-PCF $u/v/\phi\ (x, y_n, t)$

2D SPATIAL PROJECTION

USING PARABOLIC CYLINDER FUNCTIONS

Yang *et al.* (2003; 2007a; 2007b; 2007c) Yang & Hoskins (2013), Ferrett *et al.* (2020)

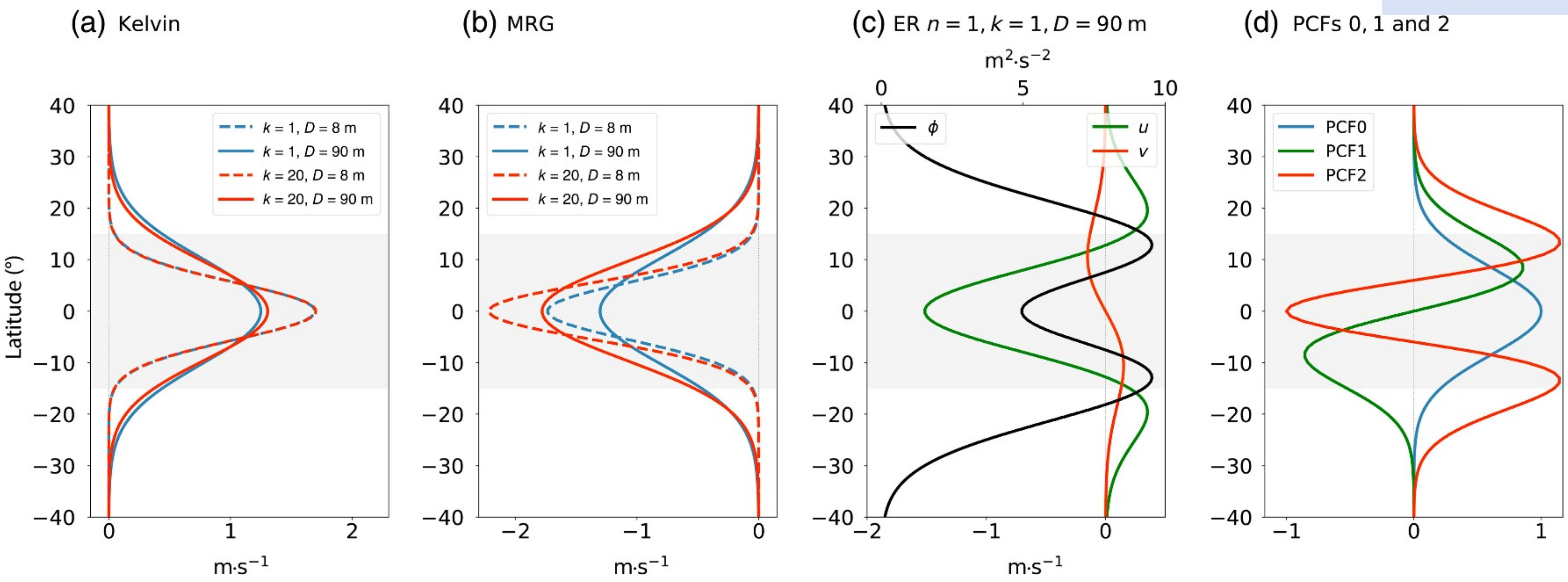

FIGURE 2 Latitudinal profiles of different equatorial wave solutions. Spherical solutions for (a) Kelvin wave zonal wind u' and (b) mixed Rossby–gravity wave (MRG) meridional wind v', both for $D = 8$ m and $D = 90$ m and for $k = 1$ and $k = 20$, as well as (c) the $n = 1$ equatorial Rossby wave (ER) u', v', and geopotential ϕ' for $k = 1$ and $D = 90$ m. These curves were produced using the software developed by Swarztrauber and Kasahara (1985). (d) Parabolic cylinder functions (PCFs) 0, 1, and 2 for $y_0 = 6°$. The 15° S–15° N belt used for averaging throughout the paper is shaded in grey [Colour figure can be viewed at wileyonlinelibrary.com]

Kelvin Waves

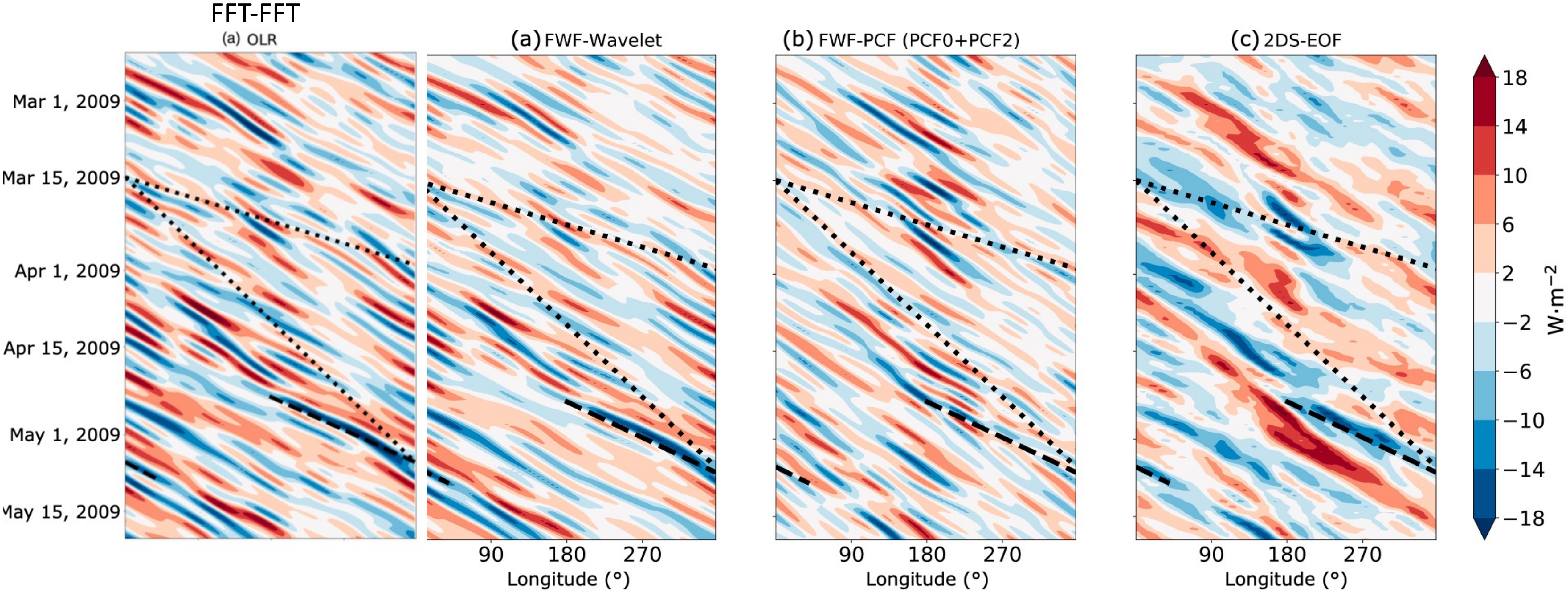

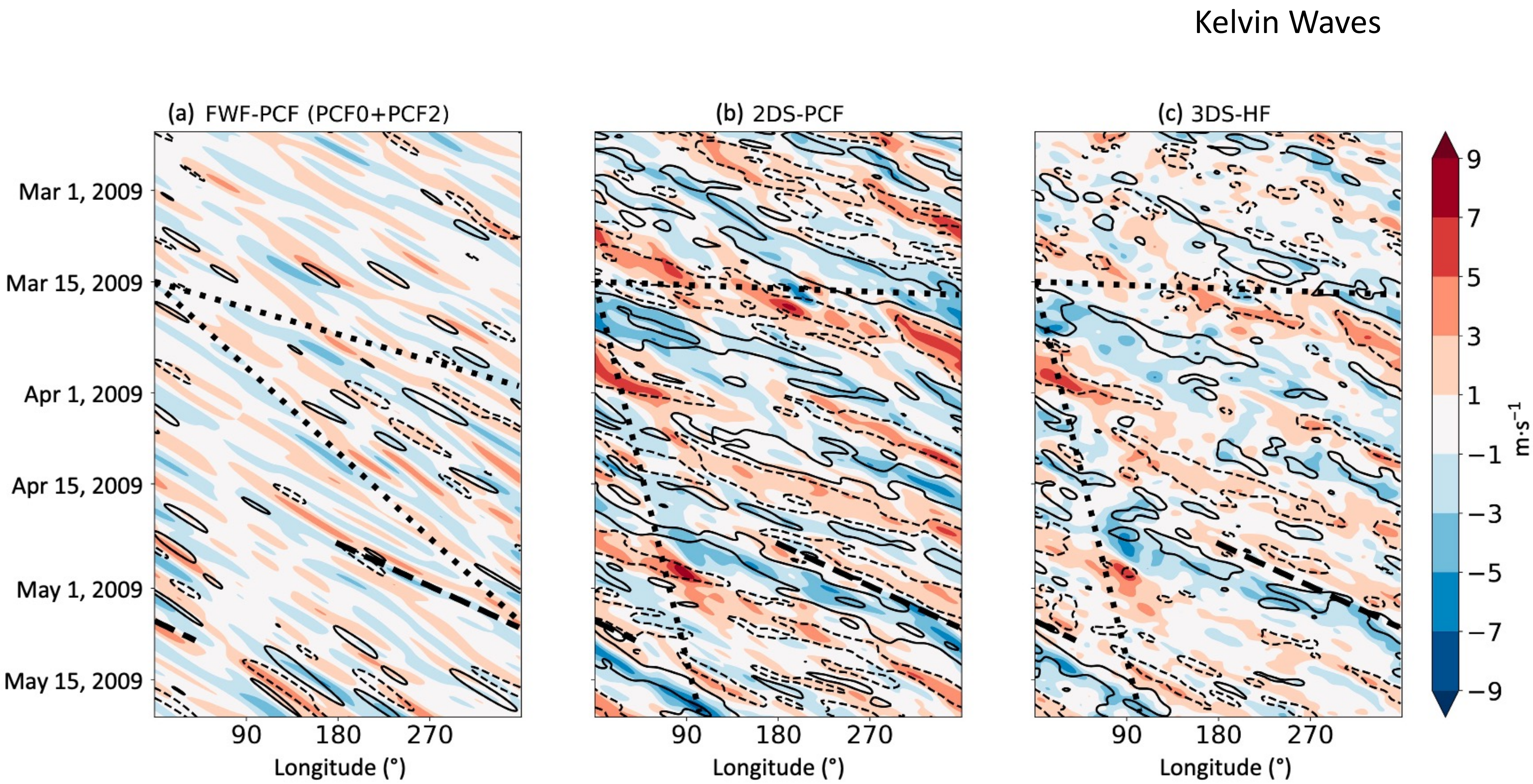
Kelvin Waves
(a) FWF-PCF (PCF0+PCF2)
(b) 2DS-PCF
(c) 3DS-HF
Mar 1, 2009
Mar 15, 2009
Apr 1, 2009
Apr 15, 2009
May 1, 2009
May 15, 2009
90
180
270
Longitude (°)
9
7
5
3
1
−1
−3
−5
−7
−9
m·s⁻¹

Equatorial Rossby Waves

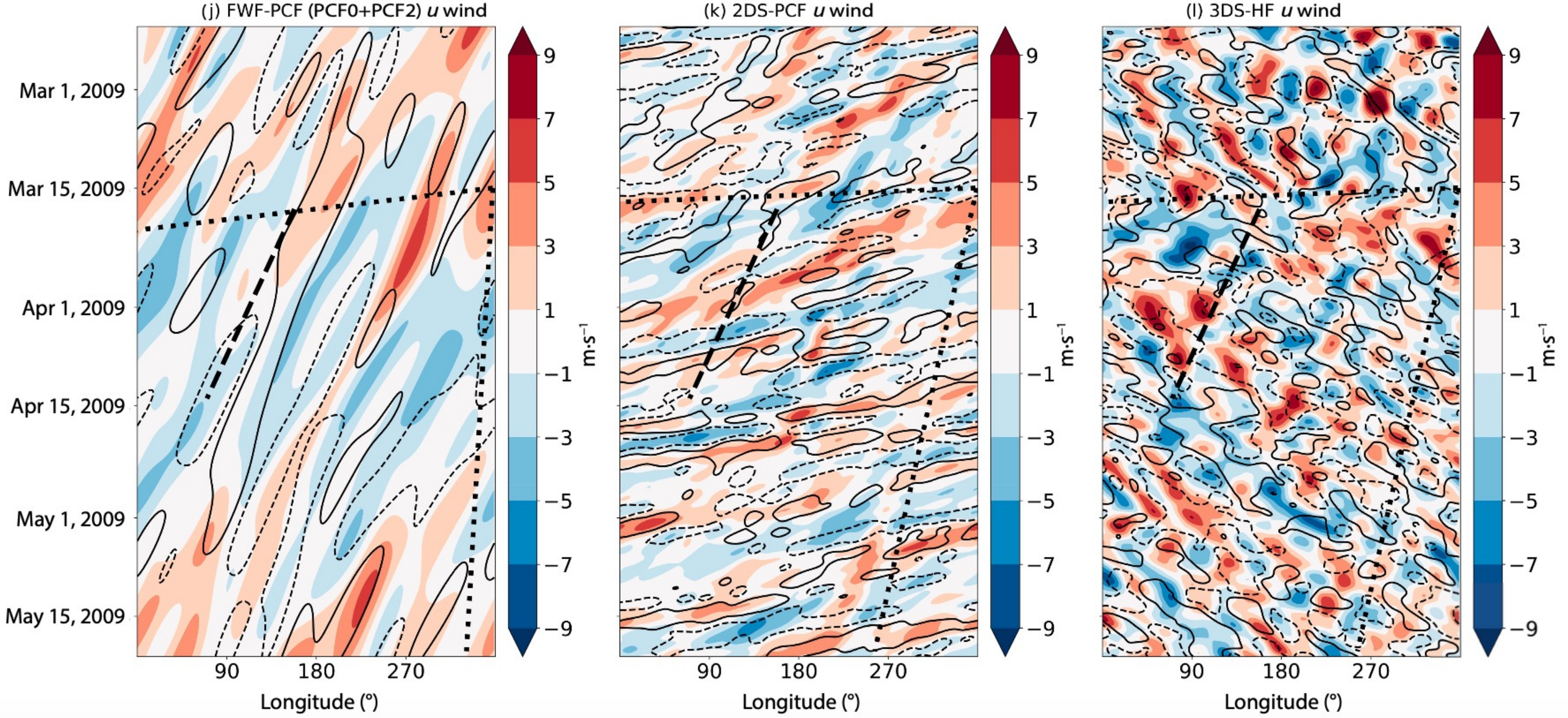

Observed structure of CCEWs

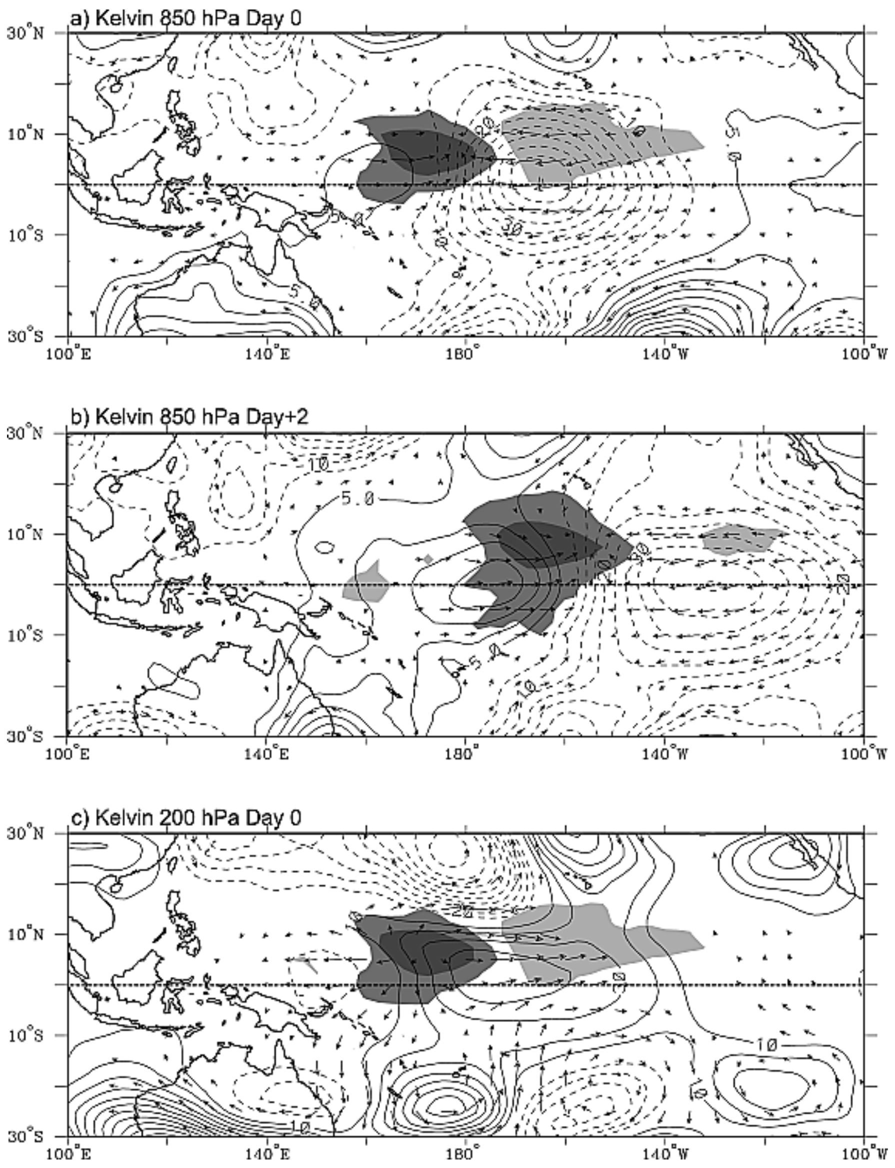

Maps of anomalous Tb (shading), geopotential height (contours), and wind (vectors) associated with a −20 K perturbation in **Kelvin wave Tb at the base point 7.5°N, 172.5°E,** for (a) day 0 at 850 hPa, (b) day +2 at 850 hPa, and (c) day 0 at 200 hPa. The contour interval is 5 m in Figures 7a and 7b and 10 m in Figure 7c, with negative contours dashed. Dark (light) shading is for negative (positive) Tb perturbations of ±10 K and 3 K. Tb and wind vectors are locally significant at the 95% level, with the largest vectors around 2 m s−1.

Kiladis 2009

Observed structure of CCEWs

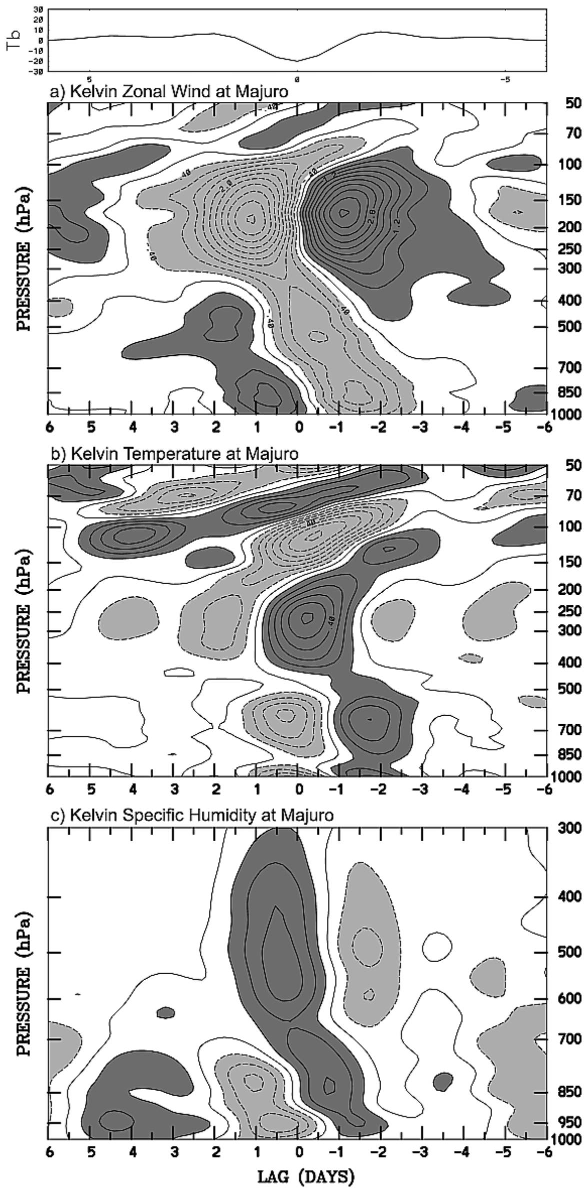

[Kiladis 2009]

Maps of anomalous Tb (shading), geopotential height (contours), and wind (vectors) associated with a −20 K perturbation in Kelvin wave Tb at the base point 7.5°N, 172.5°E, for (a) day 0 at 850 hPa, (b) day +2 at 850 hPa, and (c) day 0 at 200 hPa. The contour interval is 5 m in Figures 7a and 7b and 10 m in Figure 7c, with negative contours dashed. Dark (light) shading is for negative (positive) Tb perturbations of ±10 K and 3 K. Tb and wind vectors are locally significant at the 95% level, with the largest vectors around 2 m s−1.

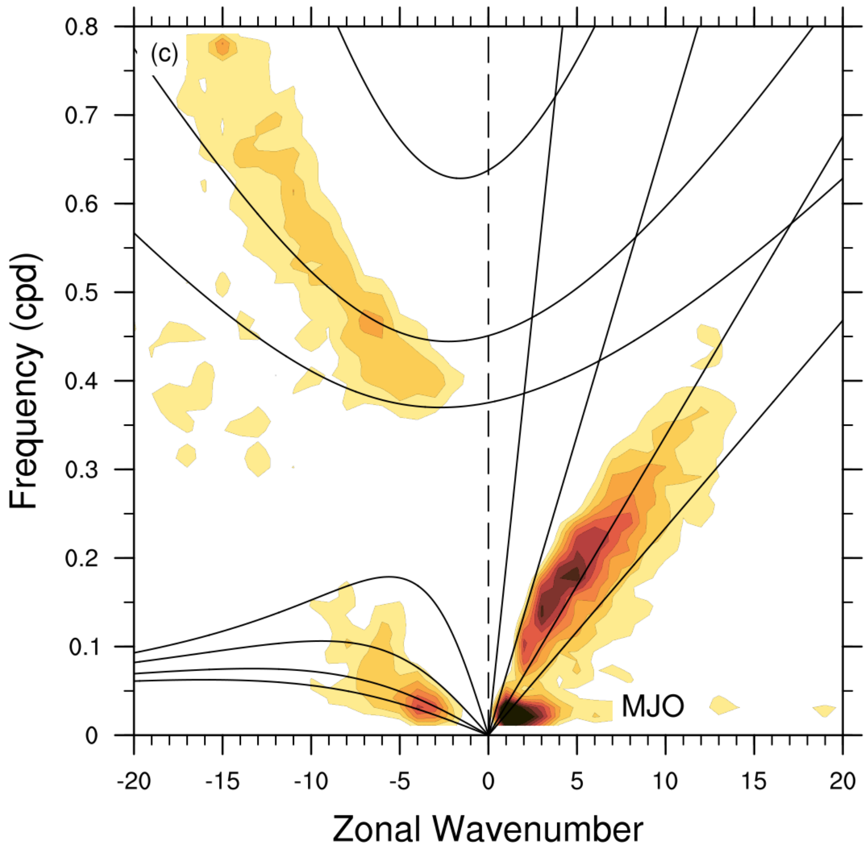

What are the mechanisms underlying convectively coupled waves (CCEW) ?

How do convective parametrizations impact the simulation of CCEWs ?

Are CCEWs important for sub-seasonal predictions within and outside the tropics?

Dias, J., Gehne, M., Kiladis, G. N., & Magnusson, L. (2023). The role of convectively coupled equatorial waves in sub-seasonal predictions. Geophysical Research Letters, 50, e2023GL106198

Dias, J., Tulich, S. N., Gehne, M., & Kiladis, G. N., 2021: Tropical Origins of Weeks 2–4 Forecast Errors during the Northern Hemisphere Cool Season, Mon. Weather Rev, 149(9), 2975-2991.

Dias J. and G. N. Kiladis, 2019: The Influence of Tropical Forecast Errors on Higher Latitude Predictions. Geophys. Res. Lett., 46, 4450-4459

Dias, J., M. Gehne, G. N. Kiladis, N. Sakaeda, P. Bechtold, and T. Haiden, 2018: Equatorial waves and the skill of NCEP and ECMWF numerical weather prediction systems. Mon. Wea. Rev., 146(6):1763-1784.

Composites: KW over the Pacific - JJA

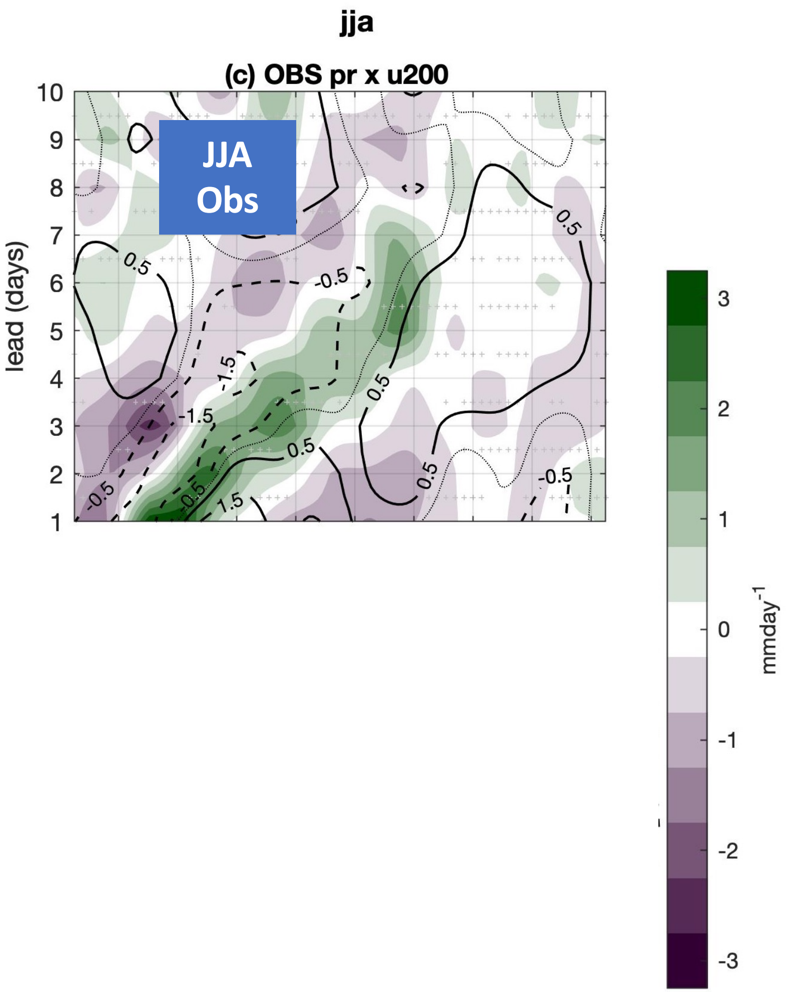

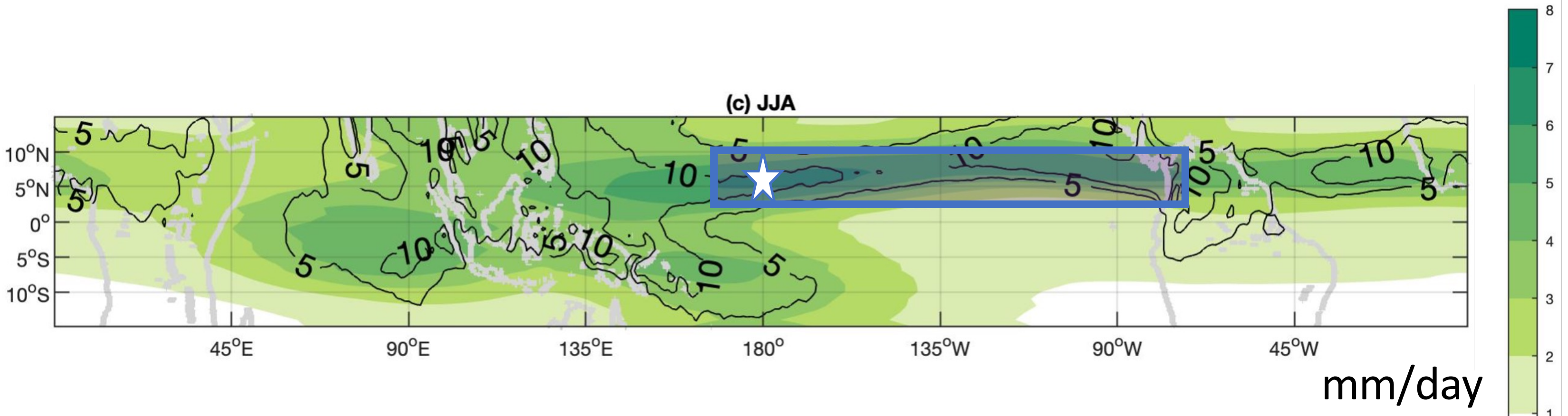

- ***Day 0 in the composites correspond to peak dates in CCKW filtered amplitude at a basepoint;***
- ***Shading shows precipitation anomalies and contours show zonal winds at 200hPa.***

Composites: KW over the Pacific - JJA

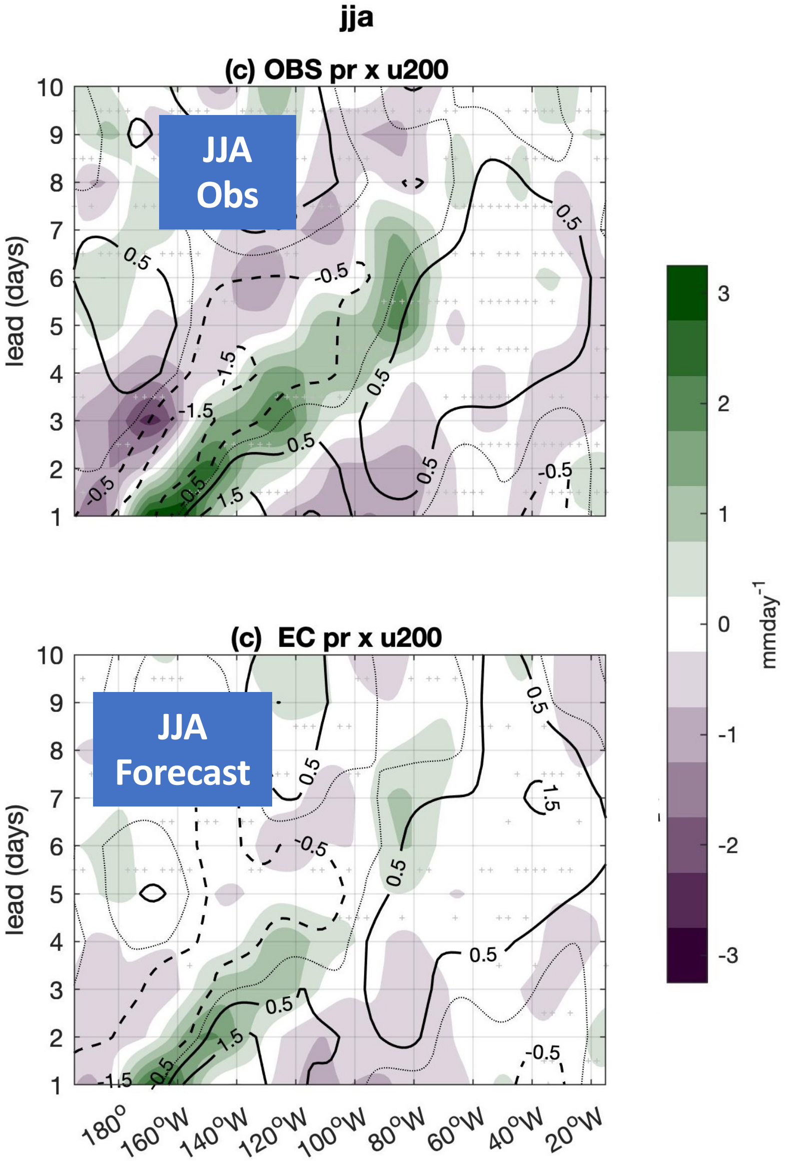

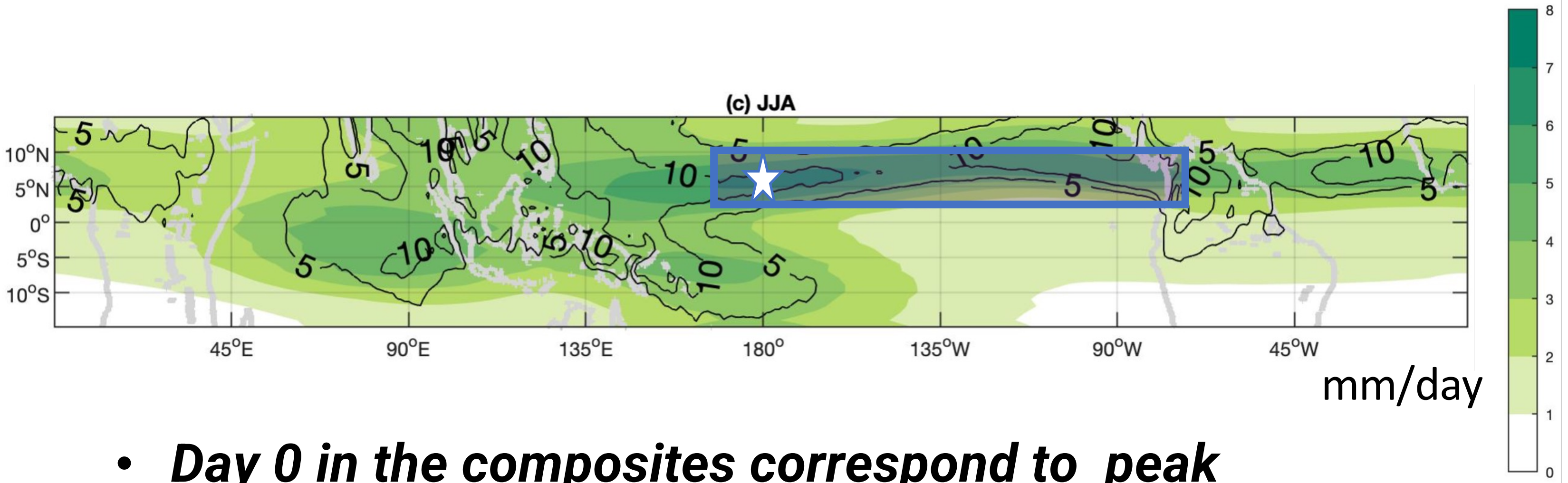

- *Day 0 in the composites correspond to peak dates in CCKW filtered amplitude at a basepoint;*
- *Shading shows precipitation anomalies and contours show zonal winds at 200hPa.*

CCEW amplitude is underestimated in the ECMWF

Composites: KW over the Pacific - JJA

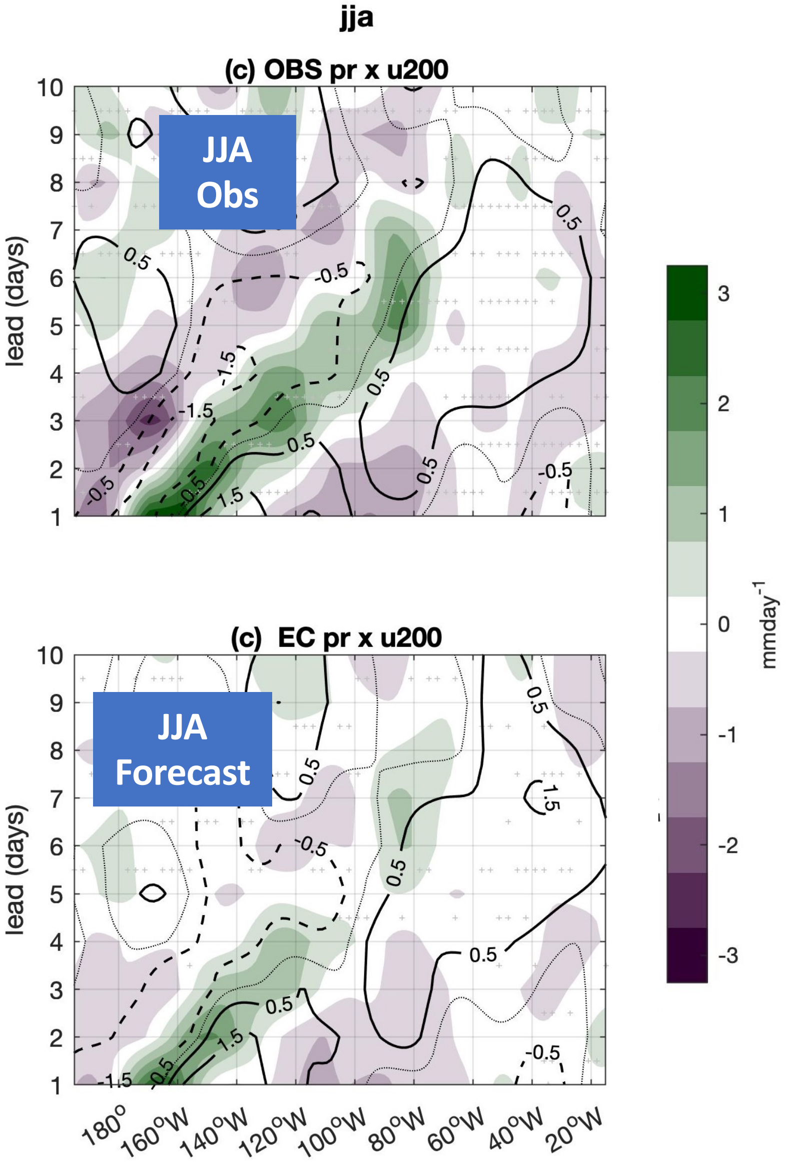

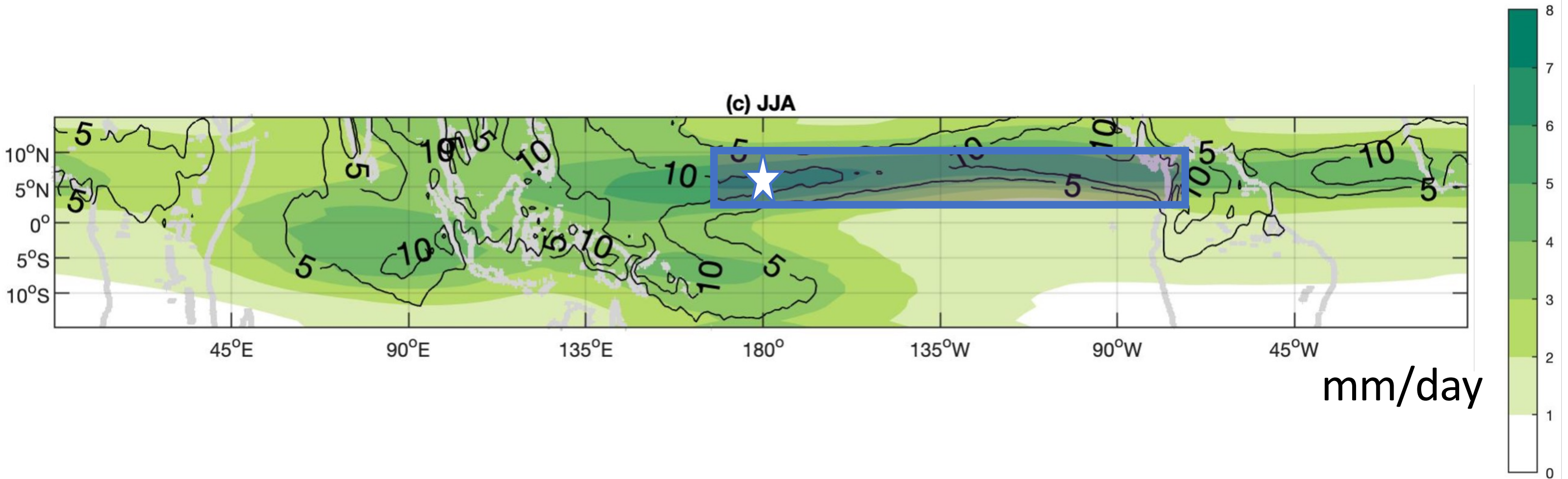

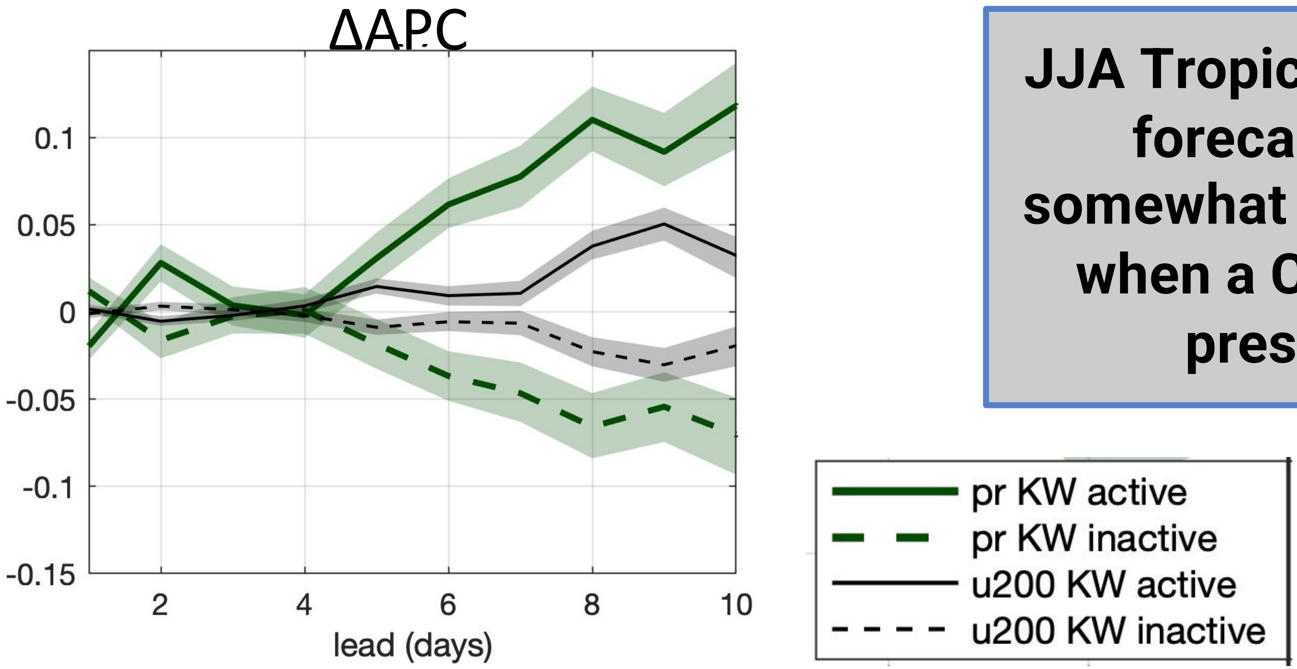

JJA Tropical Pacific forecasts is somewhat improved when a CCKW is present

KW over the Pacific: JJA, MAM, SON, DJF

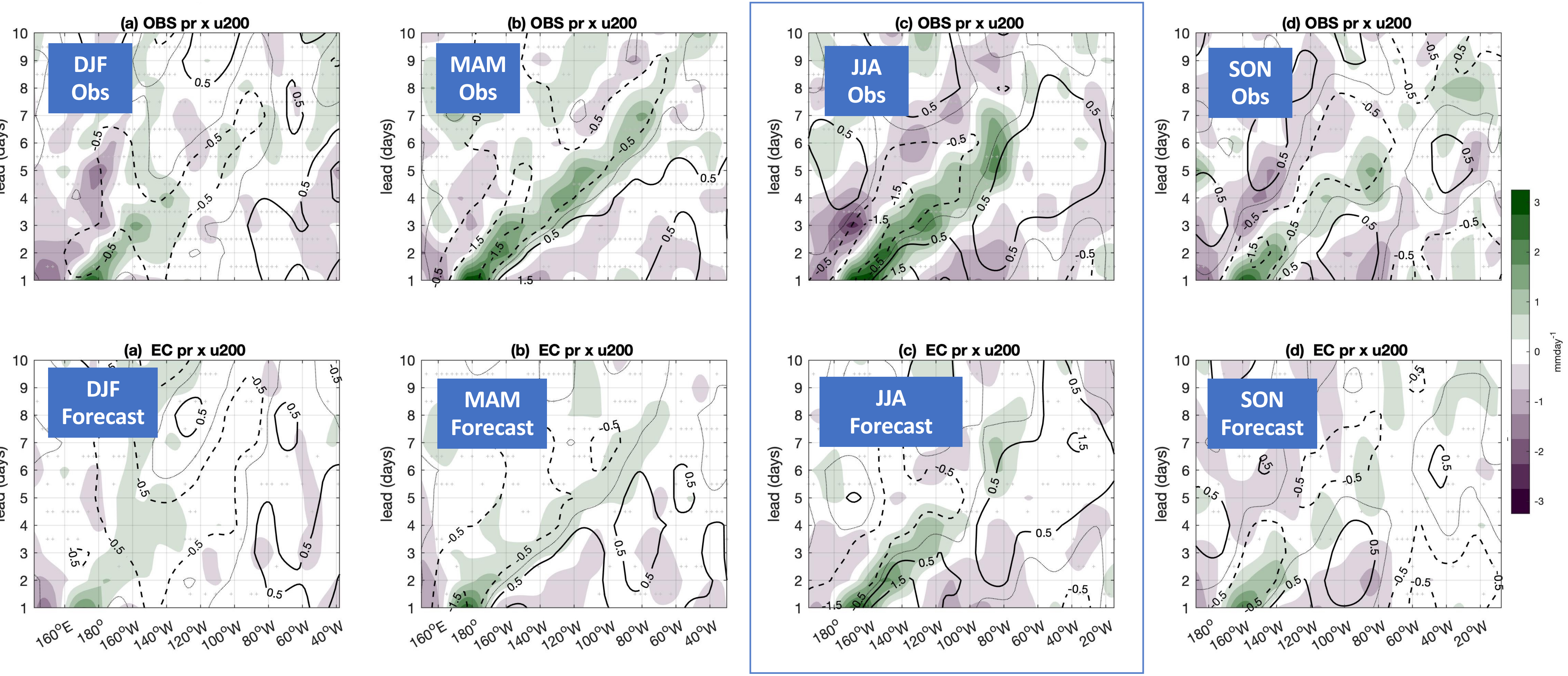

juliana.dias@noaa.gov

KW over the Pacific: JJA, MAM, SON, DJF

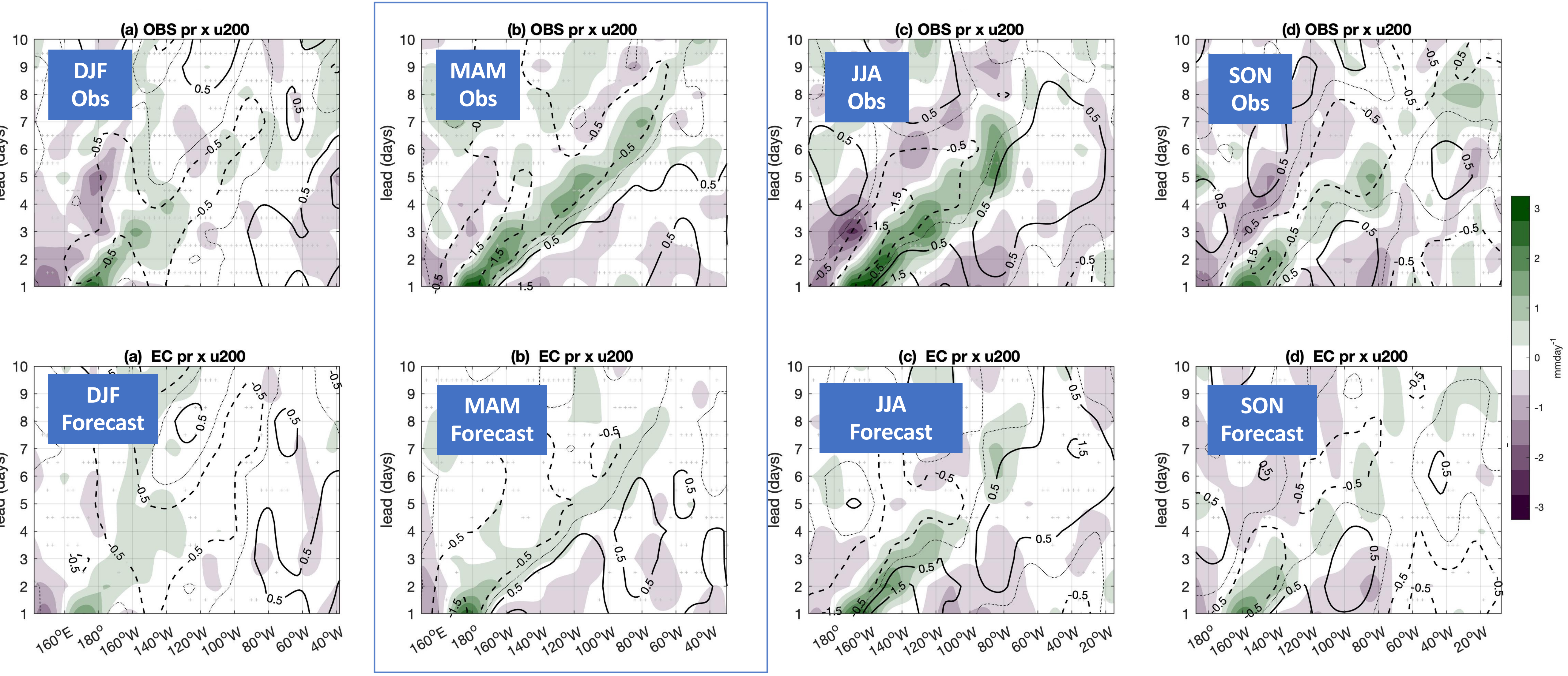

juliana.dias@noaa.gov

KW over the Pacific: JJA, MAM, SON, DJF

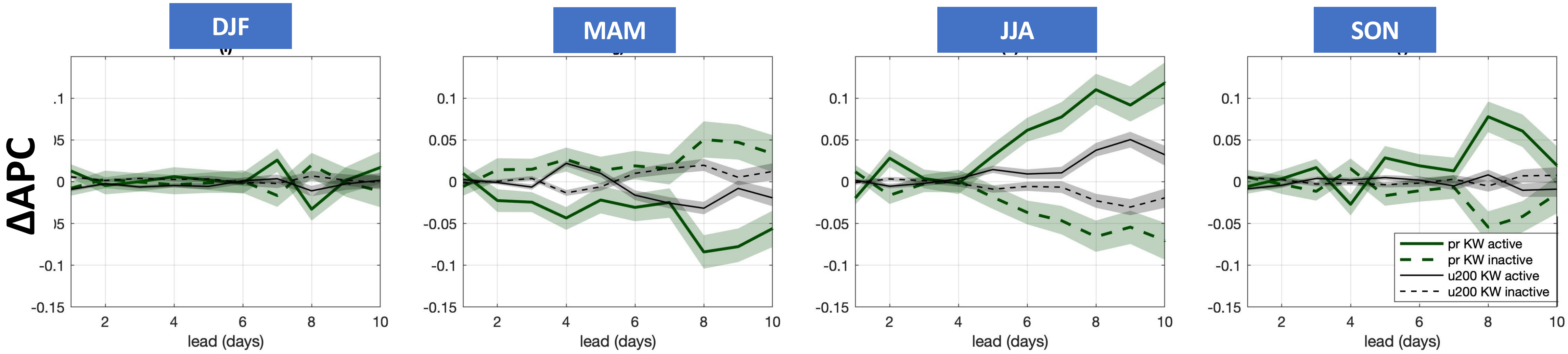

juliana.dias@noaa.gov

KW over the Pacific: JJA, MAM, SON, DJF